THE CHARACTERIZATION OF A BUILDING-INTEGRATED MICROALGAE PHOTOBIOREACTOR

by

Aaron Outhwaite

Submitted in partial fulfilment of the requirements
for the degree of Master of Applied Sciences

at

Dalhousie University
Halifax, Nova Scotia
August 2015

Table of Contents

List of Tables v
List of Figures vi
Abstract x
List of Abbreviations Used xi
Acknowledgements xii
Chapter 1 Introduction 1
1.1 Characterization of a Building-Integrated Microalgae Photobioreactor 5
Chapter 2 BIMP Design Fundamentals 7
2.1 Introduction 7
2.2 BIMP Design Characterization 8
2.3 Growth Limiting Factors 16
2.3.1 Light 16
2.3.2 Temperature 19
2.3.3 Nutrients 21
2.3.4 Carbon 24
2.4 Discussion 26
Chapter 3 BIMP Modeling Fundamentals 28
3.1 Introduction 28
3.2 System Description 29
3.3 BIMP System Growth Modeling 30
3.3.1 Continuous Photobioreactor 31
3.3.2 Fed-batch Photobioreactor 34
3.4 Growth Rate Expressions 35
3.4.1 Monod Growth Rate 35
3.4.2 Haldane Growth Rate 37
3.4.3 Maximum Growth Rate 39
3.4.4 Multiplicative Growth Rate 40
3.5 BIMP Light Dynamics 43
3.5.2 Light-Dependent Growth Rate 49

3.6 BIMP Temperature Dynamics 51
3.6.1 Temperature-Dependent Growth Rate 56
3.7 BIMP Nutrient Dynamics 56
3.7.1 Rainwater 58
3.7.2 Human Urine 60
3.7.3 Nutrient-Dependent Growth rate 61
3.8 BIMP CO_2 Dynamics 62
3.8.1 Biological Phase 63
3.8.2 Gas Phase 63
3.8.3 Liquid Phase 66
3.8.4 CO_2-Dependent Growth Rate 68
3.9 Discussion 68
Chapter 4 Modeling Light Dynamics in a BIMP System 70
4.1 Introduction 70
4.2 System Description 70
4.3 Mathematical Model 71
4.3.1 Solar model 72
4.3.2 Biological model 72
4.4 Results 73
4.5 Sensitivity Analysis 76
4.6 Discussion 76
Chapter 5 Modeling Temperature Dynamics in a BIMP System 79
5.1 Introduction 79
5.2 System Description 79
5.3 Mathematical Model 81
5.3.1 Temperature model 81
5.3.2 Biological model 83
5.4 Results 83
5.5 Sensitivity Analysis 86
5.6 Discussion 86

Chapter 6 Conclusions 88
References 93
Appendix A Equilibrium Equations for BIMP Nutrient System 104
Appendix B MATLAB Code 107
B.1 Monod 107
B.2 Haldane 109
B.3 Light Main 110
B.4 Solar Function 112
B.5 Light-Temperature Main 114
B.6 Temperature function 116

List of Tables

Table 2.1: Design Features for Outdoor Microalgae PBR Systems (adapted Ugwu et al., 2008). 9

Table 2.2: Classification of Different Wastewater Effluent in Terms of Total Kjeldahl Nitrogen (TKN) and Total Phosphorus (TP) (adapted from Cai et al., 2013; Christenson and Sims, 2011). 23

Table 3.1: Reported Maximum Specific Growth Rate μ_{max} (h^{-1}) Values for PBR Systems Growing the Microalgae Species *C. vulgaris*. 40

Table 3.2: Composition of Fresh Human Urine (FMU) and Stored Human Urine (SHU) (adapted from Udert et al., 2003a). 60

Table 4.1: Meteorological Data for Halifax Nova Scotia Canada (adapted from Green Power Labs, 2009; Duffie and Beckman, 2006). 72

Table 4.2: Summary of BIMP Light Model Parameters for Microalgae Species *C. vulgaris*. 73

Table 4.3: Final BIMP Biomass Concentrations After seven-day Growth Simulation for the Four Equinox Months When Starting from a Concentration of 1 g L^{-1} Microalgae Biomass in the System. 75

Table 5.1: Outdoor Temperature Statistics and Double Cosine Model Calibration Data for Halifax Nova Scotia Canada (Environment Canada, 2015; Chow and Levermore, 2007). 81

Table 5.2: Summary of BIMP Heat Transfer Model Parameters. 82

Table 5.3: Summary of BIMP Temperature Model Parameters for Microalgae Species *C. vulgaris*. 83

Table 5.4: Final BIMP Biomass Concentrations after Seven-Day Growth Simulation for the Four Equinox Months When Starting from a Concentration of 1 g L^{-1} Microalgae Biomass in the System. 85

Table A.1: Equilibrium Reactions for BIMP Nutrient System 106

List of Figures

Fig. 1.1. The ecological footprint of the 29 largest cities in the Baltic region of Europe, showing ecosystem appropriation for city resource production (left), and ecosystem appropriation for city waste assimilation (adapted from Folke et al., 1997). 2

Fig. 1.2. Ecological Life Support System Concept. 4

Fig. 2.1. Examples of outdoor microalgae PBR systems, including (A) open pond (B) flat- plate (C) horizontal tubular (D) vertical column. 8

Fig. 2.2. BBS process flow diagrams for BIMP integration within the built environment. External environmental factors include (1) Sunlight (2) Outdoor temperature, and (3) Precipitation. Habitation dynamics include (4) Source separated urine (5) Low quality indoor air, and (6) Indoor Temperature. BBS dynamics include the generation and discharge of (7) Vermicompost (8) Municipal solid waste, and (9) Greywater, and requires the input of (10) External foodstuffs. BBS influent streams to the BIMP include (11) Nutrients (12) CO_2, and (13) Electricity, while BIMP output to the BBS for recovery include (14) High quality indoor air, (15) Heat, and (16) Microalgae effluent. 11

Fig. 2.3. Schematic diagram of BIMP system within a theoretical BBS construct. 12

Fig. 2.4. Schematic diagram of metabolism requirements within a theoretical BBS construct. 13

Fig. 2.5. Schematic diagram of food production system within theoretical BBS construct. 14

Fig. 2.6. Schematic diagram of water usage within theoretical BBS construct. 15

Fig. 2.7. Schematic diagram of energy recovery within theoretical BBS construct. 16

Fig. 2.8. Microalgae growth rate as a function of light intensity and culture depth in flat-plate PBR. I_c light compensation point; I_s light saturation intensity; I_h light intensity value for photoinhibition onset; μ_{max} maximum microalgal growth rate; μ_d microalgae loss rate (adapted from Grobbelaar, 2010; Ogbonna and Tanaka, 2000). 18

Fig. 2.9. Variation of optimal light intensity I_{opt} with culture temperature T_w for freshwater microalgae species *C. vulgaris* (adapted from Dauta et al., 1990). 20

Fig. 2.10. Variation of maximum microalgal growth rate μ_{max} with culture temperature T_w for freshwater microalgae species *C. vulgaris* (adapted from Dauta et al., 1990). 21

Fig. 2.11. Biomass concentration (closed symbols) and urea consumption of *C. vulgaris* for different initial urea concentrations (open symbols) (●,○) 0.100 g L^{-1}; (■,□) 0.200 g L^{-1} (adapted from Hsieh and Wu, 2009). 23

Fig. 2.12. Comparison of the aqueous CO_2 fixation ability of 25 microalgal species during batch growth (adapted from Ho et al., 2011). 26

Fig. 3.1. Fundamental BIMP design schematic showing light and temperature factors. 30

Fig. 3.2. Schematic diagram for continuous PBR (c-PBR) operation during time t. 31

Fig. 3.3. Growth dynamics of algae biomass X_a (solid line) in a b-PBR based on the availability of a growth limiting substrate S_i (dash line) over 7 days, or $t = 168$ hours, for $X_a(t = 0) = 1$ g L^{-1}; $S_i(t = 0) = 3$ g^{-1}; $\mu_{max} = 0.05$ h^{-1}; $\mu_d = 0.01$ h^{-1}; $Y_{x/s,i} = 1$ g X_a g^{-1} S_i; and $K_{s,i} = 0.5$ g L^{-1}. Variable parameterization based on an idealization of literature values to show trend. 36

Fig. 3.4. Growth dynamics of algae biomass X_a (solid line) in a b-PBR based on the availability of sunlight over 7 days, or $t = 168$ hours, for $X_a(t = 0) = 1$ g L^{-1}; $\mu_{max} = 0.05$ h^{-1}; $\mu_d = 0.01$ h^{-1}; and $K_s = 100$ μmol m^{-2} s^{-1}. Sunlight described using a 12:12 daily light-dark cycle, with $S = 200$ μmol m^{-2} s^{-1} for light hours, and $S = 0$ μmol m^{-2} s^{-1} for dark hours. Variable parameterization based on an idealization of literature values to show trend. 37

Fig. 3.5 Comparison of BIMP growth rate μ with increasing substrate concentration S_i as described using Monod kinetics (solid line) and Haldane kinetics (dash line), for $\mu_{max} = 0.05$ h^{-1}; $K_{s,i} = 0.5$ g L^{-1}; and $K_{i,i} = 0.5$ g L^{-1}. Variable parameterization based on an idealization of literature values to show trend 39

Fig. 3.6. Multiplicative growth rate dynamics of algae biomass X_a (solid line) within a b-PBR based on the availability of co-limiting substrates S_1 and S_2 (dashed line) over 7 days, or $t = 168$ hours. For biomass growth $X_{a,1}$ on substrate S_1 (●,○ respectively), $X_{a,1}(t = 0) = 1$ g L^{-1}; $S_1(t = 0) = 3$ g^{-1}; $\mu_{max} = 0.05$ h^{-1}; $\mu_d = 0.01$ h^{-1}; $Y_{x/s,1} = 1$ g $X_{a,1}$ g^{-1} S_1; and $K_{s,1} = 0.5$ g L^{-1}. For biomass growth $X_{a,2}$ on substrate S_2 (■,□ respectively), $X_{a,2}(t = 0) = 0.5$ g L^{-1}; $S_2(t = 0) = 1.5$ g^{-1}; $\mu_{max} = 0.05$ h^{-1}; $\mu_d = 0.01$ h^{-1}; $Y_{x/s,2} = 0.5$ g $X_{a,2}$ g^{-1} S_2; and $K_{s,2} = 0.25$ g L^{-1}. Variable parameterization based on an idealization of literature values to show trend. 42

Fig. 4.1. Schematic for light interaction in BIMP system. 71

Fig. 4.2. A comparison between published Green Power Labs (2009) data (dashed line) and calculated (solid line) data for the monthly average daily full-spectrum solar radiation on a vertical surface facing due South in Halifax Nova Scotia Canada. 74

Fig. 4.3. MATLAB simulation of BIMP biomass growth dynamics over seven days as characterized by Monod (solid line) and Haldane (dashed line) kinetic expressions, for spatially-averaged culture PPFD in Halifax Nova Scotia Canada. (A) March (B) June (C) September (D) December. Parameterization based on values given in Table 4.1 for solar model, and Table 4.2 for biological models. 75

Fig. 4.4. Tornado plot showing the sensitivity of BIMP light-growth model inputs when varied by ± 20% of their nominal value. Hatch bar indicates change in parameter value of -20%. Solid bar indicates change in parameter value of +20%. 76

Fig. 5.1 Schematic for temperature interaction in BIMP system 80

Fig. 5.2. MATLAB simulation of daily variation in outdoor temperature (dashed line) and the resultant BIMP culture temperature (solid line) for the four equinox months in Halifax Nova Scotia Canada. (A) March (B) June (C) September (D) December. Parameterization based on values given in Table 5.2. 84

Fig. 5.3. MATLAB simulation of BIMP biomass growth dynamics over 7 days as characterized by Monod (solid line) kinetics for light, and multiplicative (dashed line) kinetic for light-temperature, in Halifax NS Canada. (A) March (B) June (C) September (D) December. Parameterization based on values given in Table 4.1 for solar model, and Tables 5.1 and 5.2 for temperature model, and Tables 4.2 and 5.3 for light and temperature biological models, respectively.
and Tables 5.1 and 5.2 for temperature model, and Tables 4.2 and 5.3 for light and temperature biological models, respectively 85

Abstract

This thesis uses an adaptive design methodology for the characterization of a building integrated microalgae photobioreactor (BIMP) system. As an integrated building component that mediates between the indoor and outdoor environments, the BIMP system is novel in that no similar applications of microalgal photobioreactor (PBR) technology are reported in the literature. As such, a preliminary analysis is needed of the BIMP system before prototyping, to understand performance issues, and to improve the fitness of the BIMP design itself. Here, the adaptive design methodology utilizes a literature review to describe the key principles and growth limiting factors in PBR systems, with a focus on light and temperature dynamics. This general analysis is followed by the specific analysis of each of light and temperature dynamics within the BIMP system, using mathematical modeling and simulation. These analyses are evaluated, and used in summary to suggest methods for improving the BIMP design.

List of Abbreviations Used

BBS	Biological Building System
BIMP	Building Integrated Microalgae Photobioreactor
b-PBR	Batch Photobioreactor
c-PBR	Continuous Photobioreactor
C	Carbon
CELSS	Closed Ecological Life Support System
CO_2	Carbon Dioxide
CSTR	Continuously-Stirred Tank Reactor
MATLAB	MATrix LABoratory
MCHP	Micro-Combined Heating and Power
N	Nitrogen
NASA	National Aeronautics and Space Administration
ODE	Ordinary Differential Equation
P	Phosphorus
PAR	Photosynthetically Active Radiation
PBR	Photobioreactor
PPFD	Photosynthetically Active Photon Flux Density
TKN	Total Kjeldahl Nitrogen
TP	Total Phosphorus
UN	United Nations

Acknowledgements

It is with sincere appreciation that I thank my supervisory team of Dr. Stephen Kuzak and Dr. Mark Gibson. Their expertise, perceptiveness, and patience gave foundation to my ideas, and the opportunity to define them. I would also like to thank Dr. Susanne Craig for her insight and provocation, and for asking the tough questions that help solidify the theoretical underpinnings of my work.

I would like to thank my parents, whose unconditional support and generosity has not only been invaluable to my thesis work, but also in making me the person I am today. My extended family has also been incredibly supportive of my work, and I thank them as well.

Finally, and most importantly, I thank my wife Elizabeth Powell. She has been, and continues to be, my inspiration.

Chapter 1 Introduction

A problem faced by cities globally is that buildings consume resources and generate wastes, which impacts both the environment and health. However, re-designing buildings so they behave as ecological machines, and bioregenerate their wastes, may be a solution to this problem.

How buildings affect their biophysical environment is of great importance, not only for the sustainability of the city, but also for the health and well-being of their occupants. The study of cities as metabolic systems involves the quantification of the inputs, outputs and storage of energy, water, nutrients, materials and wastes for an urban region (Kennedy et al., 2010). As a primary mediator between humans and their biophysical environments, buildings are a microcosm of urban metabolism theory, wherein raw materials, energy and water are converted to human biomass and wastes (Decker et al., 2000). By consuming these resources and generating waste streams, the construction and operation of buildings account for the greatest burden on natural resources of all the economic sectors (Kibert et al., 2000).

The impact that buildings have on their environment extends beyond the confines of the city, impacting the biophysical makeup of a much larger area. For instance, Folke et al. (1997) suggest that the 29 largest cities in the Baltic Sea drainage basin cover a total area of 2,216 km^2, but require open land that is approximately 200 times larger to supply the resources they require. Even more alarming is the fact that these same authors suggest that the amount of open land required to assimilate the nitrogen (N), phosphorus (P), and carbon dioxide (CO_2) generated as waste in these 29 cities is at least 400 – 1000 times larger than the size of the cities themselves.

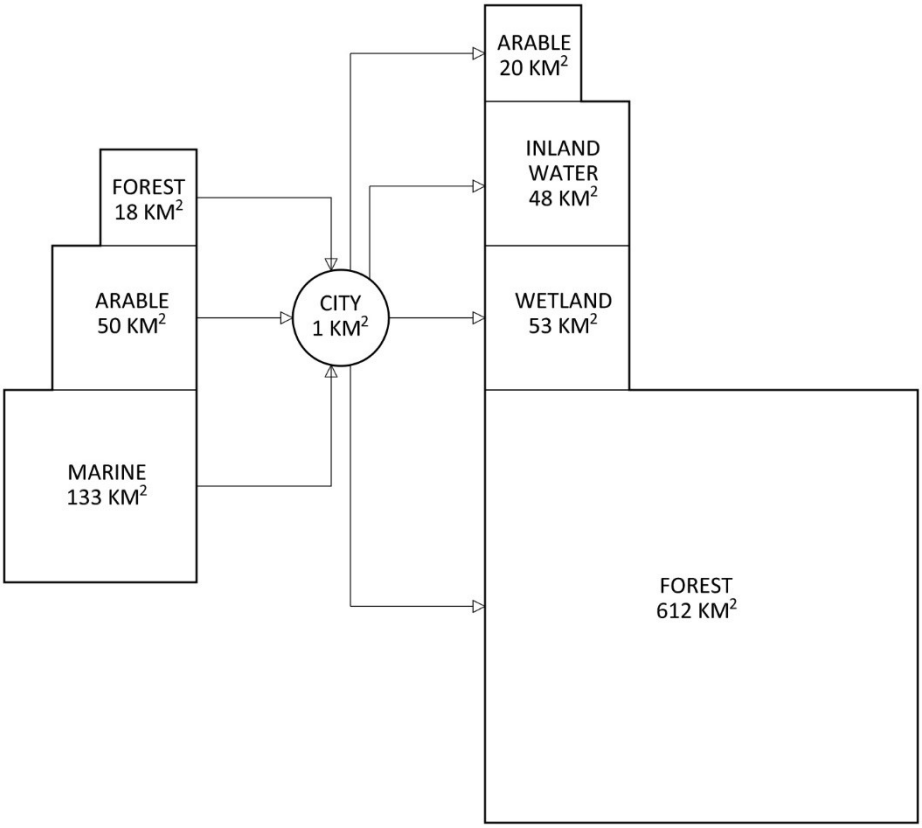

Fig. 1.1. The ecological footprint of the 29 largest cities in the Baltic region of Europe, showing ecosystem appropriation for city resource production (left), and ecosystem appropriation for city waste assimilation (adapted from Folke et al., 1997).

Contemporary urban design and infrastructure are failing to account for the drastic increase in city population expected before 2050. According to a UN report (Heilig, 2012), between 2011 and 2050, the world population is expected to increase by 2.3 billion, moving from 6.8 billion to 9.1 billion. During this same time interval, the population living in urban areas is projected to increase by 2.9 billion to a total of 6.3 billion, meaning that urban areas will house at least 70% of the world population by 2050. In North America – an already highly urbanized society – cities are expected to house at least 90% of the population by 2050.

It is not anticipated that existing city drinking water resources will be able to manage an increase in demand of such a magnitude. Further, an increase in city population

will localize and increase atmospheric pollution such that the current health issues associated with urban smog will only become exacerbated. The same is true for how the vast amounts of garbage, and human liquid and solid waste generated by an urban population is treated and disposed of. Again, it is anticipated that our already strained waste management infrastructure will be able to cope with the additional waste volume related to an increased global population. To put it simply, the contemporary methods used to design and operate cities, and the buildings they contain, are not sustainable.

Instead, a paradigm shift is required; a shift away from building typologies that are inert, to those that are alive and form a productive part of the urban metabolism. The building itself needs to behave as would a natural ecosystem, using the free resources of sunlight and rainwater for the maintenance of living systems that can bioregenerate depleted urban resources such as wastewater and CO_2 without the need to rely on – or destroy – vast exurban ecosystems. And we have a model for these types of buildings available to us, namely the biologically-based, ecological life support systems developed for space exploration.

The study of a BIMP system is based on life support systems developed by NASA and the former Soviet Union for use during manned, non-orbital long-duration space flights. These missions – expected to last at least two years – could not be effectively supported from Earth, as any attempt to leave the atmosphere with the required stores would be both uneconomical and technically unfeasible. As a result, a fundamental outline of a new life support system was developed, entailing a regenerative environment that could support human life in space using agricultural means. The earliest successful controlled ecological life support systems (CELSS), described schematically in Fig. 1.2 utilized a microalgae photobioreactor (PBR) system that could (1) provide oxygen to an enclosed environment while at the same time consume CO_2 produced by occupant respiration, (2) regenerate wastewater through the biofixation of various mineral constituents, including N and P, and (3)

provide a continuous biomass food source for consumption (Nelson et al., 2009; Gitelson et al., 2003; Eckart, 1996).

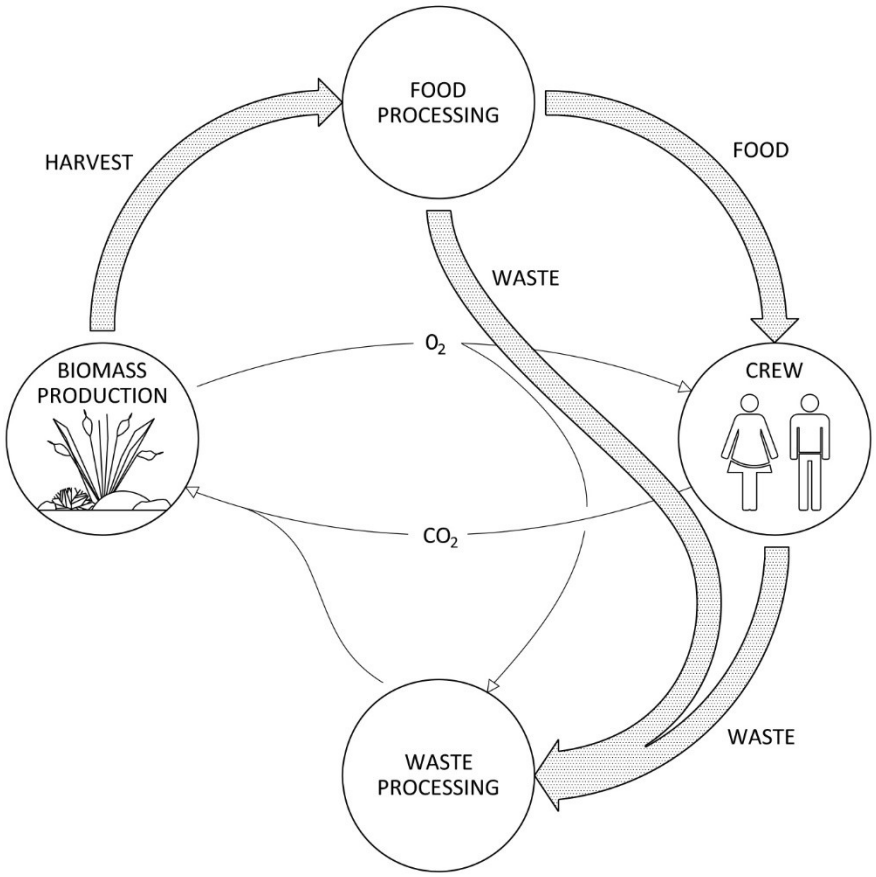

Fig. 1.2. Ecological Life Support System Concept.

Conceptually, a BIMP system is able to achieve the same results as the CELSS systems here described. However, unlike the CELSS system, the design of a BIMP system must account for both the indoor and outdoor environments. As such, the purpose of this thesis is to characterize these environmental conditions, and to determine their effect on the development of a BIMP prototype system.

1.1 Characterization of a Building-Integrated Microalgae Photobioreactor

This thesis investigates the potential utilization of a building integrated microalgae photobioreactor (BIMP) system. To convert building generated wastewater and CO_2 into useable resources, rather than discharge wastes streams into the environment. As a preliminary step toward the development of a BIMP prototype, an adaptive methodology is used to describe how sunlight and temperature affect the growth of microalgae within the BIMP system. This involves the mathematical modeling and simulation of these key factors, with a focus on improving the robustness of the BIMP design.

Therefore, this thesis uses an adaptive design methodology for the development of a BIMP system. An adaptive methodology attempts to remove uncertainly and improve robustness by increasing the understanding of a design system before it is built as a prototype. For the BIMP system, this means developing mathematical models to describe those factors considered most likely to directly affect how a prototype might be developed. Characterizing the BIMP system in such a manner will be achieved in the following chapters, here summarized briefly.

In Chapter 2, the fundamental design requirements for a BIMP system are described, including those factors that limit the growth of the microalgae within the system. These factors are inclusive of both the 'geographic' and the 'built' and include the access to sunlight, the culture temperature, as well as the availability of the nutrient resources of wastewater, and CO_2.

In Chapter 3, the basic methods for the characterization of the BIMP system through mathematical modeling and dynamic simulation are presented. Included in this chapter are the kinetic methods for describing growth limitation and inhibition, for single or co-limited microalgae cultures in a BIMP system, based specifically on

diurnal and seasonal dynamics for a particular geographic location, and on the built environment within which it is placed.

Chapter 4 describes the dynamics of growth in the BIMP system based on the incident solar radiation resource in Halifax Nova Scotia Canada. The mathematical modeling and simulation of the biological dynamics within the BIMP system are presented.

Chapter 5 describes the dynamics of growth within the BIMP system based on both the indoor and outdoor environments in Halifax. Modeling and simulation in this chapter follow a methodology similar to that in Chapter 4, with the addition of the multiplicative dynamics described in Chapter 3.

Chapter 6 summarizes the findings in Chapter 5 and 6, and several conclusions about the design of the BIMP system are made.

Chapter 2 BIMP Design Fundamentals

2.1 Introduction

As a novel biological building system (BBS), the BIMP system is akin to – but distinct from – contemporary microalgae PBR technology. This chapter introduces the design concepts used to manifest PBR systems, with a focus on how these principles affect the development of the BIMP system.

The utilization of microalgal biomass grown in PBR systems has received considerable attention in the literature, most notably in the production of biofuels (Wiley et al., 2011; Mata et al., 2009; Chisti, 2007), as well as various other chemical and food products (Borowitzka, 2013; Harun et al., 2012; Pulz and Gross, 2004). In an effort to improve process efficiencies and reduce operating costs, microalgae PBR systems have been studied empirically as part of a biorefinery concept. In these studies, natural and waste resources such as sunlight and wastewater effluent are utilized as part of the microalgal photosynthetic growth dynamic (Shurin et al., 2013; Razzak et al., 2013; Sortana and Landis, 2011). In a similar effort, microalgae PBR have been used within CELSS for the bioregeneration of the by-products of habitation, including wastewater and CO_2, for reuse within the enclosure (Ganzer and Messerschmid, 2009; Gitelson et al., 2002; Eckart, 1996).

In open systems such as a biorefinery, PBR dynamics and design are dependent on the outdoor environment, as well as on the availability of the abiotic resources such as nutrients and CO_2 needed for microalgae growth. Conversely, for closed systems such as CELSS, PBR dynamics are dependent on the indoor environment, which produces these same abiotic resources. For the BIMP system, an adaptive design approach requires the careful consideration of both the indoor and outdoor environmental factors considered most likely to affect the development of a

prototype. The purpose of this chapter is to therefore introduce these environmental factors using a literature review.

2.2 BIMP Design Characterization

In general, outdoor microalgae culturing systems that utilize solar energy are designed to have a large illuminated surface area (Ugwu et al., 2008). Common outdoor PBR of this type include open pond, horizontal tubular, vertical column, and flat-plate systems, all of which have been reviewed extensively by other authors (Wang et al., 2012; Carvalho et al., 2006; Tredici, 2004). An example for each of these types of outdoor microalgae PBR systems is shown in Fig. 2.1.

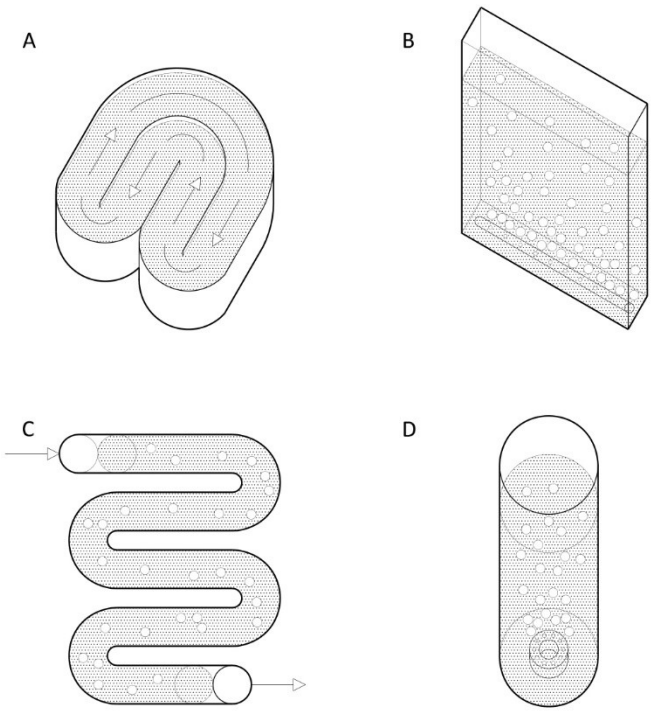

Fig. 2.1. Examples of outdoor microalgae PBR systems, including (A) open pond (B) flat- plate (C) horizontal tubular (D) vertical column.

As an integrated system in the built environment, the BIMP is designed to mediate between the indoor and outdoor environments in the form of a façade element similar

to a window. This makes the flat-plate type PBR the most obvious choice as the design basis for the BIMP system. Additionally, to avoid obstructions from environmental factors such as snow and rainwater accumulation, the BIMP system is vertically-oriented. This will have an impact on the mathematical modeling of solar radiation, which is described in detail in Chapter 3. The key design features for each photobioreactor type are presented in Table 2.1.

Table 2.1: Design Features for Outdoor Microalgae PBR Systems (adapted Ugwu et al., 2008).

Culture systems	Prospects	Limitations
Open ponds	High illuminated surface area Moderate cost; Easy to clean after cultivation;	High land requirements; Low productivity; Low long term culture stability; Limited control of growth conditions; Limited to few microalgae strains; Easily contaminated
Horizontal tubular	High illuminated surface area; Moderate productivity	High gradation for pH, O_2, CO_2 along tube length; High land requirements; High cost
Vertical column	High mass transfer; High mixing with low shear stress; Moderate productivity; Moderate scalability; Easy to sterilize	High cost; Low illuminated surface area; Limited light path with increased scale
Flat-plate	High illuminated surface area; High productivity; High mass transfer; High mixing with low shear stress; Moderate cost; Easy to sterilize	Moderate scaling issues; Moderate temperature control issues;

Flat-plate PBR are cuboids in form, with a large transparent surface facing the illumination source, and a short light path distance from that illumination source through the reactor. Usually flat-plate panel PBR are placed vertically or inclined facing the sun, though this is not always the case (Cuaresma et al., 2011). The large

illumination surface and short light path characterize the flat-plate PBR as having a high surface to volume ratio, which has the advantage of affording good light distribution accessibility within the microalgae culture medium. However, in outdoor flat-plate PBR, the solar gain afforded by the large surface area has the additional effect of causing temperature changes in the culture medium, which must be controlled to maintain optimal growth conditions (Richmond and Cheng-Wu, 2001). Nutrients for microalgal metabolism are provided based on the operational mode of the reactor; continuously for CSTR-type operation, and in sufficient density to support sustained growth dynamics in batch- or fed-batch-type operation (Yamane, 1994). Because of the short light path and limited internal volume, agitation and mixing in a flat-plate PBR is most often provided by mechanically sparging, thereby creating gas-liquid dynamics similar to those found in vertical column type airlift and bubble-column PBR (Chisti, 1989). This type of mixing has the added benefit of acting as the delivery mechanism for aqueous CO_2, a requirement for photosynthesis.

Describing the BIMP as a pseudo flat-plate PBR, and placing it within the façade means that it has both an indoor and outdoor surface, and is therefore subject to the specific environmental conditions at each of those locale. This is a non-trivial dilemma, for while outdoor environmental conditions can readily be described, the indoor environment requires a more thorough consideration. Here, a BBS concept has been developed for the purposes of rationalizing the waste/resource dynamics as are associated with habitation. These dynamics are described in Fig. 2.2.

The BBS concept described in Fig. 2.2 is not resolved in its entirety in this thesis, but is instead used to orient the characterization of the BIMP system. Explicitly then, and in summary, the geographic climate describes the amount of solar radiation incident on the exterior BIMP vertical surface, as well as the outdoor surface temperature. The indoor surface temperature, as well as the availability of the wastewater nutrients and CO_2 that are utilized for microalgae growth, are both characterized by the indoor environment of the building in which the BIMP system is placed. Therefore, the four

factors here considered to limit growth in the BIMP system are light, temperature, nutrients and CO_2, each of which is described in detail in the following section.

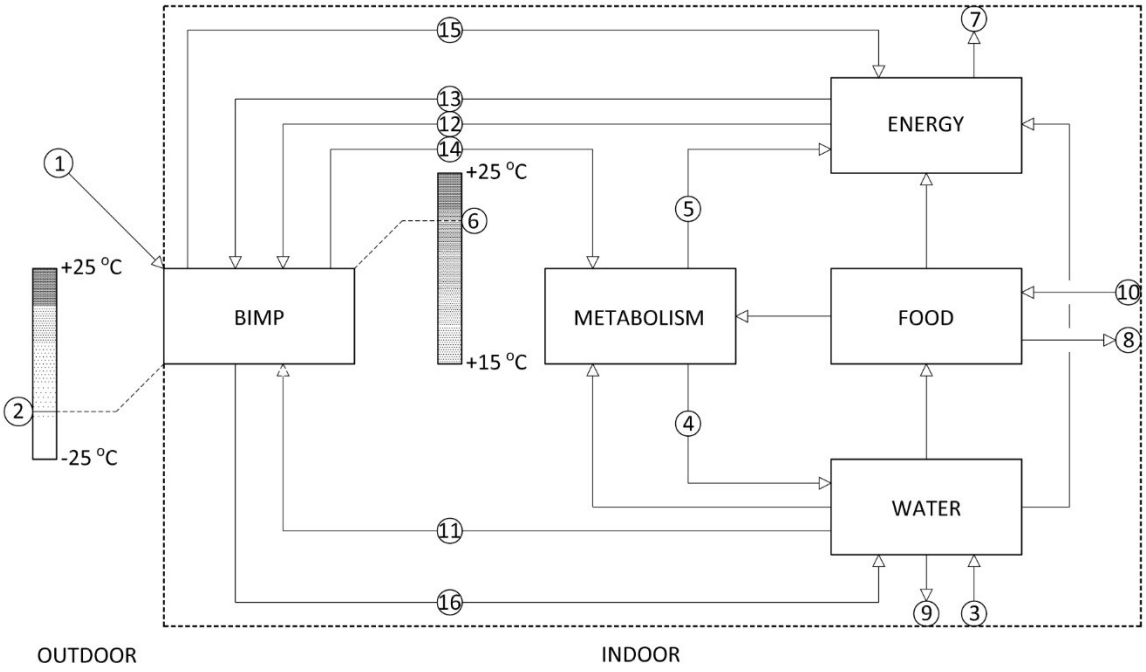

Fig. 2.2. BBS process flow diagrams for BIMP integration within the built environment. External environmental factors include (1) Sunlight (2) Outdoor temperature, and (3) Precipitation. Habitation dynamics include (4) Source separated urine (5) Low quality indoor air, and (6) Indoor Temperature. BBS dynamics include the generation and discharge of (7) Vermicompost (8) Municipal solid waste, and (9) Greywater, and requires the input of (10) External foodstuffs. BBS influent streams to the BIMP include (11) Nutrients (12) CO_2, and (13) Electricity, while BIMP output to the BBS for recovery include (14) High quality indoor air, (15) Heat, and (16) Microalgae effluent.

Each of the five individual BBS subsystems shown in Fig. 2.2 are expanded, and described in Fig. 2.3-2.7.

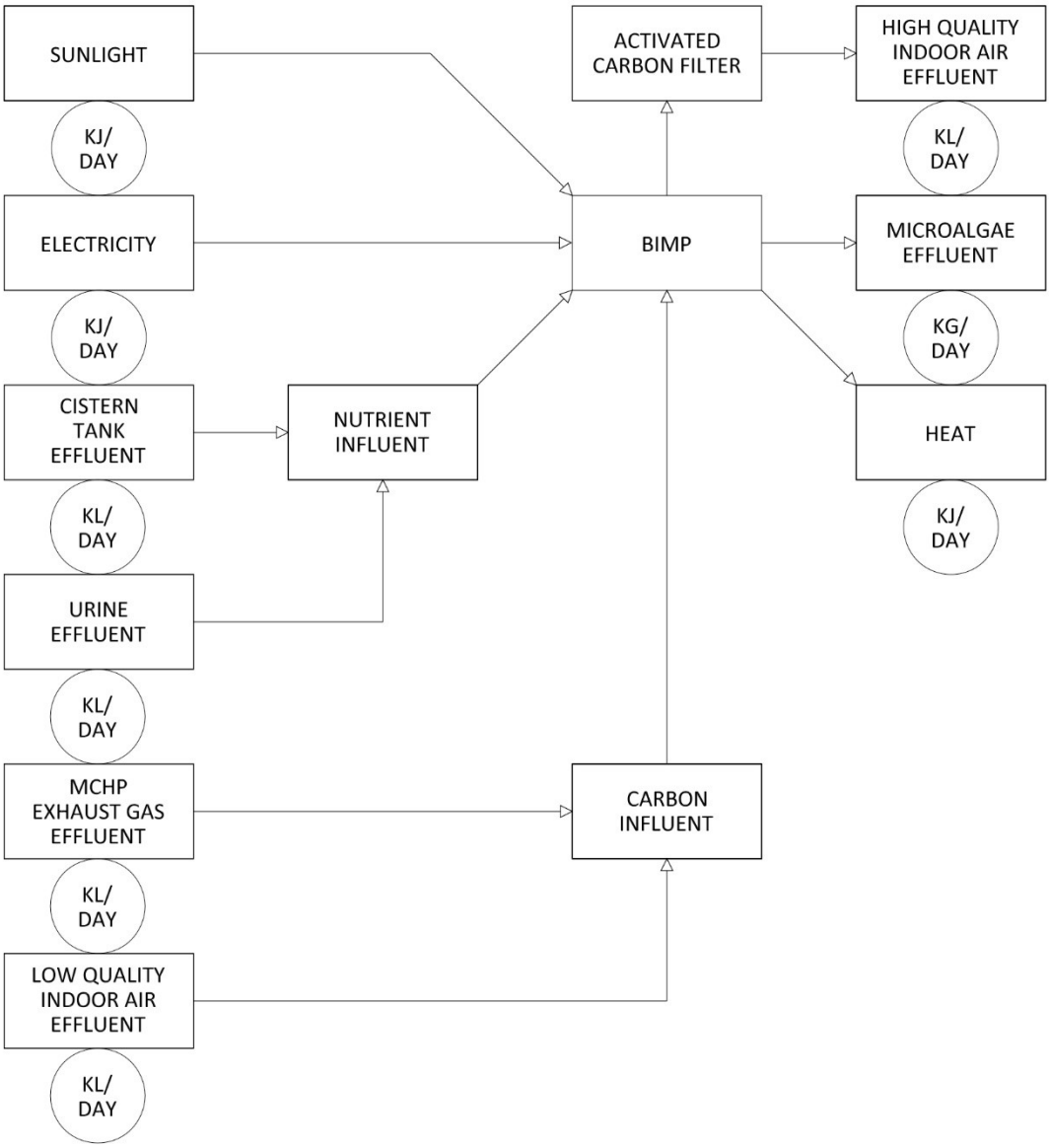

Fig. 2.3. Schematic diagram of BIMP system within a theoretical BBS construct.

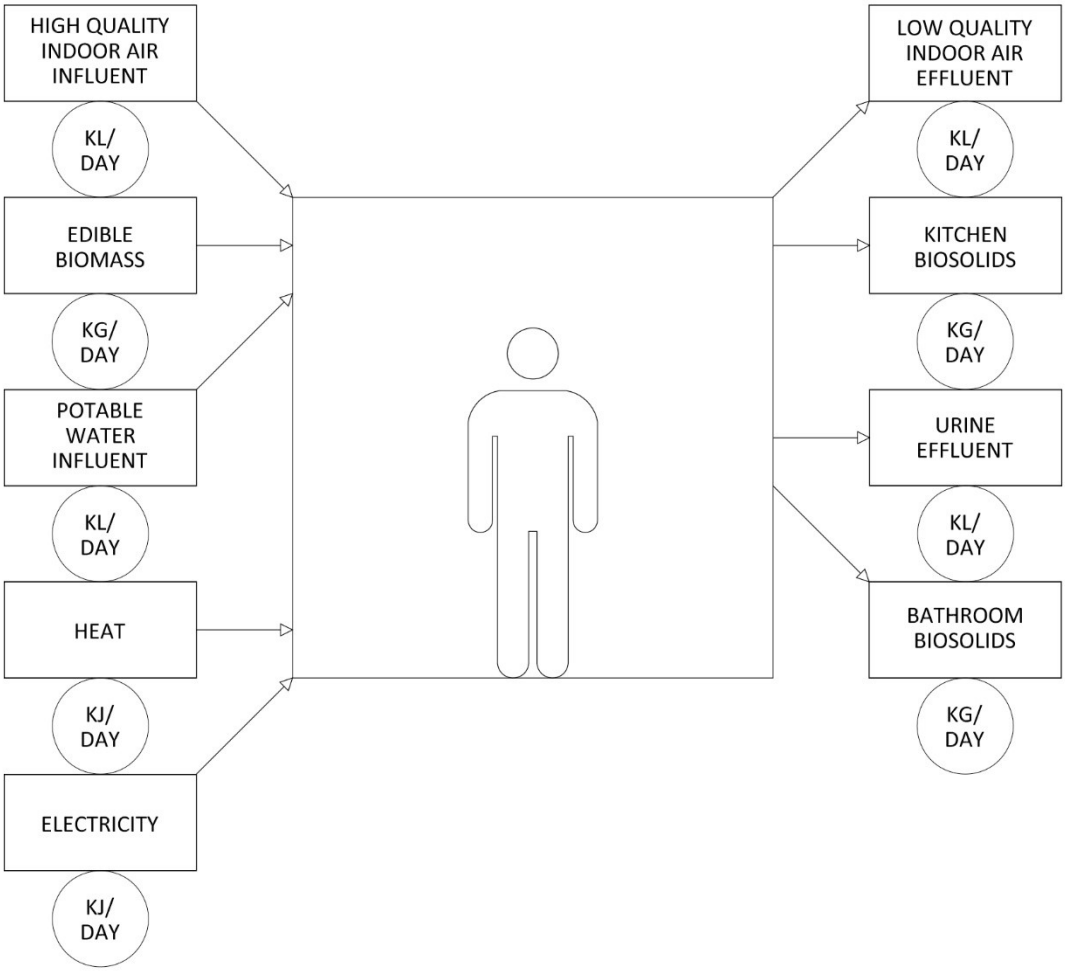

Fig. 2.4. Schematic diagram of metabolism requirements within a theoretical BBS construct.

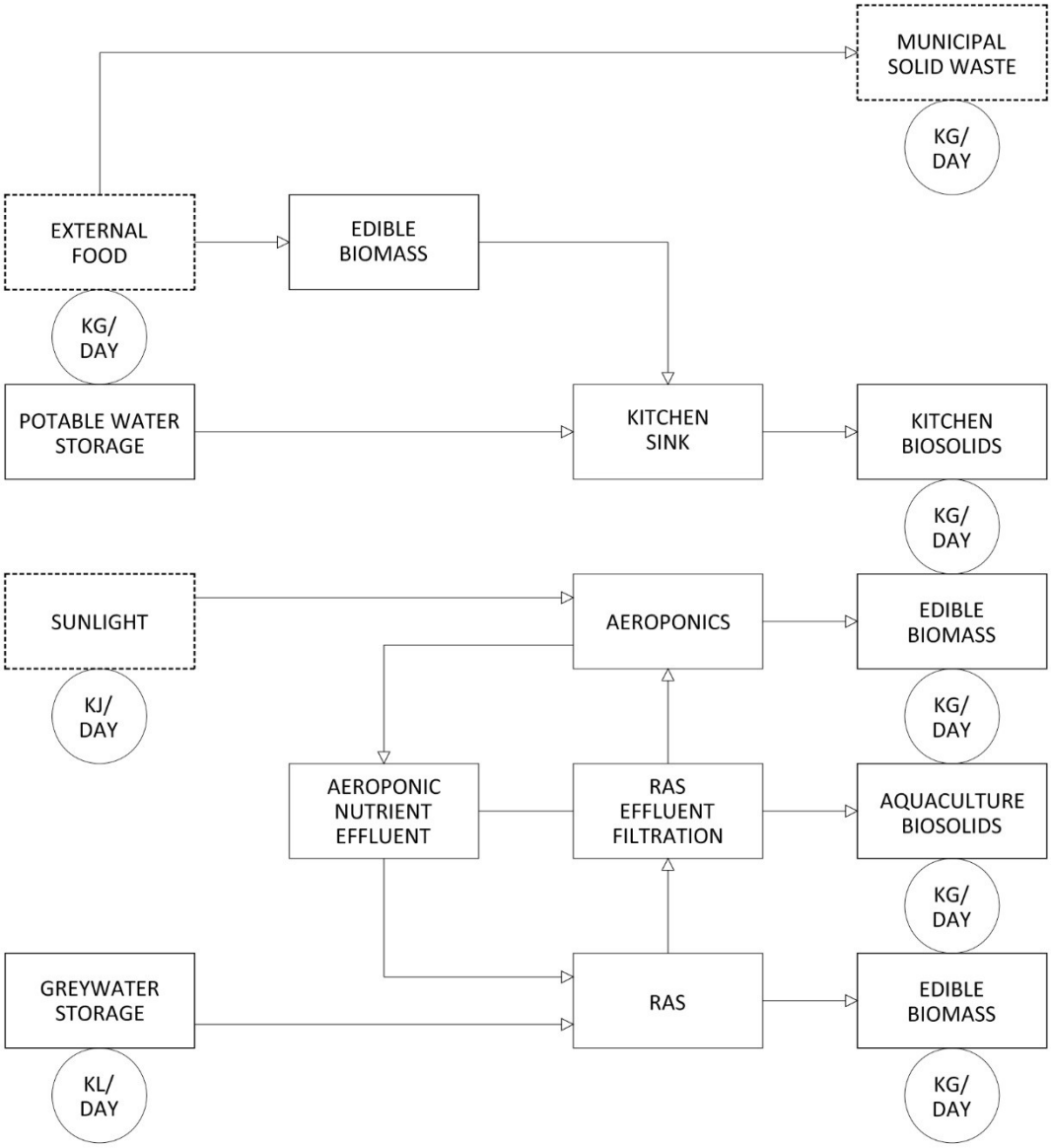

Fig. 2.5. Schematic diagram of food production system within theoretical BBS construct.

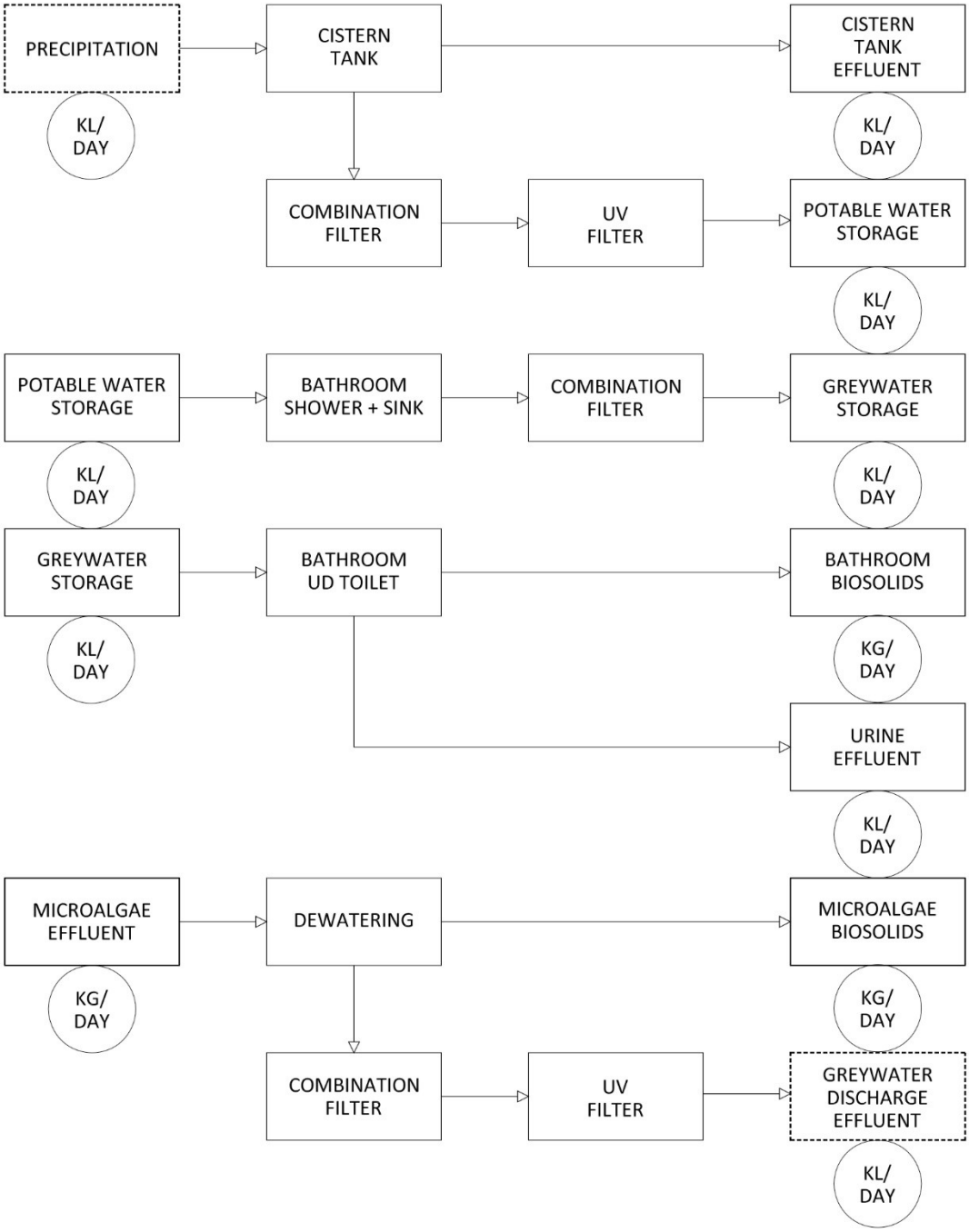

Fig. 2.6. Schematic diagram of water usage within theoretical BBS construct.

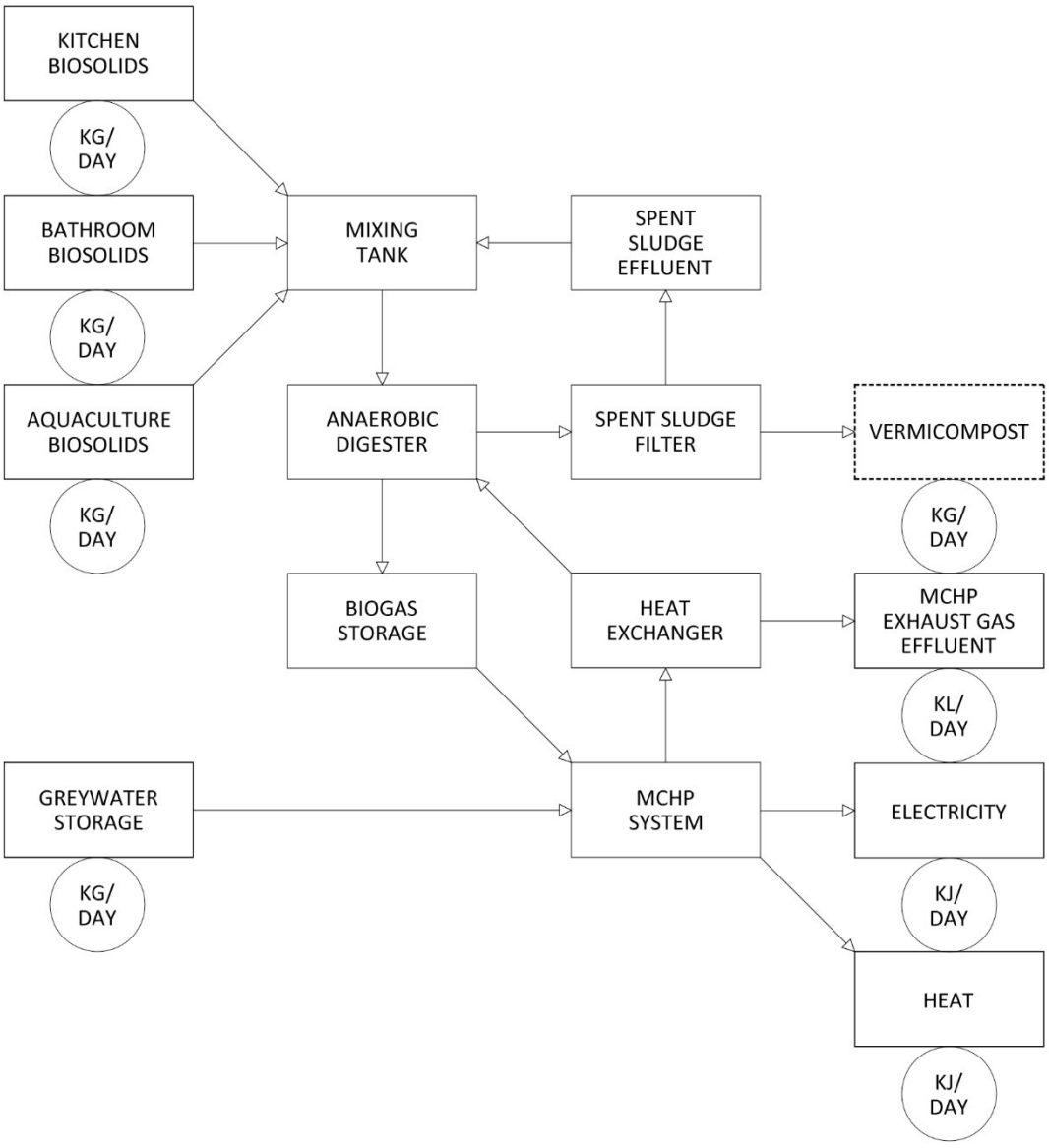

Fig. 2.7. Schematic diagram of energy recovery within theoretical BBS construct.

2.3 Growth Limiting Factors

2.3.1 Light

The amount of light that can be utilized for photosynthesis is the critical factor in determining the overall performance and bioregenerative capacity of a BIMP system. Light is electromagnetic radiation that has a wavelength between 10 and 10^6 nm, of

which the visible spectrum is between about 380–750 nm (Carvalho et al., 2011). The radiation that is usable in photosynthesis is called photosynthetically active radiation (PAR), and its wavelength range corresponds to the visible spectrum, or about 400–700 nm. Of the total solar resource that is incident on the surface of the Earth, only about 45.8% is PAR (Weyer et al., 2010). The general reaction for photosynthesis is given in Eq. 2.1 and it describes the conversion of inorganic compounds and PAR to organic matter and oxygen by autotrophs such as microalgae (Osborne and Geider, 1987).

$$CO_2 + H_2O + photons \rightarrow (CH_2O)_n + O_2 \qquad 2.1$$

It is useful here to distinguish between the different methods of reporting light energy. Often sunlight is described as a radiant flux energy, or irradiance, measured in units of power per area per time such as J m^{-2} s^{-1} (Kalogirou, 2009). However, in microalgae PBR research, irradiance is typically expressed as PAR photon flux density (PPFD), measured in units of quanta per area per time, or μmol quanta m^{-2} s^{-1}, or more conveniently, μmol m^{-2} s^{-1} (Carvalho et al., 2011). The mathematical derivation for the conversion of PAR radiant flux to PPFD is provided in Chapter 3, for the determination of the maximum theoretical BIMP photosynthetic yield. However, it is noted here that an approximate conversion factor for sunlight is 1 J m^{-2} s^{-1} PAR radiant flux equals 4.5 μmol m^{-2} s^{-1} PPFD (Masojidek et al., 2004).

In addition to the quality of light here described, the quantity of PAR incident on the exterior BIMP vertical surface is very important in determining growth dynamics. Consider that on a sunny day in equatorial regions the average solar radiation that reaches the surface of the Earth is approximately 1000 J m^{-2} s^{-1} at noon (Kalogirou, 2009). Of this, approximately 450 J m^{-2} s^{-1} is PAR radiant flux, or approximately 2000 μmol m^{-2} s^{-1} PPFD. However, the growth of microalgae is optimum at PPFD of about 200 μmol m^{-2} s^{-1}, or about $1/10^{th}$ the daily average (Kumar et al., 2011). Any exposure of the microalgae photosynthetic unit to light intensities above the saturation PPFD can impair the photosynthetic complex, resulting in decreased growth rates, cell

damage, and culture mortality (Richmond, 2004). Further, as light passes through the depth of the microalgae culture, its intensity is attenuated, meaning that a light source that is above saturation intensity at the culture surface may in fact become optimal after attenuating at some culture depth d. The response of microalgae growth to the quantity of light, or light intensity, is described in Fig. 2.8.

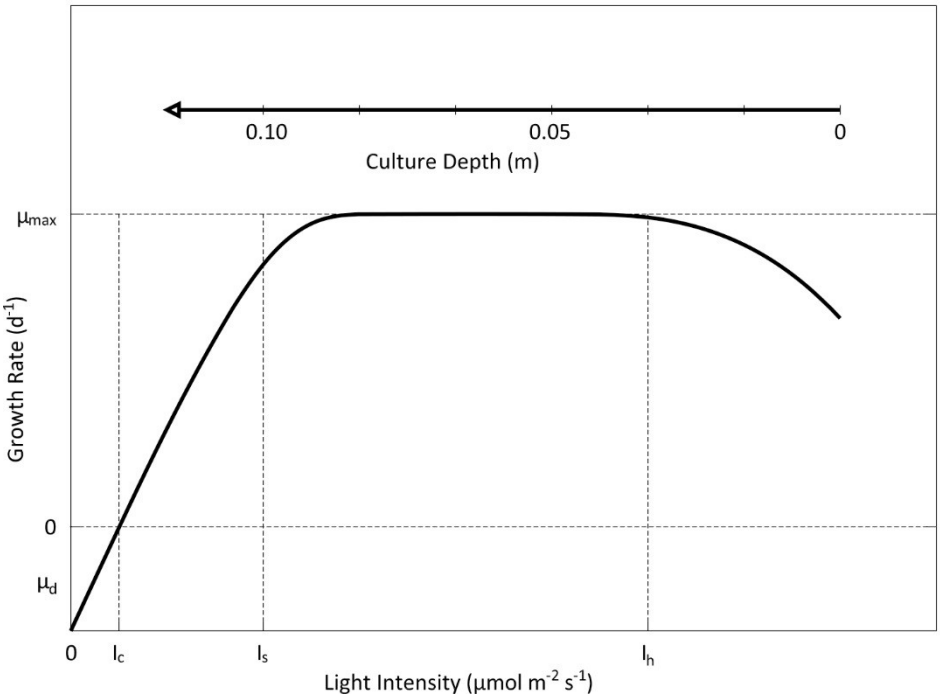

Fig. 2.8. Microalgae growth rate as a function of light intensity and culture depth in flat-plate PBR. I_c light compensation point; I_s light saturation intensity; I_h light intensity value for photoinhibition onset; μ_{max} maximum microalgal growth rate; μ_d microalgae loss rate (adapted from Grobbelaar, 2010; Ogbonna and Tanaka, 2000).

For unidirectional incident sunlight, at a culture depth d from the illuminated surface, the light compensation intensity I_c is the light level at which the microalgal growth rate is equally balanced by microalgal mortality, resulting in a net biomass accumulation of zero. As the culture depth is decreased toward the illuminated surface, more light is available for photosynthesis, and the microalgal growth rate is accelerated. Eventually, the culture depth is sufficiently shallow such that the light saturation intensity I_s is reached, and the microalgal growth rate is at its maximum. Any increase in the light intensity past the saturation value does not increase the

microalgal growth rate, and in fact, at a certain inhibition light intensity I_h, the microalgal growth rate can be seen to decline as a result of cell damage and radiation induced mortality.

In practice, for outdoor microalgae systems such as the BIMP, high microalgal growth rates can be achieved if the saturation light intensity I_s can be maintained throughout the culture by maintaining a short light path d and/or reducing the exposure time of microalgae cells to the high illuminated surface light intensities through mixing. Light availability and control is therefore the most significant factor in the adaptive design methodology for the development of a BIMP prototype. Therefore, the subject of Chapter 4 is the modeling of light dynamics in a BIMP.

2.3.2 Temperature

Microalgae grown in an outdoor PBR can only utilize the solar radiation that is photosynthetically active, and then only a fraction of the PPFD itself absorbed by the microalgae. That portion of the PPFD not absorbed is either dissipated as heat within the PBR culture medium or reflected back into the outdoor environment (Richmond, 2004). Additionally, outdoor PBR are subject not only to the PPFD, but also to the rest of the solar spectrum, including infrared and ultraviolet radiation (Masojidek et al., 2004), which can also cause temperature fluctuations within the PBR culture medium.

There is a strong correlation between light and temperature for a number of microalgae species (Sorokin and Krauss, 1962). These authors demonstrated that an increase in culture temperature caused an increase in the optimal light intensity I_{opt} for photosynthesis, as described in Fig. 2.9. Conversely, it has been shown that at low light levels, high culture temperature causes a drastic decrease in photosynthetic efficiency (Richmond, 2004). Irrespective of light, most microalgae species grown in

PBR require a culture temperature between 20 – 30 ^{o}C for optimal growth (Chisti, 2007), as is described in Fig. 2.10.

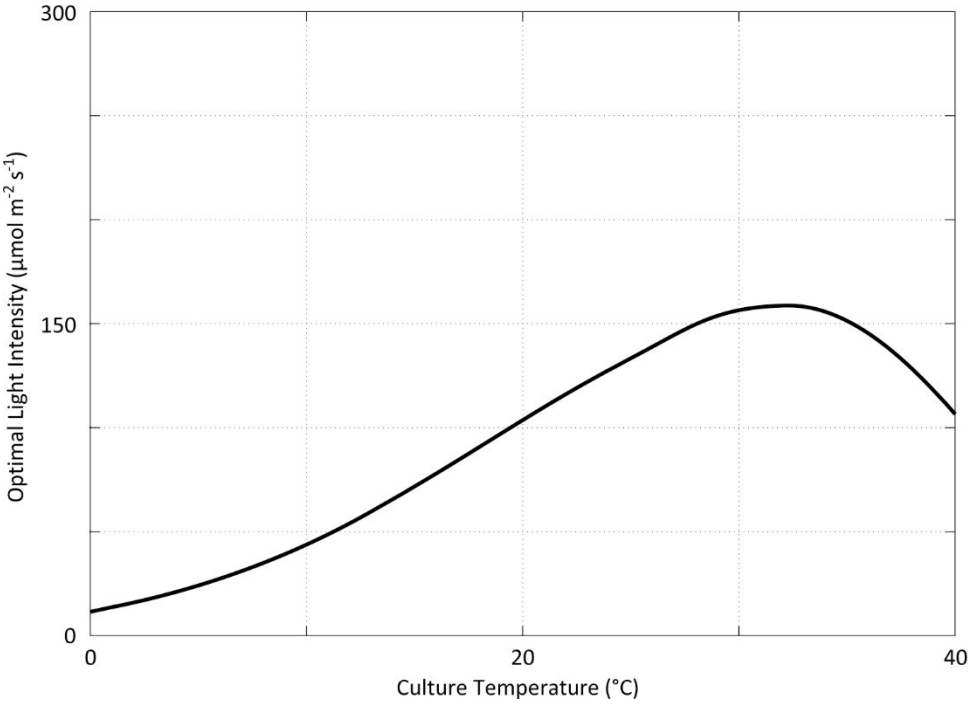

Fig. 2.9. Variation of optimal light intensity I_{opt} with culture temperature T_w for freshwater microalgae species *C. vulgaris* (adapted from Dauta et al., 1990).

However, controlling the culture temperature of outdoor PBR can be a challenging prospect. Both the amount of incident solar radiation and the outdoor ambient temperature vary based on diurnal and seasonal cycles, causing dynamic changes in outdoor PBR culture temperatures. Most often culture temperature in outdoor PBR is controlled using mechanical operations such as water cooling jackets (Miron et al., 2002), submersion in a temperature-controlled pool (Carlozzi and Sacchi, 2001), or water-spray techniques (Richmond and Cheng-Wu, 2001).

For a BIMP system, culture temperature and control will depend not only on the outdoor solar and temperature dynamics, but also on the indoor ambient room temperature. In an adaptive design methodology, temperature control is considered

a significant factor that may change the BIMP prototype design, and as such modeling the temperature dynamics in the BIMP system is the subject of Chapter 5.

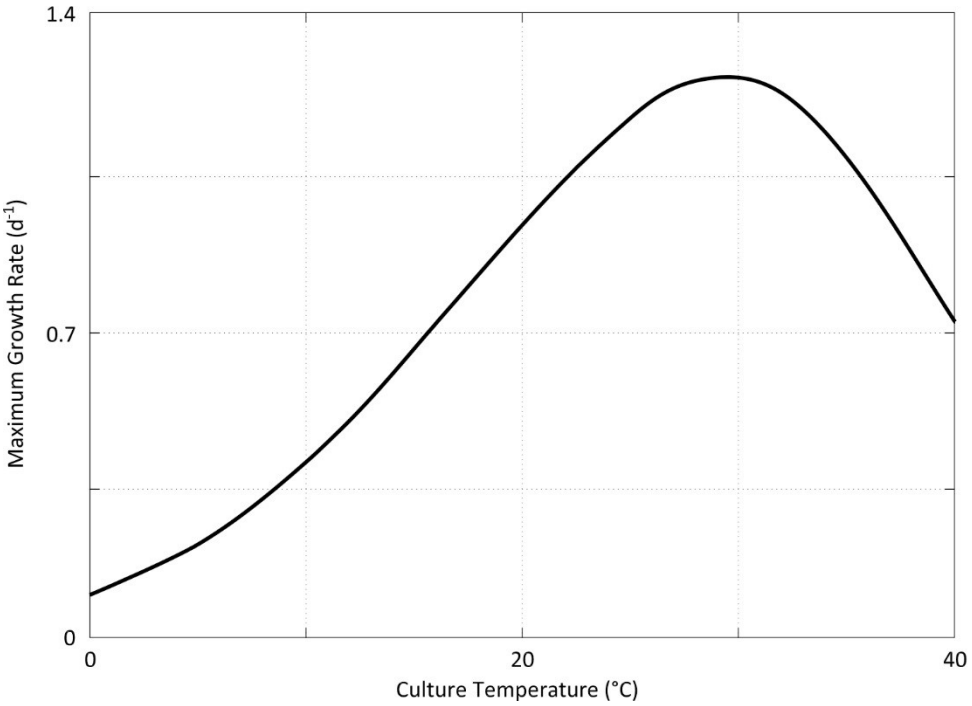

Fig. 2.10. Variation of maximum microalgal growth rate μ_{max} with culture temperature T_w for freshwater microalgae species *C. vulgaris* (adapted from Dauta et al., 1990).

2.3.3 Nutrients

The three most important nutrients for microalgae growth are carbon (C), N, and P, and their sustainable supply to any PBR is pivotal for optimizing growth conditions in an economical way (Grobbelaar, 2004). Note here that the availability of aqueous C for use in the photosynthetic process will be discussed in detail in the following section. Additional requirements include the macronutrients sulfur, calcium, magnesium, sodium, potassium, and chlorine, and in trace quantities the micronutrients iron, boron, manganese, copper, molybdenum, vanadium, cobalt, nickel, silicon, and selenium (Suh and Lee, 2003). These nutritional requirements have traditionally been provided using a purpose-built synthetic substrate, such as

BG11, Modified Allen's, and Bold's Basal media types (Sharma et al., 2011; Grobbelaar, 2004; Mandalam and Palsson, 1998). However, owing to the high costs of these industrial fertilizers, recycling wastewater as a nutrient resource for microalgae in PBR has proven to be an attractive alternative (Cai et al., 2013; Christenson and Sims, 2011; Wang et al., 2010). For instance, according to Christenson and Sims (2011), municipal wastewater can be used to support microalgae growth in PBR without growth rate limitation or supplementation with other nutrient sources, as the wastewater itself contains sufficient quantities of N, P, and micronutrients. Taking it one step further, Wang et al. (2010) suggest that not only is growth not limited by municipal wastewater nutrients, but in fact microalgae the microalgae species *C. Vulgaris* can remove N, P, and chemical oxygen demand (COD) with such efficiency that PBR technology is a viable alternative to activated sludge processes as a secondary or tertiary wastewater treatment step. These results are supported by Fig. 2.11, which describes the near complete removal of urea – the nitrogen constituent in human urine – by *C. vulgaris* within a retention time of 6 days.

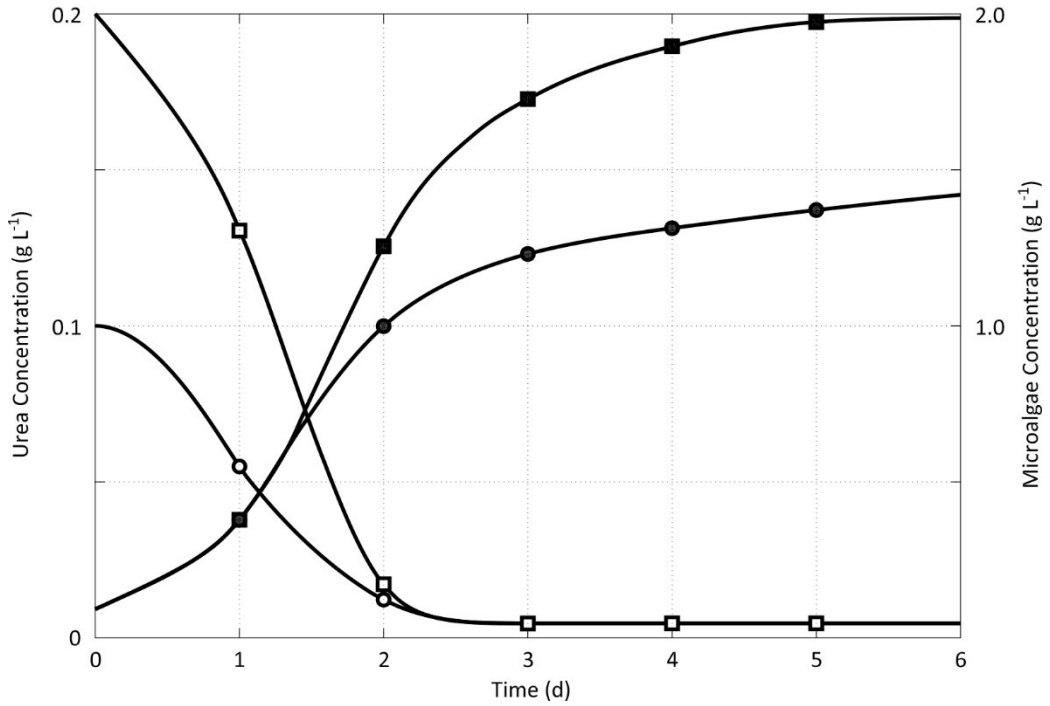

Fig. 2.11. Biomass concentration (closed symbols) and urea consumption of *C. vulgaris* for different initial urea concentrations (open symbols) (●,○) 0.100 g L^{-1}; (■,□) 0.200 g L^{-1} (adapted from Hsieh and Wu, 2009).

Table 2.2: Classification of Different Wastewater Effluent in Terms of Total Kjeldahl Nitrogen (TKN) and Total Phosphorus (TP) (adapted from Cai et al., 2013; Christenson and Sims, 2011).

Wastewater category	Description	TKN (mg L^{-1})[a]	TP (mg L^{-1})
Municipal wastewater	Weak domestic	20	4
	Medium domestic	40	8
	Strong domestic	85	15
Animal wastewater	Dairy	185	30
	Poultry	802	50
	Swine	895	168
Industrial wastewater	Textile	90	18
	Winery	110	52
	Distillery	2700	680
Anaerobic digestion effluent	Dairy manure	125	18
	Sewage sludge	427	134
	Food waste and sewage sludge	1640	296

[a] Total Kjeldahl nitrogen (NH_3+ NH_4^+)

As described in Table 2.2, there are several candidate wastewater streams that have ample N and P for use as a nutrient influent for a microalgae PBR. In practice, the utilization of building wastewater for the BIMP system would require careful monitoring and control such that harmful chemicals such as paints, solvents, and discarded pharmaceuticals would not be introduced to the system. Fouling by bacteria, mould, and other microalgae species potentially found in a stored building urine-rainwater system could also be a concern, as they would introduce a competition regime for nutrient resources in the BIMP system.

As reported by several authors, most notably Tuantet et al (2014a, b), the generation and availability of a wastewater nutrient resource within the built environment is sufficient to consider this factor as non-limiting within the BIMP system. For the purposes of predictive analysis on the BIMP prototype once built, a preliminary mathematical model describing nutrient dynamics has been include in Chapter 3.

2.3.4 Carbon

As stated in the previous section, C is one of the major macronutrients required for optimal growth of microalgae in a PBR. Microalgae growth dynamics include photoautotrophic, heterotrophic, and mixotrophic scenarios wherein either inorganic C, organic C, or a mixture of both are utilized, respectively (Yen et al., 2014). For photoautotrophic growth, such trees growing in sunlight, this means utilizing the abundant atmospheric resource of inorganic C – CO_2 – for photosynthesis. However, in contrast to terrestrial plants, microalgae grown in PBR require higher CO_2 concentrations than those found in typical outdoor environments to sustain their growth (Grobbelaar, 2004). As described in Fig. 2.7, even when intense mixing of the culture is provided, natural diffusion of CO_2 from the atmosphere, which has a concentration of approximately 400 ppm, or 400 mg L^{-1} (Tans, 2015), into the culture medium is too slow to replace the aqueous CO_2 assimilated by the microalgae in a PBR.

As such, PBR are often C limited (Riebesell et al., 1993), and additional CO_2 must be provided reliably and economically to ensure satisfactory growth dynamics. As such, microalgae PBR have been studied in depth for their ability to biofixate CO_2 from a variety of traditional emission sources, including most notably post-combustion flue gas used for municipal energy generation (Gonzalez-Lopez et al., 2012; Douskova et al., 2009; Kurano et al., 1995).

As part of the urban environment, the BIMP system can support the reduction of CO_2 at the building scale by utilizing the post-combustion CO_2 resulting from distributed micro combined heating and power (MCHP) generation systems, which are already themselves a low CO_2 option (Labis et al., 2011). Of additional relevance to the BIMP system is the use of microalgae PBR as part of bioregenerative life support systems (BLSS) for the regeneration of indoor CO_2 resulting from habitation (Li et al., 2013), and how these studies apply to the bioregeneration of indoor air within the built environment. As with nutrients, the availability of CO_2 within the built environment is considered non-limiting for the BIMP system, and as such, these considerations are left for the predictive analysis of the BIMP prototype once built. A preliminary mathematical model to this end is provided in Chapter 3.

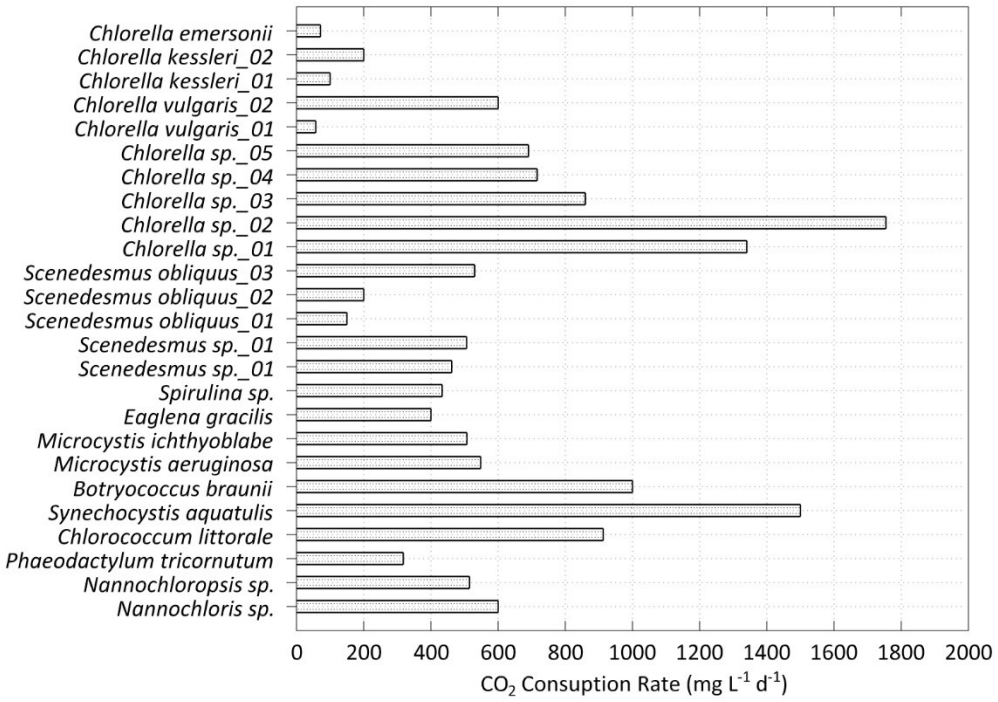

Fig. 2.12. Comparison of the aqueous CO_2 fixation ability of 25 microalgal species during batch growth (adapted from Ho et al., 2011).

2.4 Discussion

The BIMP system, as a flat-plate-type PBR integrated in the built environment, has four principle growth-limiting factors. The first of these factors is the availability of light for photosynthesis, which is a factor determined by the specific outdoor environment within which the BIMP system is placed. Light may limit microalgae growth by either being in a supply insufficient to support photosynthesis optimally, or in excess supply so as to damage the photosynthetic mechanism in the microalgae cell. The BIMP culture temperature is a limiting factor dependent on both the outdoor environment and the indoor environment, as the BIMP system is designed to mediate between the two. The culture temperature can limit growth by reducing the optimal light intensity for photosynthesis, as well as limiting the maximum growth rate. Within the adaptive design methodology used in this thesis, both light and temperature are considered factors that can change the mechanistic character of the

BIMP prototype design. As such, the mathematical modeling and analysis of these factors will be a primary consideration in the forthcoming chapters.

Nutrient limitation is based on the availability of a urine-rainwater mixture, as generated within the indoor environment. Here growth limitation can occur if the nutrient mixture is generated in insufficient quantities to maintain the algae culture in the BIMP without the need for supplemental fertilizers. Finally, C limitation is based on the availability of CO_2 gas, as generated within the indoor environment through an energy based process such as a MCHP generation system, or the metabolic process of breathing and exhausting CO_2 to the indoor atmosphere. The supply of both nutrients and CO_2 from the built environment is not deterministic in the adaptive methodology employed in this thesis in that these factors do not change how the prototype system is designed. Both nutrient and CO_2 availability in the built environment is considered sufficient to not limit growth, and the mechanistic supply of these resources is dependent on the design of subsystems to the BIMP, and not the BIMP itself. These factors are therefore not included in the analysis presented in this thesis, save the modeling efforts that are presented in Chapter 3 toward a predictive methodology in future works.

Chapter 3 BIMP Modeling Fundamentals

3.1 Introduction

This chapter presents the fundamental modeling and simulation methods required to characterize a building-integrated microalgae photobioreactor (BIMP) system. For novel applications such as a BIMP, dynamic mathematical modeling can be an invaluable prerequisite for empirical studies, when predicting process performance and optimizing operating conditions and design. The modeling of growth in a PBR is based on efforts to model oceanic phytoplankton growth dynamics using a chemostat analogy (Huisman et al., 2002; Frost and Franzen, 1992; Picket, 1975). The chemostat is theoretically akin to a CSTR, and as such, early ocean-based phytoplankton growth models have been optimized for microalgae PBR using process dynamics and control methods developed for microorganism growth in bioreactors (Bequette, 1998; Asenjo and Merchuk, 1995; Panikov, 1995).

Because PBR are designed to maximize the production of microalgae, PBR modeling has most often been used to understand and optimize the optical properties and intensity of light within the culture medium used for photosynthesis (Zonneveld, 1998; Evers, 1991; Aiba, 1982). Other abiotic factors such as culture temperature (Ras et al., 2003; Goldman and Carpenter, 1974; Eppley, 1972), as well as the concentration and character of aqueous nutrients (Ruiz et al., 2013; O'Brian, 1974; Monod, 1949), and CO_2 (Laamanen et al., 2014; Talbot et al., 1991; Gavis and Ferguson, 1974) have also been modeled for the purposes optimizing and maximizing the growth of microalgae in a PBR. These factors can independently or multiplicatively limit microalgae growth within a PBR, and beyond single-limitation modeling studies, most often multiple growth limitation modeling focuses on the interaction between two of these factors (Bernard and Remond, 2012; Lacerda et al., 2011; Baquerisse et al., 1998).

As a bioregenerative device in the built environment, a BIMP system has four fundamental interacting growth limiting factors, including light, temperature, nutrients, and CO_2. However, only two of these factors, namely light and temperature, are considered as determinants in the mechanistic characterization of a BIMP prototype. The focus of this chapter is therefore on the development of a fundamental modeling method for studying these limiting factors for their specific and interacting effects on BIMP growth *in silico*, with a specific emphasis on coupling light and temperature dynamics.

3.2 System Description

As part of the BBS concept described in Chapter 2, the characterization of a BIMP system involves the analysis of several different influent an effluent streams, each of which is dependent on an additional subsystem. The BIMP defined for this thesis is a flat-plate-type PBR that is meant to act as the threshold – or façade – between the indoor and outdoor environments. The amount of sunlight impingent on the exterior surface of the BIMP system is a condition of the geographical location, as is the outdoor temperature. The indoor temperature is a condition of the specific building in which the BIMP system is situated, as are the availability of nutrients and CO_2. It is assumed that indoor light does not contribute a significant PPFD for photosynthesis in the BIMP system. This assumption is a result of considering where exactly the BIMP system would be placed within a building. For instance, as integrated within an open living space, PPFD from indoor lights used during night time would certainly be of a quantity worth considering in the light model presented in this chapter. However, if the BIMP system were to be placed within a bathroom space, as may be preferable for the proximity to the urine-rainwater storage, then PPFD from lights would be very limited. As the specific architectural space within which the BIMP system is to be integrated has yet to be defined, the influence of indoor PPFD on the BIMP light model must be neglected. Also, as briefly stated in the introduction, this chapter focuses on the coupling of light and temperature dynamics in the BIMP system. Therefore, the

modeling of both the nutrient and CO_2 dynamics within the BIMP system are introduced in this chapter, but not solved explicitly for the BIMP system. As a result of these assumptions and definitions, the fundamental BIMP design schematic showing the light and temperature considerations developed in this chapter and subsequently for the rest of this thesis are described in Fig. 3.1.

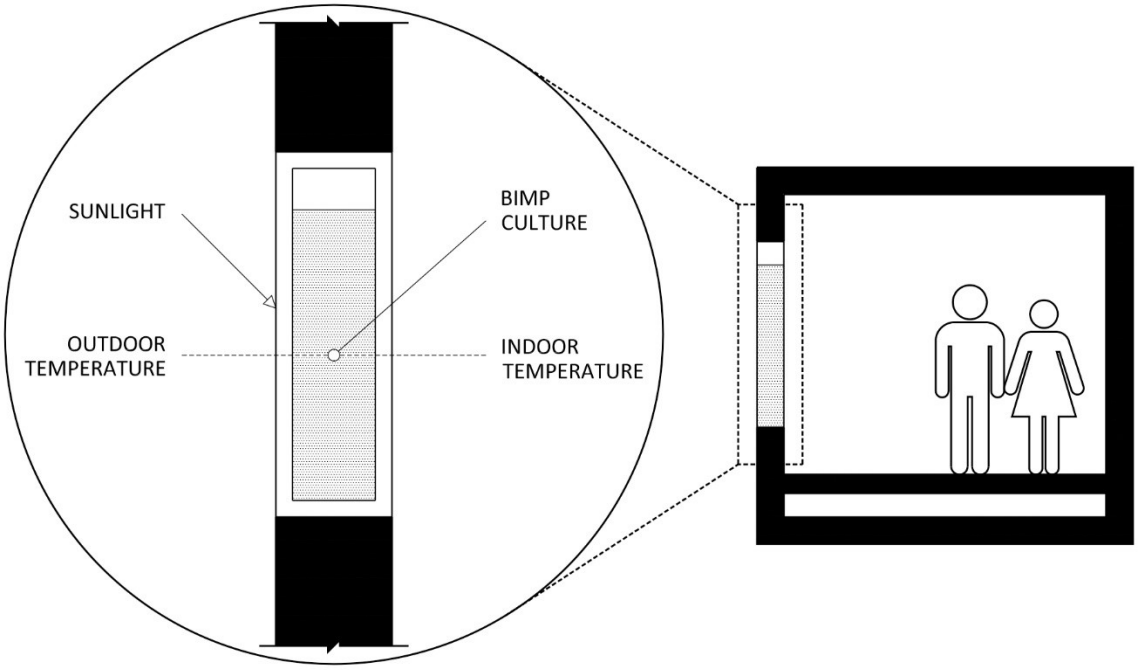

Fig. 3.1. Fundamental BIMP design schematic showing light and temperature factors.

These factors are the basis for the development of the mathematical model in the subsequent section.

3.3 BIMP System Growth Modeling

Consider a bioreactor system that utilizes a nutrient substrate to grow a microalgae product. The relationship between the quality and quantity of the substrate to the growth dynamic of the product has been extensively modeled in the literature (Dunn et al., 2003; Bequette, 1998; Bailey and Ollis, 1986). What makes PBR modeling efforts

unique to those used for bioreactors is the need to include light dynamics. As will be discussed further in Chapter 4, modeling the light dynamics in a PBR often involves treating light as a substrate akin to a liquid or gaseous influent stream. As such, this section presents an introduction to classic bioreactor modeling methods, with the additional consideration of light as a substrate.

It is assumed that the BIMP will operate as a fed-batch PBR. However, as stated in the introduction, classic PBR modeling efforts are based on an analogy with the chemostat, which are in essence CSTR reactors. As such, the following analysis first describes continuous PBR (c-PBR) dynamics, and then relates these to fed-batch PBR (b-PBR) dynamics. The MATLAB code used to simulate the modeling presented in this section is provided in Appendix E.

3.3.1 Continuous Photobioreactor

The continuous PBR (c-PBR) schematic used in the following analysis is described in in Fig. 3.2.

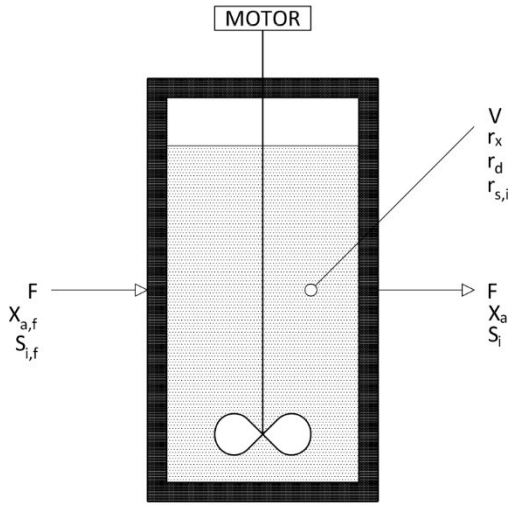

Fig. 3.2. Schematic diagram for continuous PBR (c-PBR) operation during time *t*.

It is assumed that the c-PBR is perfectly mixed and that the volume is constant, and thus $F_{in} = F_o = F$. The material balance on the microalgal biomass within the c-PBR can therefore be written as (Dunn et al., 2003):

algae accumulation = algae in + algae generation – algae out – algae death

or, expressed mathematically:

$$V \cdot \frac{dX_a}{dt} = F \cdot X_{a,f} + V \cdot r_x - F \cdot X_a - V \cdot r_d \qquad 3.1$$

Where X_a is the microalgal concentration in the c-PBR (mass cells volume^{-1}), $X_{a,f}$ is the microalgal concentration in the c-PBR feed stream, F is the volumetric flow rate to and from the c-PBR (volume time^{-1}), r_x is the rate of microalgal cell generation (mass cells volume^{-1} time^{-1}), r_d is the rate of microalgal cell death (mass cells volume^{-1} time^{-1}), and V is the c-PBR volume.

Similar to the material balance as described in Eq. 3.1 for microalgae biomass in the BIMP, a material balance on a substrate S_i utilized for growth in the c-PBR can be described as:

substrate accumulation = substrate in – substrate out – substrate consumption

or, mathematically as:

$$V \cdot \frac{dS_i}{dt} = F \cdot S_{i,f} - F \cdot S_i - V \cdot r_{s,i} \qquad 3.2$$

where S_i is the substrate concentration in the c-PBR (mass substrate volume^{-1}), $S_{i,f}$ is the substrate concentration in the c-PBR feed stream, and $r_{s,i}$ is the rate of substrate i consumption (mass substrate volume^{-1} time^{-1}).

By dividing through by V and by defining F/V as the dilution rate D, Eq. 3.1 and Eq. 3.2 become, respectively:

$$\frac{dX_a}{dt} = D \cdot X_{a,f} + r_x - D \cdot X_a - r_d \quad 3.3$$

$$\frac{dS_i}{dt} = D \cdot S_{i,f} - D \cdot S_i - r_{s,i} \quad 3.4$$

The rate of microalgal cell generation r_x in Eq. 3.3 is described in terms of a specific growth rate μ (time^{-1}) as (Bequette, 1998):

$$r_x = \mu \cdot X_a \quad 3.5$$

The rate of microalgal loss r_d through cell death, respiration, and other loss mechanisms r_d in Eq. 3.3 is described in terms the specific growth rate μ, the algal density X_a, and a dimensionless constant φ as (Bechet et al., 2013):

$$-r_d = -\varphi \cdot \mu \cdot X_a \quad 3.6$$

Often, Eq. 3.6 is expressed in terms of a specific loss rate μ_d (time^{-1}) (Concas et al., 2012) such that:

$$-r_d = -\mu_d \cdot X_a \quad 3.7$$

There exists a relationship between the rate at which cells grow and the rate that substrate concentration is reduced in the PBR as a result of this growth. This relationship is described using a yield coefficient, defined as the mass of cells produced per mass of substrate consumed (Bequette, 1998), or:

$$Y_{x/s,i} = \frac{r_x}{r_{s,i}} \quad 3.8$$

By substitution of Eq. 3.5 into Eq. 3.8, and through rearrangement, the rate of substrate consumed can be written as:

$$r_{s,i} = \frac{\mu \cdot X_a}{Y_{x/s,i}} \tag{3.9}$$

By substituting Eq. 3.5 and Eq. 3.9 into Eq. 3.3 and Eq. 3.4, respectively, and by assuming that there exists no biomass in the c-PBR feed stream ($X_{a,f}$ = 0), modeling equations for biomass growth and substrate consumption in the c-PBR are:

$$\frac{dX}{dt} = (\mu - \mu_d - D) \cdot X_a \tag{3.10}$$

$$\frac{dS_i}{dt} = D \cdot \left(S_{i,f} - S_i \right) - \frac{\mu \cdot X_a}{Y_{x/s,i}} \tag{3.11}$$

3.3.2 Fed-batch Photobioreactor

For fed-batch growth in a photobioreactor, there is no dilution rate, and thus Eq. 3.10 takes the form of the Malthusian model (Ratledge and Kristiansen 2006), or:

$$\frac{dX_a}{dt} = (\mu - \mu_d) \cdot X_a \tag{3.12}$$

while the change in substrate concentration S_i described by Eq. 3.11 becomes:

$$\frac{dS_i}{dt} = -\frac{\mu \cdot X_a}{Y_{x/s,i}} \tag{3.13}$$

These equations are here described as a means of introducing the BIMP system growth dynamics. As built, the BIMP system would rely on these kinetic expressions for the predictive modeling of performance, based on the utilization of both nutrients and CO_2 as substrates. When light is treated as a substrate, Eq. 3.12 remains valid for

the description of the microalgae growth rate, while Eq. 3.13 has no physical meaning. This position is defended in the next section.

3.4 Growth Rate Expressions

The specific growth rate μ described previously is not constant, but instead must vary based on the microalgae density X_a in the BIMP. Several mathematical expressions have been developed to relate $\mu = f(X_a, S_i)$ in the literature. Here, two of the most common methods for describing growth rate kinetics for PBR systems are described.

3.4.1 Monod Growth Rate

The Monod growth rate expression is a general kinetic model that is used to describe the relationship between the growth rate μ of a microorganism, and the availability, or concentration, of a growth limiting substrate S_i, or:

$$\mu = \mu_{max} \cdot \frac{S_i}{K_{s,i} + S_i} \tag{3.14}$$

where μ_{max} is the maximum growth rate of the microorganism under non-limiting conditions, and $K_{s,i}$ is the half-saturation constant, which describes the theoretical value of the substrate concentration S_i when μ/μ_{max} is equal to 0.5. Notice that the ratio $S_i/(K_{s,i} + S_i)$ is unitless and must be $0 \leq S_i/(K_{s,i} + S_i) \leq 1$, meaning that the specific growth rate μ is bound as $0 \leq \mu \leq \mu_{max}$, a consideration that is important in the forthcoming analyses.

Recall that a specific substrate S_i may be described as limiting within the BIMP system. Utilizing the Monod rate expression, and solving the coupled ordinary differential equations (ODE) given in Eq. 3.12 and Eq. 3.13 using MATLAB describes the dynamic growth of microalgae in a b-PBR based on single substrate limitation, as is shown in Fig. 3.3.

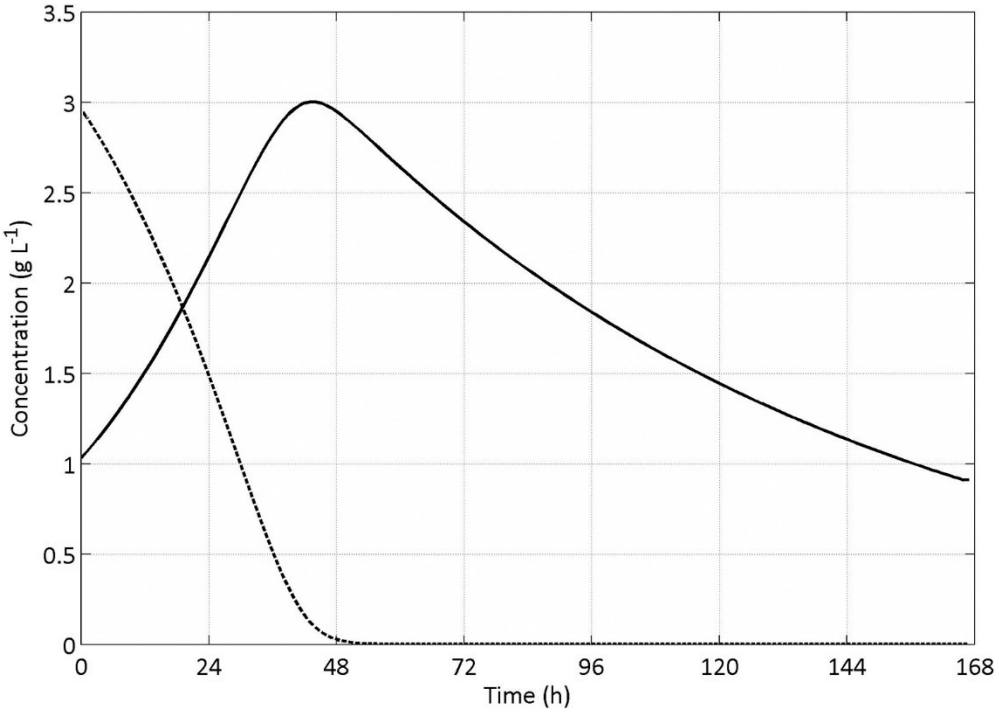

Fig. 3.3. Growth dynamics of algae biomass X_a (solid line) in a b-PBR based on the availability of a growth limiting substrate S_i (dash line) over 7 days, or $t = 168$ hours, for $X_a(t = 0) = 1$ g L^{-1}; $S_i(t = 0) = 3$ g^{-1}; $\mu_{max} = 0.05$ h^{-1}; $\mu_d = 0.01$ h^{-1}; $Y_{x/s,i} = 1$ g X_a g^{-1} S_i; and $K_{s,i} = 0.5$ g L^{-1}. Variable parameterization based on an idealization of literature values to show trend.

Based on b-PBR operating principles, only a fixed – and limiting – amount of substrate S_i is available for growth over the duration of the growth cycle. When the substrate is exhausted, the growth expression given in Eq. 3.12 becomes governed by the specific loss rate term μ_d, and therefore the microalgae density X_a in the b-PBR declines as shown in Fig. 3.3. When sunlight is considered a limiting substrate S_i in a p-PBR, these limitation conditions are no longer fixed, but instead vary with the diurnal cycle. The dynamics of microalgae growth in a b-PBR with sunlight as the substrate are presented in Fig. 3.4.

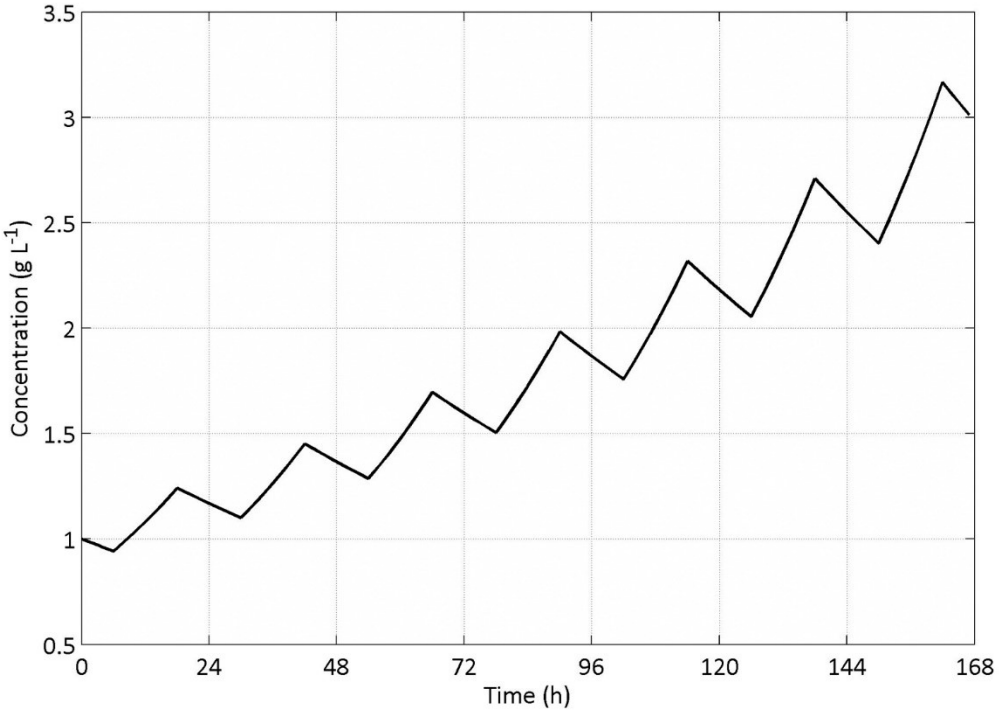

Fig. 3.4. Growth dynamics of algae biomass X_a (solid line) in a b-PBR based on the availability of sunlight over 7 days, or $t = 168$ hours, for $X_a(t = 0) = 1$ g L^{-1}; $\mu_{max} = 0.05$ h^{-1}; $\mu_d = 0.01$ h^{-1}; and $K_s = 100$ µmol m^{-2} s^{-1}. Sunlight described using a 12:12 daily light-dark cycle, with $S = 200$ µmol m^{-2} s^{-1} for light hours, and $S = 0$ µmol m^{-2} s^{-1} for dark hours. Variable parameterization based on an idealization of literature values to show trend.

In Fig. 3.4, the same exponential growth as is described in Fig. 3.3 is seen for the 12 hour light cycle, after which during the 12-hour dark cycle, no sunlight is available for photosynthesis, and the loss rate μ_d dominates the dynamics. The sawtooth dynamic is a consequence of light-dark cycles repeating over a seven-day period, and is a trend that will appear again in Chapter 4.

3.4.2 Haldane Growth Rate

In a microalgae b-PBR system, the amount of substrate that is available for growth affects the system as described by the dynamics shown in Fig. 3.3, wherein the substrate is depleted in response to biomass growth, thereby creating a limit to

growth with time. In certain cases, biomass growth is actually inhibited by the presence of an excess of an otherwise consumable substrate, such as was described for photoinhibition in Fig. 2.3. As such, the Haldane growth rate (Aiba, 1982) was developed, which adjusts the Monod expression given in Eq. 3.14 through the inclusion of an inhibition term, as:

$$\mu = \mu_{max} \cdot \frac{S_i}{K_{s,i} + S_i + \frac{S_i^2}{K_{i,i}}} \qquad 3.15$$

where $K_{i,i}$ is the inhibitory constant, describing the point at which the microalgal culture is limited by too much substrate, thereby creating a decline in the b-PBR growth rate. A comparison between the uninhibited Monod growth rate and the inhibited Haldane growth rate is given in Fig. 3.5.

The inclusion of inhibitory kinetics actually causes the growth rate to decrease despite an increase in consumable substrate. This is an important consideration in the BIMP system, wherein the sunlight intensity may have a significant impact on the growth dynamics due to the photoinhibition effect. Both Monod and Haldane kinetics will be used in Chapter 4 to describe the characteristics of light limitation in the BIMP system.

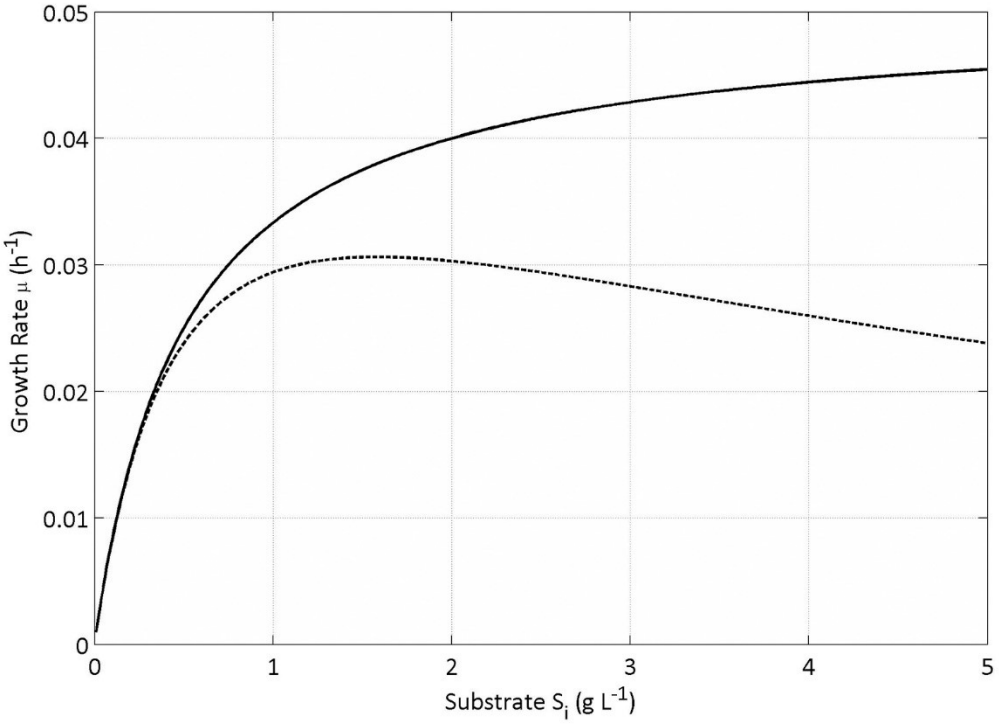

Fig. 3.5 Comparison of BIMP growth rate μ with increasing substrate concentration S_i as described using Monod kinetics (solid line) and Haldane kinetics (dash line), for $\mu_{max} = 0.05$ h^{-1}; $K_{s,i} = 0.5$ g L^{-1}; and $K_{i,i} = 0.5$ g L^{-1}. Variable parameterization based on an idealization of literature values to show trend.

3.4.3 Maximum Growth Rate

The maximum specific growth rate μ_{max} within a b-PBR system is the growth rate that can be theoretically achieved if no limitation occurs, and microalgae growth is ideal. For ideal conditions and with $\mu_d = 0$, Eq. 3.12 can be solved exactly as:

$$X_a = X_{a,o} \cdot \exp(\mu \cdot t) \qquad 3.21$$

where $X_{a,o}$ is the initial microalgae concentration, X_a is the microalgae concentration at some time t, and μ is the microalgae growth rate. Of note in Eq. 3.21 are the units of μ, which by definition must be $1/t$, with the most often reported unit scale being either h^{-1} or d^{-1}. Representationally, the unit of time used to describe μ_{max} suggest

that this is the maximum growth rate that can occur during that time interval. Thus, a daily μ_{max} value has questionable applicability to hourly modeling and simulation efforts, such as are used in this thesis to characterize a BIMP system. Additionally, the maximum growth rate is found experimentally by sampling X and plotting this versus experimental time t; the maximum slope of the resulting curve is the μ_{max} of the experimental system. As shown in Table 3.1, even for experiments using the same microalgae species and the same time interval, the maximum specific growth rate μ_{max} can vary significantly, based on different individual PBR operational characteristics.

Table 3.1: Reported Maximum Specific Growth Rate μ_{max} (h^{-1}) Values for PBR Systems Growing the Microalgae Species *C. vulgaris*.

Reference	μ_{max} (h^{-1})
Silva et al., (1984)	0.230
Lee, (2001)	0.110
Lee, (2001)	0.081
Filali et al., (2011)	0.080
Huisman et al., (2007)	0.070
Concas et al., (2012)	0.064
Sasi et al., (2011)	0.040

This is a common problem when trying to parameterize mathematical modeling efforts such as those used in this thesis to characterize the BIMP system. Because such variance exists in the literature, a sensitivity analysis will be used in Chapters 4 and 5 to determine the effect that varying key model parameters has on the growth dynamics in the BIMP system, thereby improving the fitness of the characterization efforts.

3.4.4 Multiplicative Growth Rate

The previous analysis has demonstrated how a single substrate may limit and inhibit growth in a microalgae b-PBR. However, as is most often the case, more than one

substrate in the system can limit growth, thereby giving rise to co-limitation dynamics. Microalgae nutritional requirements include more than one mineral substrate, and instead include many macro and micro nutrients, as was described in Chapter 2. The multiplicative growth rate assumes (Bae and Rittmann., 1995) that if two or more of these mineral nutrient substrates S_i are present in sub-optimal concentrations, then both will directly limit the growth of microalgae in a b-PBR, with the limitation effects being multiplicative. For two limiting substrates, this can be described as:

$$\mu = \mu_{max} \cdot \left(\frac{S_1}{K_{s,1} + S_1}\right) \cdot \left(\frac{S_2}{K_{s,2} + S_2}\right) \tag{3.16}$$

where S_1 and S_2 represent two unique substrates that the microalgae culture utilize for growth. Notice that the multiplicative growth rate is composed of the Monod growth rate expression; Eq. 3.16 could just as easily be written for the Haldane growth rate expression. The dynamics of the multiplicative growth rate are given in Fig. 3.6.

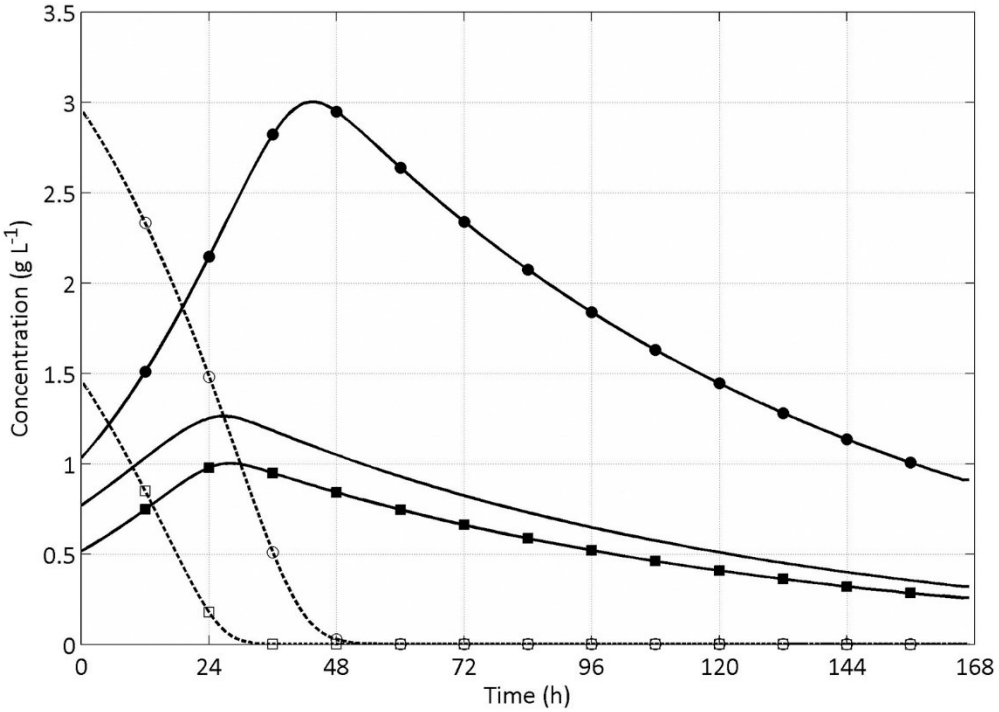

Fig. 3.6. Multiplicative growth rate dynamics of algae biomass X_a (solid line) within a b-PBR based on the availability of co-limiting substrates S_1 and S_2 (dashed line) over 7 days, or $t = 168$ hours. For biomass growth $X_{a,1}$ on substrate S_1 (●,○ respectively), $X_{a,1}(t = 0) = 1$ g L^{-1}; $S_1(t = 0) = 3$ g^{-1}; $\mu_{max} = 0.05$ h^{-1}; $\mu_d = 0.01$ h^{-1}; $Y_{x/s,1} = 1$ g $X_{a,1}$ g^{-1} S_1; and $K_{s,1} = 0.5$ g L^{-1}. For biomass growth $X_{a,2}$ on substrate S_2 (■,□ respectively), $X_{a,2}(t = 0) = 0.5$ g L^{-1}; $S_2(t = 0) = 1.5$ g^{-1}; $\mu_{max} = 0.05$ h^{-1}; $\mu_d = 0.01$ h^{-1}; $Y_{x/s,2} = 0.5$ g $X_{a,2}$ g^{-1} S_2; and $K_{s,2} = 0.25$ g L^{-1}. Variable parameterization based on an idealization of literature values to show trend.

The specific case of two-substrate limitation demonstrated in Fig. 3.6 can be generalized to a condition of multiple substrate limitation, or:

$$\mu = \mu_{max} \cdot \prod_1^n \left(\frac{S_n}{K_{s,n} + S_n} \right) \qquad 3.17$$

where $S_1, S_2, S_3 \ldots S_n$ are specific substrate species within the microalgal culture medium that may limit growth. Generalizing the term $S_n/(K_{s,n} + S_n)$ as a specific

limiting function $f(L_n)$, the multiplicative growth rate expression given in Eq. 3.17 becomes:

$$\mu = \mu_{max} \cdot \prod_1^n f(L_n) \qquad 3.18$$

where $L_1, L_2, L_3 \ldots L_n$ are specific growth rate limiting functions. For the BIMP system, four specific growth limiting factors have been described in Chapter 2, including the availability of sunlight for photosynthesis, the culture temperature as influenced by both the outdoor and indoor environment, as well as the availability of building generated nutrient and CO_2 resources. Rewriting Eq. 3.18 to include each of these specific limiting functions yields:

$$\mu = \mu_{max} \cdot f(\overline{I}_{avg}) \cdot f(T_{avg}) \cdot f\left(\left[S_{tot,i}\right]_L\right) \cdot f([CO_2]_L) \qquad 3.19$$

As an adaptive method for the design development of the BIMP system, this thesis will explore the interaction between two limiting factors, such that Eq. 3.19 becomes:

$$\mu = \mu_{max} \cdot f(\overline{I}_{avg}) \cdot f(T_{avg}) \qquad 3.20$$

where $\overline{I}_{avg}$ is the average solar radiation incident on the BIMP, and T_{avg} is the average BIMP culture temperature. The utilization of Monod and Haldane kinetics, and the application of multiplicative kinetics described by Eq. 3.20 are expanded upon in Chapters 4 and 5. In the following sections, each of the four limiting functions described by Eq. 3.19 are described mathematically.

3.5 BIMP Light Dynamics

The modeling of the monthly average hourly sunlight incident on a vertical surface is well described in the literature (Chwieduk, 2009; Kalogirou, 2009; Duffie and

Beckman, 2006), and has been applied to PBR systems in the literature (Pruvost et al., 2011; Sierra et al., 2008; Grima et al., 1999; Fernandez et al., 1998). Typically, these works utilize the Beer-Lambert approximation to average the incident PAR through the volume of the PBR culture medium. For instance, Grima et al (1999) employ a stepwise approach for the averaging the PAR radiation in their continuous tubular PBR system, which includes the definition of a PAR model and the use of the Beer-Lambert relationship to describe the spatially averaged PAR amount at any depth d within the PBR culture. To describe light-limited growth within a microalgae PBR, these authors then couple these light dynamics with an empirically-derived, photoinhibition growth rate model similar to the Haldane kinetic expression described in previously in this chapter. Conversely, Pruvost et al., (2011) utilize an empirically uninhibited Monod type model to describe the biological growth rate dynamics in their PBR system. According to Bechet et al., (2013), when coupled with the Beer-Lambert relationship, both Monod and Haldane type expressions have been used to predict microalgae growth rates for a wide range of light-limited or -inhibited PBR systems with a high level of accuracy.

For this thesis, it is assumed that the Liu and Jordon (1960) Isotropic Diffuse Sky Model, as describe by Duffie and Beckman (2006) is sufficiently accurate to describe the solar resource available for utilization in the BIMP system, despite its computational ease in relation to more complex solar models (Evseev and Kudish, 2009; Loutzenhiser et al., 2007). It is also assumed that the surface azimuth angle, or surface tilt deviation from due South, is zero. This is considered optimal for flat-plate solar collectors in the northern hemisphere (Duffie and Beckman, 2006).

The total monthly average daily incident solar radiation on a horizontal surface $\overline{H}$ is composed of two components, namely the direct beam radiation component, and the diffuse sky radiation component, such that:

$$\overline{H} = \overline{H}_b + \overline{H}_d \qquad 3.21$$

For the monthly average day N, the total solar intensity $\overline{H}$ has been defined empirically and published for major cities in Canada. To define each of the beam and diffuse components in Eq. 3.21, a second published empirically defined component is used. This is the clearness factor $\overline{K}_t$, and it accounts for the attenuation of extraterrestrial solar radiation as it passes through the atmosphere. Using empirically derived formulae, the clearness factor can be used to describe the correlation between the monthly average daily horizontal diffuse sky radiation $\overline{H}_d$ and horizontal total radiation $\overline{H}$ at the surface of the earth:

For $\omega_s \leq 81.4^o$ and $0.3 \leq \overline{K}_t \leq 0.8$:

$$\frac{\overline{H}_d}{\overline{H}} = 1.391 - 3.560 \cdot \overline{K}_t + 4.189 \cdot \overline{K}_t^2 - 2.137 \cdot \overline{K}_t^3 \qquad 3.22$$

For $\omega_s > 81.4^o$ and $0.3 \leq \overline{K}_t \leq 0.8$:

$$\frac{\overline{H}_d}{\overline{H}} = 1.311 - 3.022 \cdot \overline{K}_t + 3.427 \cdot \overline{K}_t^2 - 1.821 \cdot \overline{K}_t^3 \qquad 3.23$$

Here, the criteria for selecting the appropriate empirical correlation is based on calculating the sunset hour angle ω_s for the average monthly day N using the following relationship:

$$\omega_s = cos^{-1}(-tan\,\phi \cdot tan\,\delta) \qquad 3.24$$

where latitude $\phi = 44.4^o$ for Halifax. The declination angle δ describes the angular position of the sun at solar noon with respect to the equator, and is calculated as:

$$\delta = 23.45 \cdot sin\left[\frac{360}{365} \cdot (284 + N)\right] \qquad 3.25$$

As the BIMP relies on the diurnal light-dark cycle, the monthly average daily solar intensity value $\overline{H}$ must be converted to a monthly average hourly value. The monthly average day length $\overline{N}$ is a description of how many sunlight hours are available during each monthly average day, and is calculated using the sunset hour angle using the following equation:

$$Day\ length = \frac{2}{15} \cdot \omega_s = \overline{N} \tag{3.26}$$

Dividing the monthly average day length gives an estimation of the number of sunlight hours before and after local solar time. Then, the specific solar hour angle ω can be determined for the midpoint of each sunlight hour using:

$$\omega = \pm 0.25 \cdot (\#\ of\ minutes\ from\ local\ solar\ noon) \tag{3.27}$$

For example, for January in Halifax, the monthly average day number is $N = 17$, and by calculating declination $\delta = -20.92$ degrees using Eq. 3.25, the sunset hour angle is found to be $\omega_s = 67.78$ degrees from Eq. 3.24. The day length is then $\overline{N} = 9.04$ hours from Eq. 3.26, meaning there are approximately 4.5 hours of sunlight before and after solar noon. The corresponding specific solar hours are then calculated using Eq. 3.27 for the midpoint of each solar hour before and after noon.

For each solar hour defined by Eq. 3.26, the monthly average daily solar intensity can be converted to an hourly solar intensity. This is achieved by defining a ratio r_t, given as:

$$r_t = \frac{\overline{I}}{\overline{H}} \tag{3.28}$$

where $\bar{I}$ is the average hourly radiation on a horizontal surface (MJ m^{-2} hr^{-1}). The ratio r_t can be determined for each solar hour using the specific solar hour angle ω and the sunset hour angle ω_s as follows:

$$r_t = \frac{\pi}{24} \cdot (a + b\ cos\,\omega) \cdot \left(\frac{cos\,\omega - cos\,\omega_s}{sin\,\omega_s - \frac{\pi\omega_s}{180} \cdot cos\,\omega_s} \right) \quad 3.29$$

where the coefficients a and b are given as:

$$a = 0.409 + 0.5016 \cdot sin(\omega_s - 60) \quad 3.30$$
$$b = 0.6609 + 0.4767 \cdot sin(\omega_s - 60) \quad 3.31$$

Similar to Eq. 3.28, an expression for the ratio of hourly total diffuse radiation on a horizontal surface r_d is:

$$r_d = \frac{\bar{I}_d}{\bar{H}_d} \quad 3.32$$

Where $\bar{I}_d$ is the average hourly diffuse radiation on a horizontal surface (MJ m^2 h^{-1}), and the expression for r_d is given as:

$$r_d = \frac{\pi}{24} \cdot \left(\frac{cos\,\omega - cos\,\omega_s}{sin\,\omega_s - \frac{\pi\omega_s}{180} \cdot cos\,\omega_s} \right) \quad 3.33$$

Note here that Eq. 3.28 to Eq. 3.33 must be calculated for each solar hour defined by the day length calculation given in Eq. 3.26, using the specific solar hour angle defined for that solar hour by Eq. 3.27. Then, for each daily solar hour, and in a manner similar to that described in Eq. 3.21, the total hourly radiation on a horizontal surface is expressed using beam $\bar{I}_b$ and diffuse $\bar{I}_d$ components as:

$$\bar{I} = \bar{I}_b + \bar{I}_d \quad 3.34$$

For a tilted surface, the hourly beam radiation $\overline{I}_{b,t}$ diffuse radiation $\overline{I}_{d,t}$ reflected radiation $\overline{I}_{r,t}$ and total radiation $\overline{I}_t$ are estimated through a summation of the beam, diffuse, and reflected radiation components incident on the surface itself:

$$\overline{I}_t = \overline{I}_{b,t} + \overline{I}_{d,t} + \overline{I}_{r,t} \tag{3.35}$$

For the isotropic diffuse sky model, the beam, diffuse, and reflected solar radiation components in Eq. 4.15 are term-expanded as:

$$\overline{I}_t = \overline{I}_b \cdot R_b + \overline{I}_d \cdot \left(\frac{1 + cos\,\beta}{2}\right) + \overline{I} \cdot \left(\frac{1 - cos\,\beta}{2}\right) \cdot \rho_g \tag{3.36}$$

where ρ_g is the ground reflectance – or albedo – of the area surrounding the vertical surface, and $\beta = 90^{\circ}$ is the angle of surface tilt. The ratio R_b for a tilted surface is given as:

$$R_b = \frac{cos\,\theta}{cos\,\theta_z} = \frac{cos(\phi - \beta) \cdot cos\,\delta \cdot cos\,\omega + sin(\phi - \beta) \cdot sin\,\delta}{cos\,\phi \cdot cos\,\delta \cdot cos\,\omega + sin\,\phi \cdot sin\,\delta} \tag{3.37}$$

Thus, for any calendar day *N*, Eq. 3.36 can be solved to describe the hourly solar radiation incident on the vertical exterior surface of the BIMP, for each daily solar hour defined by Eq. 3.26.

As a photosynthetic organism, microalgae are only able to utilize a specific spectral range within the incident solar resource. This range, commonly referred to as PAR, has a spectrum between λ = 400–700 nm (Richmond, 2004). Only the PAR radiation is useful in the BIMP system to support photosynthesis, so the monthly average hourly solar radiation incident on the BIMP system described by Eq. 3.36 must be reduced by the ratio of PAR to full spectrum solar energy. This ratio has been calculated by Weyer et al., (2010) as 0.458.

A second attenuation of the monthly average hourly solar resource is caused by the BIMP system itself: light incident on the BIMP exterior glazed surface will be reflected to a certain degree, thereby attenuating the solar resource. Here a simple correlation is made between the PAR spectrum, and the visible light spectrum, the latter of which is also λ = 400–700 nm. As such, published data on visible light transmission of common glazing materials can be used to approximate the PAR transmission through the exterior BIMP glazing. Average visible light transmittance values for various glazing products are described by the Canadian Housing and Mortgage Company (2004) as between 81 – 89% PAR. Based on the PAR and attenuation reductions here described, the average monthly hourly PAR that has passed through the exterior BIMP translucent surface and is impingent on the exterior vertical culture surface is:

$$\overline{I}_i = 0.458 \cdot 0.89 \cdot \overline{I}_t = 0.408 \cdot \overline{I}_t \qquad 3.38$$

In the following section, the average monthly hourly PAR value described in Eq. 3.38 is spatially averaged through the volume of the BIMP culture medium, for the description of the light-limited growth rate.

3.5.2 Light-Dependent Growth Rate

The characterization of the light-dependent growth rate in the BIMP system is dependent on the spatially-averaged PAR density $\overline{I}_{avg}$, which can be determined by averaging the incident solar radiation $\overline{I}_i$ through the culture depth d of the BIMP system. This is achieved using a modified form of the Beer-Lambert relationship, as described by Yun and Park (2003) as:

$$\overline{I}(X, z) = \overline{I}_i \cdot \exp(-k_m \cdot X_a \cdot z) \qquad 3.39$$

where $\overline{I}_i$ and $\overline{I}(X, z)$ are the radiation intensity at the BIMP interior culture surface and at any point z (m) from the illuminated surface within the culture medium,

respectively. The variable X describes the microalgae biomass density (g m^{-3}) within the BIMP, while the parameter k_m represents the mass attenuation coefficient of the culture medium (m^2 g^{-1}). For rectangular photobioreactor geometries, Richmond (2004) integrated the Beer-Lambert expression given in Eq. 3.39 through the culture depth d to determine the spatially averaged PAR $\overline{I}_{avg}$ available within the BIMP:

$$\overline{I}_{avg} = \int_0^d \frac{\overline{I}(X,z) \cdot dz}{d} \tag{3.40}$$

For the assumption that the BIMP system is completely mixed, and by using substitution and solving Eq. 3.40, the spatially-averaged PAR density within the BIMP for photosynthesis $\overline{I}_{avg}$ is given as:

$$\overline{I}_{avg} = 0.408 \cdot \overline{I}_t \cdot \frac{1 - exp(-k_m \cdot X_a \cdot d)}{k_m \cdot X_a \cdot d} \tag{3.41}$$

Using Monod kinetics, the spatially-averaged PAR density dependent microalgal biomass growth rate function $f_1(\overline{I}_{avg})$ in the BIMP system is given as:

$$f_1(\overline{I}_{avg}) = \left(\frac{\overline{I}_{avg}}{K_s + \overline{I}_{avg}}\right);\ 0 \le f_1(\overline{I}_t) \le 1 \tag{3.42}$$

where K_s is the half-saturation constant for light-dependent microalgal growth. Here, $f_1(\overline{I}_{avg})$ is extended using Haldane kinetics to include the effects of light saturation, or:

$$f_2(\overline{I}_{avg}) = \left(\frac{\overline{I}_{avg}}{K_s + \overline{I}_{avg} + \frac{\overline{I}_{avg}}{K_i}^2}\right);\ 0 \le f_2(\overline{I}_t) \le 1 \tag{3.43}$$

where K_i is the inhibition constant for light-dependent microalgal growth.

3.6 BIMP Temperature Dynamics

For outdoor PBR systems, the impact of the geographically specific environment on the culture temperature has not been extensively modeled in the literature. Gutierrez et al., (2008) performed a heat balance on a stand-alone, outdoor batch open tank PBR, and described variation in culture temperature with time as dependent on five heat transfer mechanisms, which include solar gain, convection, evaporation, radiation, and conduction. In addition, these authors described the change in PBR tank body temperature with time, important in their work for the conductive heat transfer mechanism. Goetz et al., (2011) use a similar approach, but for an outdoor horizontal continuous flat-plate-type PBR. Here, the authors replace the term describing conduction between the PBR and the culture medium with a convective term, as is typical for flow conditions. Bechet et al., (2010) described an outdoor batch vertical tubular PBR, and assumed there is no temperature gradient between the PBR material and the culture medium, thereby affording an analysis with only one PBR system temperature changing with time. For the BIMP system, the indoor building environment must also be considered in the heat transfer analysis, a condition not considered in the aforementioned studies, nor in the PBR literature. Published work on the solar gain through building windows is useful in this analysis, most notably the work of Chow et al., (2011a, 2011b), who modeled a window system as a solar thermal heating device.

For the BIMP system, a heat balance is used to describe the temperature change within the exterior translucent surface. Based on the characteristics of the incident solar radiation $\bar{I}_t$, as well as the average daily outdoor temperature T_o and the BIMP culture temperature T_w, the temperature change in the exterior BIMP surface is given as:

$$m_1 \cdot C_{p,1} \cdot \frac{dT_1}{dt} = Q_{s,1} - Q_{r,1} - Q_{c,1} - Q_{k,1} \qquad 3.44$$

where T_1 is the temperature of the BIMP exterior translucent surface, while m_1 (kg) and $C_{p,1}$ (J kg^{-1} K^{-1}) are the mass and heat capacity of that surface, respectively. The heat transfer mechanism $Q_{s,1}$ is the total possible heat gain from the sun for a given geographic location and BIMP orientation, $Q_{r,1}$ is the amount of heat radiated as a loss from the outside BIMP surface to the exterior environment, and $Q_{c,1}$ represents the convective heat transfer from the exterior surface to the outdoor environment. Because the BIMP operates in a fed-batch mode, the conductive heat transfer mechanism dominates across the exterior BIMP surface. As such, $Q_{k,1}$ represents the conductive heat transfer through the exterior surface between the outdoor environment and the BIMP culture medium. Each of these heat transfer mechanisms is term expanded and described through the following equations:

$$Q_{s,1} = \alpha_1 \cdot A_1 \cdot \bar{I}_t \quad 3.45$$

$$Q_{r,1} = \varepsilon_1 \cdot \sigma \cdot A_1 \cdot (T_1^4 - T_{sky}^4) \quad 3.46$$

$$Q_{c,1} = h_{c,1} \cdot A_1 \cdot (T_1 - T_o) \quad 3.47$$

$$Q_{k,1} = h_{k,1} \cdot A_1 \cdot (T_1 - T_w) \quad 3.48$$

Here, α_1 (-) and ϵ_1 (-) are the absorptivity and emissivity of the BIMP exterior translucent surface, respectively, while A_1 (m^2) is the illuminated area of that surface. The Stefan-Boltzmann constant σ is equal to 5.67037(10)$^{-8}$ (W m^{-2} K^{-4}).

The effective sky temperature T_{sky} (K) used to describe radiation from the atmosphere is expressed empirically as a function of the outdoor temperature T_o (Duffie and Beckman, 2006), as:

$$T_{sky} = 0.0552 \cdot T_o^{1.5} \quad 3.49$$

The outdoor temperature T_o for the average day in any given month is described statistically for weather stations in Canada using a daily average minimum temperature T_{min}, a daily average maximum temperature T_{max}, and a daily average temperature T_{avg}. To convert the monthly average daily outdoor temperatures to a monthly average hourly outdoor temperature, the Double Cosine Model as described by Bilbao et al. (2002) and Chow and Levermore (2007) is used. The Double Cosine Model provides a method of calculating and linking together the hours of occurrence of the daily maximum and minimum temperatures using three sinusoidal segments as given by the following expressions:

For $1 \leq t < t_{T_{min}}$:

$$T_o(t) = T_{avg} + cos\left[\frac{\pi \cdot \left(t_{T_{min}} - t\right)}{24 + t_{T_{min}} - t_{T_{max}}}\right] \cdot \frac{T_{amp}}{2} \qquad 3.50$$

For $t_{T_{min}} \leq t \leq t_{T_{max}}$:

$$T_o(t) = T_{avg} + cos\left[\frac{\pi \cdot \left(t - t_{T_{min}}\right)}{t_{T_{max}} - t_{T_{min}}}\right] \cdot \frac{T_{amp}}{2} \; ; \qquad 3.51$$

For $t_{T_{max}} < t \leq 24$:

$$T_o(t) = T_{avg} + cos\left[\frac{\pi \cdot \left(24 + t_{T_{min}} - t\right)}{24 + t_{T_{min}} - t_{T_{max}}}\right] \cdot \frac{T_{amp}}{2} \qquad 3.52$$

where $T_o(t)$ is the monthly average hourly outdoor temperature calculated for each hour t between 12:30 am (t = 1) and 11:30 pm ($t = 24$), $t_{T_{min}}$ is the hour of occurrence of the daily average minimum temperature T_{min} , and $t_{T_{max}}$ is the hour of occurrence of the daily average maximum temperature T_{max} . The monthly mean temperature amplitude T_{amp} is defined as the difference between the monthly average maximum and minimum temperatures.

The convective heat transfer coefficient between the exterior translucent BIMP surface and the outdoor environment $h_{c,1}$ (W m^{-2} K^{-1}) is a function of the wind speed V (m s^{-1}) (Duffie and Beckman, 2006), and is expressed as:

$$h_{c,1} = (5.7 + 3.8 \cdot V) \tag{3.53}$$

The conductive heat transfer coefficient $h_{k,1}$ (W m^{-2} K^{-1}) through the exterior surface is expressed as a relationship between the thermal conductivity k_1 (W m^{-1} K^{-1}) and depth d_1 (m) of the material (Incropera et al., 2007), or:

$$h_{k,1} = \frac{k_1}{d_1} \tag{3.54}$$

Similar to the analysis presented for the exterior BIMP surface but for conditions characterized by the indoor environment, the change in temperature in the inside surface of the BIMP can be described using a heat balance based on the indoor environment, namely the internal temperature T_i. As such, the rate of change in temperature for the interior translucent BIMP surface is given as:

$$m_2 \cdot C_{p,2} \cdot \frac{dT_2}{dt} = Q_{s,2} - Q_{r,2} - Q_{c,2} - Q_{k,2} \tag{3.55}$$

where T_2 is the temperature of the BIMP interior translucent surface. The heat transfer mechanism $Q_{s,2}$ is the total possible heat gain from the sun as transmitted through both the exterior BIMP surface and the culture medium, $Q_{r,2}$ is the amount of heat radiated from the inside BIMP surface to the indoor environment, and $Q_{c,2}$ represents the convective heat transfer from the interior surface to the indoor environment. And, as for the exterior surface 2 represents the conductive heat transfer through the interior surface between the outdoor environment and the BIMP culture medium.

Again term expanding these heat transfer mechanism results in the following equation set:

$$Q_{s,2} = \tau_1 \cdot \tau_w \cdot \alpha_2 \cdot A_2 \cdot \bar{I}_t \quad 3.56$$

$$Q_{r,2} = \varepsilon_2 \cdot \sigma \cdot A_2 \cdot (T_2^4 - T_{sur}^4) \quad 3.57$$

$$Q_{c,2} = h_{c,2} \cdot A_2 \cdot (T_2 - T_i) \quad 3.58$$

$$Q_{k,2} = h_{k,2} \cdot A_2 \cdot (T_2 - T_w) \quad 3.59$$

The terms τ_1 (-) and τ_w (-) represent the transmissivity of the exterior BIMP surface and the culture medium, respectively. The effective indoor surface temperature T_{sur} is assumed equivalent to the indoor temperature T_i (Chow et al., 2011a, b). The indoor convective heat transfer coefficient $h_{c,2}$ is simply defined as Eq. 3.53 without the wind speed term (Carlos et al., 2011), or 5.7 W m^{-2} K^{-1} when converted to the normal unit set used in this chapter. As both the interior and exterior BIMP surfaces are the same material, the conductive heat transfer coefficient $h_{k,2}$through the interior BIMP surface between the culture medium and the indoor environment is defined using Eq. 3.54.

The change in the BIMP culture temperature T_w is dependent on the expressions developed for the change in exterior and interior translucent BIMP surface temperatures $T_1$and T_2, respectively, as described by the following heat balance:

$$m_w \cdot C_{pw} \cdot \frac{dT_w}{dt} = Q_{s,w} - Q_{k,1} - Q_{k,2} \quad 3.60$$

with the term expansion resulting in the following equation set:

$$Q_{s,w} = \tau_1 \cdot \alpha_w \cdot A_w \cdot \bar{I}_T \quad 3.61$$

In the following section, these heat transfer analyses will be used to determine the BIMP culture temperature defined by Eq. 3.60.

3.6.1 Temperature-Dependent Growth Rate

The effect that temperature has on the growth rate of microalgae is described by Quinn et al. (2011) using two expressions that relate culture medium temperature T_w to the activity of the ribulose-1,5-bisphosphate carboxylase/oxygenase – or RuBisCo – enzyme, which catalyzes the preliminary carbon fixation activities in the microalgae cell. These expressions are:

$$\varphi_T = \exp\left(\frac{E_a}{R \cdot T_{opt}} - \frac{E_a}{R \cdot T_w}\right) \tag{3.62}$$

$$f(T_w) = \frac{2 \cdot \varphi_T}{1 + (\varphi_T)^2}; 0 \leq f(T_w) \leq 1 \tag{3.63}$$

where E_a (J mol^{-1}) is the activation energy of the RuBisCo enzyme, and R (J K^{-1} mol^{-1}) is the universal gas constant. The optimal culture temperature T_{opt} (K) is the temperature at which microalgae growth is ideal and not temperature limited, and T_w is the actual culture temperature.

3.7 BIMP Nutrient Dynamics

In this section, a microalgae nutrient resource consisting of human urine and rainwater is theoretically defined. As described in Fig. 1.1, an urban region has a large demand on exurban water resources, requiring both freshwater inputs, and large ecosystem regions for the treatment of wastewater that is generated. Instead, this section proposes the BIMP system as an in-situ wastewater treatment device, able to bioregenerate a human urine/wastewater mixture, without the need of an exurban ecosystem.

The BIMP nutrient medium is described as a mixture of stored rainwater collected from an urban environment as mixed with stored human urine, as provided from a wastewater source separation system. The influence of nutrients on biomass growth includes the definition of the chemical composition of a urine-rainwater mixture to be used as a nutrient feed, the specific uptake of various aqueous chemical species by microalgae within the BIMP, and the resulting effect on the BIMP system pH.

Rainwater collected from an urban environment changes pH as it passes through the various stages of harvesting; Despins et al., (2009) describe a range of pH 5.8 for rural environments, to 8.2 for industrial areas. Also, rainwater in various North American regions demonstrate different pH values based on various climatic factors, including proximity to sea spray, heavy industry, and urbanized areas. Here it is assumed that rainwater entering the catchment area only has aqueous C species present, and other species such as N and sulfur dioxides absorbed from the atmosphere are neglected. This assumption is then used as a first approximation for rainwater pH.

Stored human urine differs from fresh human urine in chemical composition, based mainly on the hydrolysis of urea according to the following reaction (Udert et al., 2003a, b):

$$NH_2(CO)NH_2 + 2H_2O \rightarrow NH_3 + NH_4^+ + HCO_3^- \qquad 3.64$$

The formation of ammonia and bicarbonate in the hydrolyzed urine system causes the pH to increase, resulting in the formation of various precipitates (Udert et al., 2003a). These precipitates settle in the urine storage tank, and as such, it is here assumed that the stored urine utilized within the BIMP is drawn from the supernatant, while settled precipitates would be collected and utilized elsewhere. It is also assumed that upon mixing the source-separated urine and rainwater, new precipitates will not form due to very low concentrations of calcium and magnesium in rainwater (Udert et al., 2003b), and ammonia in situ will remain so, and not volatilize within the BIMP system.

It is assumed that C species in rainwater and urine mix additively to form a new TIC, whereby the change in pH caused by rainwater dilution – and resulting change in pH – results in a new equilibrium point, and a new TIC profile after mixing. Also, C species are not removed from the system based on biological uptake in this study, and instead the specific species concentrations of TIC are utilized here to calculate changes in the system pH, based on the nutrient metabolism of microalgae within the BIMP. At any given time, the TIC profile can be determined based on the system pH here described, and are utilized as inputs to the BIMP system modeling of aqueous CO_2 uptake by microalgae, as described in the next section.

All equilibrium constants for the equilibrium equations are for 25 °C, and variations based on the change in BIMP liquid temperature are neglected. Also, it is assumed that no complex species exist that have equilibrium dynamics outside those characterized by the equations in Appendix A.

3.7.1 Rainwater

To determine the pH of rainwater based on the presence of C species, the electro-neutrality condition must be described. The electro-neutrality expression describes the balance between the concentrations of C cation and anion species, as well as the concentrations of hydrogen $[H^+]$ and hydroxyl $[OH^-]$ species present, and is given as (Stumm and Morgan, 1996):

$$[H^+] = [HCO_3^-] + 2 \cdot [CO_3^{2-}] + [OH^-] \qquad 3.65$$

Where concentrations $[H^+]$ and $[OH^-]$ are related by the equilibrium reaction constant for water K_W, as provided in Appendix A. To determine the bicarbonate $[HCO_3^-]$ and carbonate $[CO_3^{2-}]$ aqueous concentrations, the equivalent carbonic acid aqueous concentration $[H_2CO_3]^*$ must first be described.

This is achieved using the dynamics of CO_2 mass transfer from the gas-phase (atmosphere) to the liquid phase (rainwater), as expressed by the equilibrium reaction (England et al., 2011):

$$[CO_2]_G + H_2O \overset{H_C}{\leftrightarrow} [H_2CO_3]^* \tag{3.66}$$

where H_C = 3.4 x 10^{-2} mol L·atm^{-1} is the Henry's constant for CO_2, the concentration $[CO_2]_G$ is equivalent to the partial pressure P_{CO_2} of CO_2 in the atmosphere. The equivalent carbonic acid concentration is the sum of aqueous CO_2 and carbonic acid described by the relationship $[H_2CO_3]^* = [CO_2]_L + [H_2CO_3]$ for open freshwater systems, and is a convention used due to the slow rate of conversion of aqueous CO_2 to carbonic acid. Thus, the equilibrium equation describing the equivalent carbonic acid concentration is given as:

$$[H_2CO_3]^* = H_C \cdot P_{CO_2} \tag{3.67}$$

Then, by expressing the equilibrium equations for bicarbonate and carbonate in terms of the equivalent carbonic acid concentration, and through substitution, the expression for electro-neutrality given in Eq. 3.65 becomes:

$$[H^+] = \frac{2 \cdot K_{C2} \cdot K_{C3} \cdot H_C \cdot P_{CO_2}}{[H^+]^2} + \frac{K_{C2} \cdot H_C \cdot P_{CO_2}}{[H^+]} + \frac{K_W}{[H^+]} \tag{3.68}$$

where, after rearranging, a polynomial equation with respect to $[H^+]$ is achieved:

$$[H^+]^3 - [H^+] \cdot \left(K_{C2} \cdot H_C \cdot P_{CO_2} + K_W\right) - 2 \cdot K_{C2} \cdot K_{C3} \cdot H_C \cdot P_{CO_2} = 0 \tag{3.69}$$

For an atmospheric partial pressure P_{CO_2} = 4 x 10^{-4} atm (equivalent to a concentration of $[CO_2]_G$ = 400 ppm), Eq. 3.69 can be solved using the *roots* function in MATLAB, yielding a concentration $[H^+]$ = 2.476 x 10^{-6} M, and a corresponding pH = 5.6 for the rainwater system here considered. This pH value is in the range of rainwater cistern

values for Canada (Despins et al., 2009). The total inorganic C (TIC) in the rainwater system can be described as:

$$[TIC] = [CO_2]_L + [H_2CO_3] + [HCO_3^-] + [CO_3^{2-}] \quad 3.70$$

where the equilibrium equations for each species in Eq. 3.70 utilize Eq. 69. The equilibrium equations for rainwater are provided in Appendix A.

3.7.2 Human Urine

Based on the formation of precipitates, as well as the volatilization of ammonia within the source-separated urine system, the difference between chemical species density in fresh and stored human urine are described in Table 3.2.

Table 3.2: Composition of Fresh Human Urine (FMU) and Stored Human Urine (SHU) (adapted from Udert et al., 2003a)

Species	Fresh urine	Stored urine
Ammonia (g N m^{-3})	254	1720
Urea (g N m^{-3})	5810	73
Phosphate (g P m^{-3})	367	76
Calcium (g m^{-3})	129	28
Magnesium (g m^{-3})	77	1
Sodium (g m^{-3})	2670	837
Potassium (g m^{-3})	2170	770
Sulphate (g SO_4 m^{-3})	748	292
Chloride (g m^{-3})	3830	1400
Carbonate (g C m^{-3})	-	966
Total COD (g O_2 m^{-3})	8150	1650
pH	7.2	9.0

For the chemical species described in Table 3.2, the relevant equilibrium equations and reactions for the urine-rainwater system are described in Appendix A. Stored urine has two important characteristics. First, stored urine is diluted with water, as part of mechanism used to separate it from solid wastes in a source separation system. Second, the pH = 9 of the stored urine is suboptimal for *C. Vulgaris* growth

(Mayo, 1997), and therefore must be buffered prior to utilization within the BIMP. The requirements of electro-neutrality within the BIMP suggest that the concentration $[H^+]$ – and thus the pH – can be described as follows:

$$[OH^-] + [HCO_3^-] + 2 \cdot [CO_3^{-2}] + [H_2PO_4^-] + 2 \cdot [HPO_4^{-2}] + 3 \cdot [PO_4^{-3}] + 2 \cdot [SO_4^{-2}] + [Cl^-] = [H^+] + [NH_4^+] + 2 \cdot [Ca^{+2}] + 2 \cdot [Mg^{+2}] + [Mg^+] + [Na^+] + [K^+] \quad 3.71$$

3.7.3 Nutrient-Dependent Growth rate

To describe the change in macronutrient concentration in the BIMP system, the yield coefficient $Y_{S_{tot,i}}$ for each must be defined, as is described in Chapter 3. For each macronutrient in the BIMP culture medium, the rate of biological nutrient uptake $d\left[S_{tot,i}\right]_X$ can be described as follows:

$$\frac{d\left[S_{tot,i}\right]_X}{dt} = -\mu_{max} \cdot X_a \cdot Y_{S_{tot,i}} \quad 3.72$$

The change in macronutrient concentration in the BIMP culture medium can then be defined as:

$$\frac{d\left[S_{tot,i}\right]_L}{dt} = \left[S_{tot,i}\right]_i + \frac{d\left[S_{tot,i}\right]_X}{dt} \quad 3.73$$

Using the multiplicative growth kinetics described by Eq. 3.18, the nutrient limitation function is given as:

$$f\left(\left[S_{tot,i}\right]_L\right) = \prod_{i=1}^{n} \frac{\left[S_{tot,i}\right]_L}{K_{S_{tot,i}} + \left[S_{tot,i}\right]_L};\ 0 \leq f\left(\left[S_{tot,i}\right]_L\right) \leq 1 \quad 3.74$$

3.8 BIMP CO_2 Dynamics

This section introduces the mathematical modeling of the dynamics of BIMP CO_2 utilization. Here, the model describes the mechanism of bubbling CO_2 into the BIMP at various concentrations, and the corresponding dynamics of mass transfer, and biological uptake that result. An important consideration in this chapter is the mechanism by which microalgae fixate aqueous C. To ensure that the biological models for microalgal uptake of C remain consistent, and an assumption must be made whether microalgae preferentially uptake a specific aqueous C type. Concas et al., (2012) assume that *C. Vulgaris* are indifferent in their selection of aqueous C species, while Pegallapati and Nirmalakhandan (2012) select bicarbonate [HCO_3^-] based on the prevalence of the aforementioned species in the pH range of 6.8 – 7.4, considered ideal for *C. Vulgaris*.

A secondary consideration here is the dynamics present with the utilization of urban wastewater – either source separated urine, or secondary and/or tertiary wastewater effluent – as aqueous C species are more than likely present as a result of urease degradation of urea, thereby changing again the dynamics of the model. As part of a comprehensive urban waste strategy, the BIMP is challenged with using said wastewater, thereby creating a meta-variable set that is rarely discussed and/or modeled within the literature.

The influence of aqueous CO_2 on biomass growth as described in this section includes the definition CO_2 gas-liquid mass transfer from bubbles sparged to the BIMP culture medium, the dynamics of CO_2 hydrolysis, and the specifics of biological uptake of aqueous CO_2 species by microalgae within the BIMP. Also of interest here is the power required to sparge the CO_2 (Hulatt and Thomas, 2011).

3.8.1 Biological Phase

The biological uptake of CO_2 is similar to that described in Appendix C for nutrients, or:

$$\frac{d[CO_2]_{L,X}}{dt} = -\mu_{max} \cdot X_a \cdot Y_{S_i/A} \quad 3.75$$

3.8.2 Gas Phase

Gas-liquid mass transfer of CO_2 from sparged air to the BIMP microalgal culture medium is defined by both time and space; the former being a function of the gas holdup ϵ within the BIMP culture, while the latter a function of the BIMP culture medium height y. To state this more directly, sparged air entering that enters the bottom of the BIMP will continuously undergo gas-liquid mass transfer as bubbles rise through the height of the culture medium, meaning the CO_2 concentration within the bubbles at the base of the BIMP will be greater than the CO_2 concentration of the bubbles entering the BIMP headspace. In general, across the volume of the BIMP culture medium, the gas-liquid mass transfer rate is defined as:

$$\frac{d[CO_2]_G}{dt} = F_G \cdot ([CO_2]_{G,i} - [CO_2]_{G,o}) \quad 3.76$$

Where $[CO_2]_i$ is the concentration of CO_2 in bubbles sparged at the base of the BIMP, while $[CO_2]_o$ is the concentration of CO_2 in sparged bubbles leaving the BIMP culture medium and entering the headspace. Consider then, a differential volume within the BIMP, as characterized by the height dimension dz. The gas-liquid mass transfer J_{dz} for the differential volume V_{dz} is described by Chisti (1989) as:

$$J_{dz} = k_L a_L \cdot ([CO_2]_L^* - [CO_2]_L) \cdot V_{dz} \quad 3.77$$

Where $V_{dz} = (1 - \epsilon) \cdot A \cdot dz$ describes the available aqueous culture medium within the differential volume for gas-liquid mass transfer. Also, by definition during steady-state BIMP operation, the rate of gas-liquid mass transfer within the differential volume V_{dz} must be:

$$J_{dz} = F_G \cdot [CO_2]_{G,i} - F_G \cdot ([CO_2]_{G,i} + d[CO_2]_{G,dz}) = -F_G \cdot d[CO_2]_{G,dz} \quad 3.78$$

Thus, the amount of CO_2 transferred from the gaseous phase to the aqueous BIMP phase within the differential volume can be described by equating Eq. 3.77 with Eq. 78 and rearranging, or:

$$\frac{d[CO_2]_{G,dz}}{dz} = k_L a_L \cdot ([CO_2]_L^* - [CO_2]_L) \cdot (1 - \epsilon) \cdot \frac{A}{F_G} \quad 3.79$$

where $[CO_2]_L^* = H_c \cdot [CO_2]_{G,dz}$, for H_c as the Henry Constant for CO_2 between gas and BIMP culture medium. Eq. 3.79 can is now rearranged and to solve using boundary conditions characteristic of the BIMP:

$$\int_{[CO_2]_{G,i}}^{[CO_2]_{G,o}} \frac{d[CO_2]_{dz}}{(H_c \cdot [CO_2]_{G,dz} - [CO_2]_L)} = -k_L a_L \cdot (1 - \epsilon) \cdot \frac{A}{F_G} \cdot \int_o^y dz \quad 3.80$$

Thus, by solving Eq. 3.80 and rearranging yields the concentration of CO_2 leaving the gaseous bubble phase and entering the headspace of the BIMP. Assuming no gas-liquid mass transfer between the headspace and BIMP culture medium, the amount of CO_2 leaving the BIMP is described as:

$$[CO_2]_{G,o} = \frac{1}{H_c} \cdot \left[\left((H_c \cdot [CO_2]_{G,i} - [CO_2]_L) \cdot \exp\left(\frac{(k_L a_L \cdot (1 - \epsilon) \cdot A \cdot y}{F_G} \right) \right) + [CO_2]_L \right] \quad 3.81$$

Returning then to Eq. 3.76, the rate of CO_2 transferred from the sparged gas phase to the liquid phase within the BIMP is:

$$\frac{d[CO_2]_G}{dt} = F_G \cdot \left[[CO_2]_{G,i} - \frac{1}{H_c} \cdot \left[\left((H_c \cdot [CO_2]_{G,i} - [CO_2]_L) \cdot \exp\left(\frac{(k_L a_L \cdot (1-\epsilon) \cdot A \cdot y)}{F_G} \right) \right) + [CO_2]_L \right] \right] \quad 3.82$$

By design, the BIMP behaves as a pneumatically-agitated bubble column reactor with a rectangular shape factor. For this type of reactor, Acien-Fernandez et al., (2012) present empirical relationships describing both the mass transfer coefficient $k_L a_L$ and gas holdup ϵ, as dependent on the power input through gas sparging per unit reactor culture medium volume:

$$k_L a_L = 2.39(10)^{-4} \cdot \left(\frac{P_G}{V_L} \right)^{0.86} \quad 3.83$$

$$\epsilon = 3.32(10)^{-4} \cdot \left(\frac{P_G}{V_L} \right)^{0.97} \quad 3.84$$

The power input per volume factor P_G/V_L is a function of the superficial gas velocity in the aerated zone of the reactor, the density of the reactor culture medium, and gravitational acceleration:

$$\frac{P_G}{V_L} = \rho_L \cdot g \cdot U_G \quad 3.85$$

Where the superficial gas velocity U_G is defined as the flow rate of aeration gas per area of aeration zone, or:

$$U_G = \frac{Q_G}{A_G} \tag{3.86}$$

3.8.3 Liquid Phase

If it is assumed that *C. Vulgaris* preferentially uptake aqueous CO_2 then the amount of C in that form available for photosynthesis may limit growth, based on the dynamics of CO_2 hydrolysis with respect to pH within the BIMP culture medium. For the hydrolysis of CO_2 the following overall chemical equilibria equations (England et al., 2011) are considered.

$$[CO_2]_L + H_2O \overset{K_{c1}}{\leftrightarrow} H_2CO_3 \tag{3.87}$$

$$H_2CO_3 \overset{K_{c2}}{\leftrightarrow} HCO_3^- + H^+ \tag{3.88}$$

$$HCO_3^- \overset{K_{c3}}{\leftrightarrow} H^+ + CO_3^{-2} \tag{3.89}$$

Here, the variables K_i (for i =C_1, C_2, C_3) represent the equilibrium constant for each reaction, respectively. These equilibrium constants are related to the reaction rates for each CO_2 hydrolysis reaction by the relationship proposed by Erickson et al., (1987):

$$K_{ci} = \frac{k_{+i}}{k_{-i}} \tag{3.90}$$

where k_{+i} represents the forward reaction rate of the ith reaction, while k_{-i} represents the reverse reaction rate of the ith reaction. Along with the characteristics of biological uptake of $[CO_2]_L$ in situ, the reaction rates $k_{\pm i}$ are utilized with respect

to the dynamic concentration of each C species within the BIMP to determine the availability of $[CO_2]_L$ for microalgal photosynthesis. This is described as:

$$V_L \cdot \frac{d[CO_2]_L}{dt} = \frac{d[CO_2]_G}{dt} + \frac{d[CO_2]_{L,X}}{dt} + [CO_2]_{L,i} + k_{-1} \cdot [H_2CO_3] - k_1 \cdot [CO_2]_L \quad 3.91$$

The rate of change of concentration for each C species – those not $[CO_2]_L$ – are dependent on the kinetics of Eq. 3.91, as well as the initial concentration of each species present as a result of utilizing a urine-rainwater mixture as the BIMP nutrient source. These concentrations are therefore given as:

$$V_L \cdot \frac{d[H_2CO_3]}{dt} = [H_2CO_3]_i + k_1 \cdot [CO_2]_L + k_{-2} \cdot [H^+] \cdot [HCO_3^-] - k_{-1} \cdot [H_2CO_3] - k_2 \cdot [H_2CO_3] \quad 3.92$$

$$V_L \cdot \frac{d[HCO_3^-]}{dt} = [HCO_3^-]_i + k_2 \cdot [H_2CO_3] + k_{-3} \cdot [H^+] \cdot [CO_3^{-2}] - k_{-2} \cdot [H^+] \cdot [HCO_3^-] - k_3 \cdot [HCO_3^-] \quad 3.93$$

$$V_L \cdot \frac{d[CO_3^{-2}]}{dt} = [CO_3^{-2}]_i + k_3 \cdot [HCO_3^-] - k_{-3} \cdot [H^+] \cdot [CO_3^{-2}] \quad 3.94$$

where $[H^+]$ is defined based on the nutrient chemical equilibria and electro-neutrality requirements for the BIMP nutrient media and microalgal uptake dynamics presented in Appendix A.

3.8.4 CO_2-Dependent Growth Rate

Using the Monod growth kinetics described in Chapter 3, the CO_2 limitation function is given as:

$$f([CO_2]_L) = \frac{[CO_2]_L}{K_c + [CO_2]_L};\ 0 \leq f([CO_2]_L) \leq 1 \qquad 3.95$$

3.9 Discussion

This chapter introduces the b-PBR dynamic modeling method, where the microalgae biomass concentration X_a is shown to be dependent on a specific growth rate μ, for which two kinetic expressions are described, including the uninhibited Monod growth rate and the inhibited Haldane growth rate. For the former of these expressions, the depletion of a single substrate S_i in a b-PBR system is shown to limit the growth of the microalgae, as described in Fig. 3.3. This analysis is extended to the specific case of sunlight as substrate, which is not exhausted with the b-PBR, but instead varies diurnally, resulting in a sawtooth microalgae growth dynamic, as described in Fig. 3.4. As was described in Chapter 2, the sunlight intensity may be such that it limits growth through photoinhibition, a concept introduced using a comparison between the Monod and Haldane growth rates as described in Fig. 3.5. A brief review of the empirical derivation of the maximum specific growth rate μ_{max} was presented. As described in Table 3.1, there exists a large variance in the literature for values of μ_{max} , even in systems using the same microalgae species. This is a consequence of the individual PBR system dynamics that are present in these studies, and as such, this thesis will utilize a sensitivity analysis in the modeling characterization of the BIMP system.

The analysis of the growth rate for a single-limiting substrate is extended to the case of multiple-limitation dynamics, where two or more substrate $S_1, S_2, S_3, \dots, S_n$ can co-limit growth, as described using the multiplicative growth rate. For the scenario of

two co-limiting substrates S_1 and S_2 , the multiplicative growth rate is describe in Fig. 3.6. The multiplicative growth rate expression is then generalized in terms of a specific limiting function $f(L_n)$, and applied to the BIMP system by defining four unique limiting functions, one each for sunlight $f(\bar{I}_{avg})$, culture temperature $f\left(T_{avg}\right)$, nutrients $f\left(\left[S_{tot,i}\right]_L\right)$, and CO_2 $[CO_2]_L$. The analysis of a single limiting function $f(\bar{I}_{avg})$ on the growth dynamic in the BIMP system is the subject of Chapter 4. The analysis of BIMP system multiplicative growth kinetics $f(\bar{I}_{avg}) \cdot f\left(T_{avg}\right)$ is the subject of Chapter 5.

Chapter 4 Modeling Light Dynamics in a BIMP System

4.1 Introduction

As described in Chapter 2, microalgae grown in PBR systems have specific light requirements that must be maintained to ensure photosynthesis is not limited or inhibited. As such, this chapter presents an analysis of the single-limitation growth dynamics in the BIMP system, as defined by the available outdoor PPFD resource.

4.2 System Description

The influence of light on biomass growth as described in this chapter includes the definition of the total monthly average daily solar resource incident on a horizontal terrestrial surface, and the conversion of this to a monthly average hourly vertical solar resource $\overline{I}_t$. As stated in Chapter 3, the influence of indoor light on the BIMP system is neglected. The hourly solar radiation is then reduced by two mechanistic principles: the first reduction is to quantify the PPFD value that could be utilized by microalgae for photosynthesis; the second reduction is a result of reflecting a small portion of the PPFD from the exterior vertical translucent material surface of the BIMP system. These considerations and the BIMP system analyzed in this section are presented in Fig 4.1.

The average PPFD available for photosynthesis $\overline{I}_{avg}$ at any depth d within the BIMP system is determined using the Beer-Lambert relationship, which is spatially averaged throughout the rectangular culture profile. Here it is assumed that the BIMP has an illuminated culture surface area of 1 m^2. Finally the biological utilization of light by microalgae in the BIMP system is described using two kinetic theories for growth.

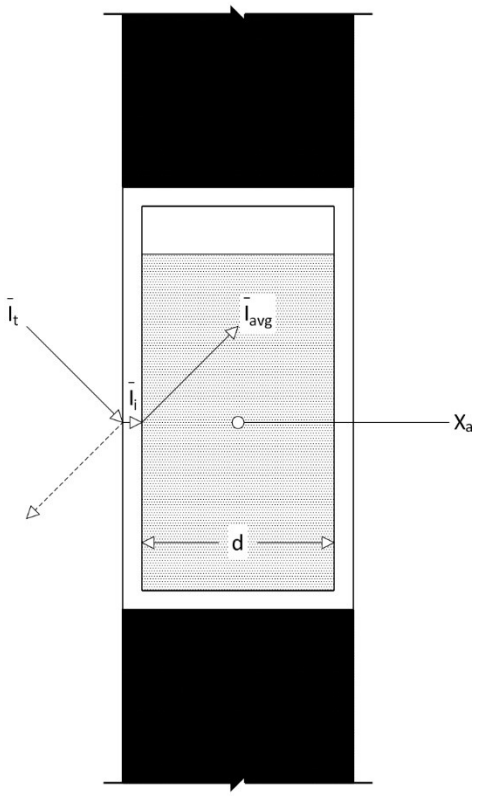

Fig. 4.1. Schematic for light interaction in BIMP system.

4.3 Mathematical Model

Using Eq. 3.12 in Chapter 3 with the specific light-growth rate function, the biomass growth rate for the light-limited BIMP system can be calculated using:

$$\frac{dX_a}{dt} = \left[\mu_{max} \cdot f_i\left(\overline{I}_{avg}\right) - \mu_d\right] \cdot X_a \qquad 4.1$$

where $\overline{I}_{avg}$ is the spatially-averaged PPFD in the BIMP system, as defined in Chapter 3 for both Monod and Haldane kinetics. The following section describes the model inputs, including any assumptions that are made. The model is based on the theoretical cultivation of the microalgae species *C. vulgaris*.

4.3.1 Solar model

For the determination of incident solar radiation on a vertical surface in Halifax, published meteorological data, as described in Table 4.1, are here utilized.

Table 4.1: Meteorological Data for Halifax Nova Scotia Canada (adapted from Green Power Labs, 2009; Duffie and Beckman, 2006).

	Jan	Feb	Mar	Apr	May	Jun	Jul	Aug	Sep	Oct	Nov	Dec
N	17	47	75	105	135	162	198	228	258	288	318	344
$\overline{H}$	5.58	8.78	12.64	15.52	18.07	19.98	19.73	17.57	14.33	9.65	5.69	4.54
$\overline{K_t}$	0.41	0.46	0.48	0.44	0.44	0.48	0.47	0.50	0.50	0.45	0.39	0.35
ρ_g	0.70	0.70	0.40	0.30	0.20	0.20	0.20	0.20	0.20	0.30	0.40	0.70

The assumed ground reflectance values presented in Table 4.1 are based on those found in the literature corresponding to winter months with high reflectance due to snow cover, and summer months with low reflectance due to vegetation and absorptive materials such as asphalt. For the purposes of the analysis presented in the Results section, the dynamics of light-growth in the BIMP system will be simulated for the four equinox months of March, June, September, and December. It is assumed that these four months will be sufficient to characterize light in the BIMP system.

4.3.2 Biological model

The growth of microalgae in the BIMP system is assumed to follow batch dynamics, as described by Eq. 3.12 in the previous chapter. The specific biological parameters for *C. vulgaris* that are used in the simulation efforts here presented are summarized in Table 4.2.

Table 4.2: Summary of BIMP Light Model Parameters for Microalgae Species *C. vulgaris*.

Parameter	Nomenclature	Value	Unit	Reference
Mass attenuation coefficient	k_m	0.334	$m^2\ g^{-1}$	Huesemann et al., (2013)
Culture depth	d	0.05	m	Hu et al., (1996)
Half-saturation constant	K_s	15.90	$\mu mol\ m^{-2}\ s^{-1}$	Yun and Park, (2003)
Light inhibition constant	K_i	200	$\mu mol\ m^{-2}\ s^{-1}$	Kumar et al., (2011)
Maximum growth rate	μ_{max}	0.07	h^{-1}	Huisman et al., (2002)
Microalgae loss rate	μ_d	0.006	h^{-1}	Concas et al., (2012)

As was described in Chapter 3, a great deal of variation exists in the literature for the values presented in Table 4.1. An effort has been made to use median or common values from the literature, and a sensitivity analysis in the following section was used to determine the validity of this parameterization. For the purposes of the modeling study, it is assumed that the microalgae are well mixed and uniformly distributed throughout the BIMP culture, that there are no other limitation mechanisms in the BIMP system other than light, and that the physical characteristics of the *C. vulgaris* do not change during the length of the simulation.

4.4 Results

To validate the solar model, the following comparison between reported values for the monthly average daily solar radiation on vertical surface in Halifax (Green Power Labs, 2009) to that calculated by the solar model presented in this chapter is made. The comparison was achieved by summing the monthly average hourly values calculated, and converting to the same unit set as was used in the published work. These results are presented in Fig. 4.2.

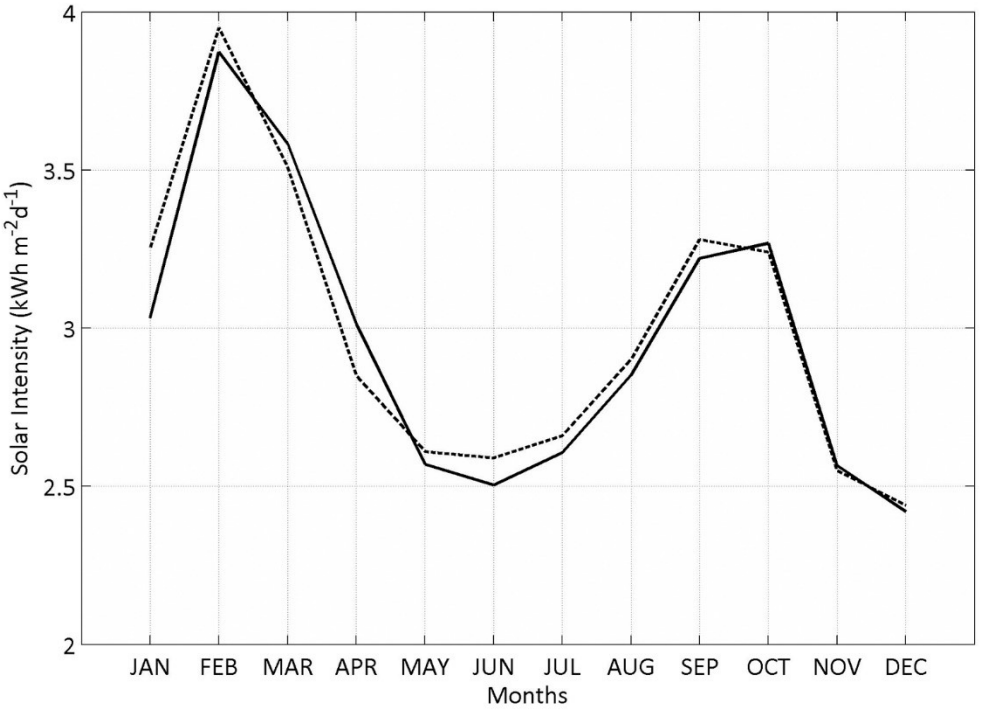

Fig. 4.1. A comparison between published Green Power Labs (2009) data (dashed line) and calculated (solid line) data for the monthly average daily full-spectrum solar radiation on a vertical surface facing due South in Halifax Nova Scotia Canada.

A good agreement is seen in Fig. 4.2 between the published and calculated solar intensities, indicating that the solar radiation model has a high degree of fitness. The solar model is spatially-averaged through the BIMP depth using Eq. 3.41, and a seven-day simulation was run in MATLAB using and Euler approximation with a time step of 0.042, and an initial microalgae concentration of 1 g L^{-1} for each of the four equinox months using both Monod and Haldane kinetics, as described in Fig. 4.3.

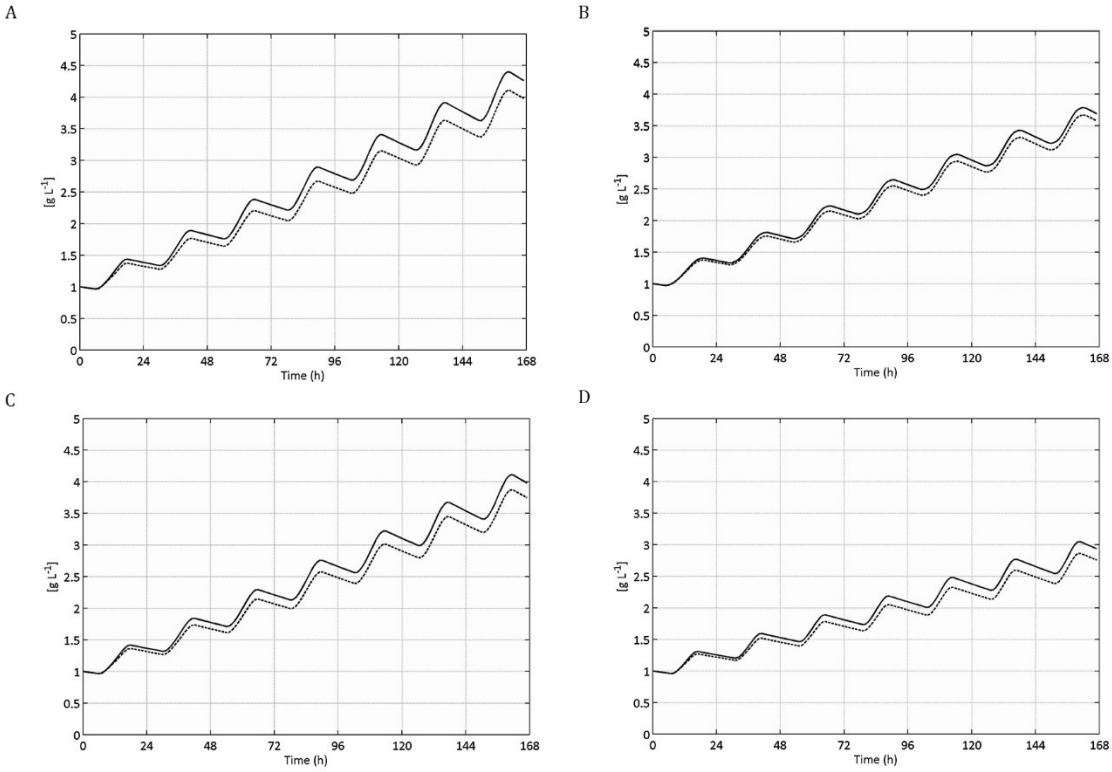

Fig. 4.3. MATLAB simulation of BIMP biomass growth dynamics over seven days as characterized by Monod (solid line) and Haldane (dashed line) kinetic expressions, for spatially-averaged culture PPFD in Halifax Nova Scotia Canada. (A) March (B) June (C) September (D) December. Parameterization based on values given in Table 4.1 for solar model, and Table 4.2 for biological models.

The final microalgae density in the BIMP system for each of the four months described in Fig. 4.3 is summarized in Table 4.3.

Table 4.3: Final BIMP Biomass Concentrations After seven-day Growth Simulation for the Four Equinox Months When Starting from a Concentration of 1 g L^{-1} Microalgae Biomass in the System.

Month	Monod (g L^{-1})	Haldane (g L^{-1})	Reduction
March	4.40	4.12	-6.7%
June	3.79	3.67	-3.2%
September	4.11	3.87	-5.8%
December	3.05	2.86	-6.2%

4.5 Sensitivity Analysis

A graphical method (Frey and Patil, 2002) is here employed to perform a sensitivity analysis on selected inputs to the light-growth model. The sensitivity analysis increased and decreased Monod parameter values by ± 20%, and the MATLAB simulation was performed to determine the biomass concentration after seven-days, as compared to a normal value of 4.40 g L^{-1}, as given in Table 4.3 for the Monod simulation in March. A tornado plot was then generated from these tabulated data, as shown in Fig. 4.4.

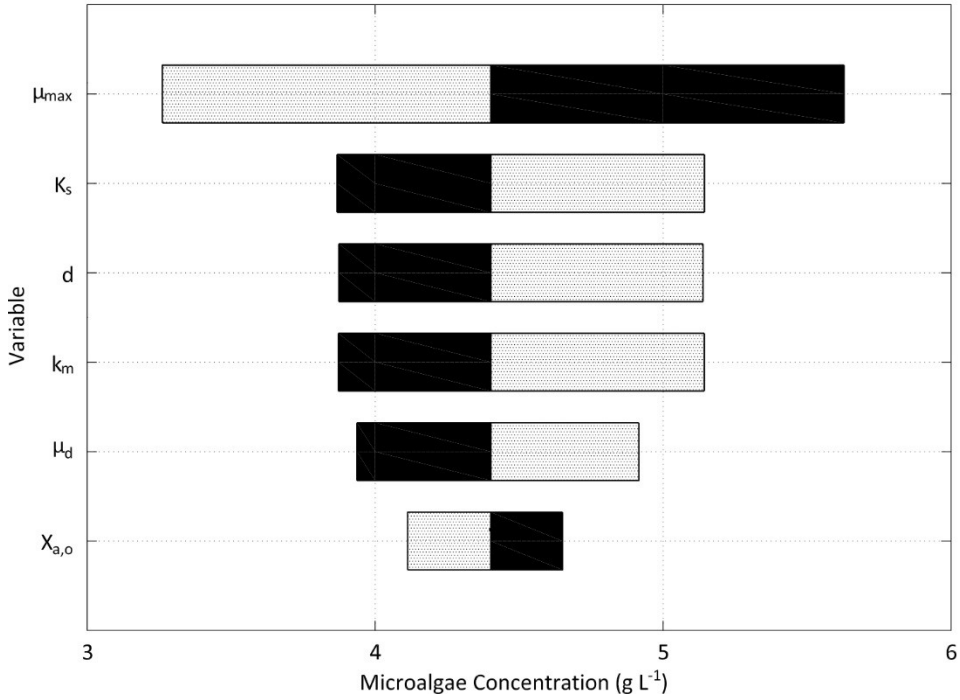

Fig. 4.4. Tornado plot showing the sensitivity of BIMP light-growth model inputs when varied by ± 20% of their nominal value. Hatch bar indicates change in parameter value of -20%. Solid bar indicates change in parameter value of +20%.

4.6 Discussion

As described in Fig. 4.3, there is a relatively small reduction in overall BIMP culture density after the seven-day simulation as a result of using the Haldane expression to

account for photoinhibition. This is due to two separate but coupled conditions. First, Halifax has a comparatively low solar intensity as compared to the average PPFD reported in Chapter 2 that reaches a horizontal surface. Second, when the horizontal solar resource is converted to a vertical solar resource, this PPFD is again reduced. The modest reduction in overall microalgae density that results from using the Haldane kinetics is in good agreement with the work of Cuaresma et al., (2011), who suggest that photoinhibition is rarely seen in a vertical flat-plate-type PBR, even in regions where the PPFD is much greater than Halifax. For an initial microalgae concentration of 1 g L^{-1}, the BIMP system here described is able to increase the density to at least 3 g L^{-1} at the end of the seven-day simulation for each of the four months described here. These data are in good agreement with the work of Quinn et al (2011), whose modeling efforts are based on empirical data collected from an industrial PBR system, and describe a similar increase in microalgae density over the same time period. This suggests that the BIMP system will not be light limited during the daytime in the Halifax region, and will have a biomass productivity consistent with the literature.

The sensitivity of the parameters described in Fig. 4.4 and used in light-growth modeling also support this preliminary conclusion, as a change of ± 20% does not dramatically decrease the overall growth potential of the BIMP system. The outlier to this statement is the maximum growth rate, which is shown to have the most significant impact as a parameter on the light-growth dynamics in the BIMP system. To improve the confidence in the parameterization of the maximum growth rate for the BIMP system, laboratory experiments where *C. vulgaris* populations are grown as a function of time under solar conditions similar to those here presented are required. Perhaps the most interesting outcome of the sensitivity analysis is the increase in overall productivity of the BIMP system when the culture depth d is decreased. A reduction in cultural depth by definition must increase the spatially averaged PPFD using the Beer-Lambert expression, creating greater availability of photons for

microalgae photosynthesis. This result, along with other considerations from this chapter, will be discussed in greater detail in Chapter 6.

Chapter 5 Modeling Temperature Dynamics in a BIMP System

5.1 Introduction

In addition to light, photoautotrophic organism survival and growth is strongly dependent on the temperature of the ecological system which they inhabit. For microalgae grown in a BIMP system, this habitat is the enclosed aqueous culture medium, which is subject to both outdoor and indoor environmental factors. As such, this chapter presents an analysis of the multiplicative growth dynamics in a BIMP system, as defined by the culture temperature and the availability of light.

5.2 System Description

The influence of temperature on biomass growth as described in this chapter includes the definition of the amount of solar radiation incident on the exterior surface of the BIMP, the mechanism of heat transfer resulting from this solar resource passing through each material phase of the BIMP assembly, and the resulting temperature profile within. Concurrently, the influence of the outdoor and indoor ambient temperatures on transient heat transfer mechanisms to and from the BIMP system are described. A schematic showing these heat transfer mechanisms as they relate to the BIMP system is described in Fig. 5.1.

Several assumptions are made with respect to the formulation of the temperature-growth model presented in this chapter. First, it is assumed that the BIMP operates in a fed-batch mode with an illuminated culture surface area of 1 m^2, with both the interior and exterior BIMP translucent surfaces constructed of the same material. The BIMP culture medium is assumed to be completely mixed, with all physical properties, including temperature, considered to be uniform.

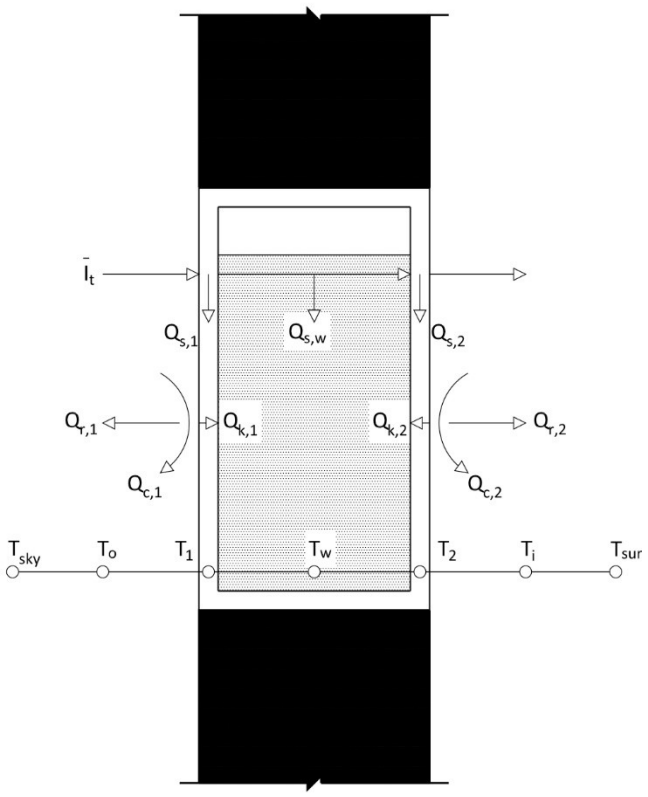

Fig. 5.1 Schematic for temperature interaction in the BIMP system

Additionally, as microalgal density and nutrient concentration in the BIMP are generally low (of the order 1 g L^{-1}), the culture medium thermophysical properties are considered equivalent to those of water at standard temperature and pressure. The BIMP headspace is assumed to be at the same temperature as the culture medium, and saturated with water. There is therefore no evaporative heat transfer from the top surface of the BIMP culture medium to the headspace. The temperature across the outside and inside translucent surfaces are assumed constant throughout the material, and thus the material temperature gradient is neglected. Additionally, the heat gain in the culture medium caused by microalgal metabolism is neglected. Finally, the fraction of solar radiation converted into algal biomass during photosynthesis is assumed constant and equal to 2.5% of the full spectrum incident solar radiation (Bechet et al., 2010).

5.3 Mathematical Model

Using Eq. 3.12 in Chapter 3 with the multiplicative growth rate function given in Eq. 3.20, the biomass growth rate for the light and temperature limited BIMP system can be calculated using:

$$\frac{dX_a}{dt} = \left[\mu_{max} \cdot f\left(\bar{I}_{avg}\right) \cdot f(T_w) - \mu_d\right] \cdot X_a \qquad 5.1$$

where $\bar{I}_{avg}$ and T_w are the spatially-averaged PPFD and BIMP culture temperature, respectively, as defined in Chapter 3. The following section describes the model inputs, including any assumptions that are made. The model is based on the theoretical cultivation of the microalgae species *C. vulgaris*.

5.3.1 Temperature model

The data described in Table 5.1 are used for the determination of the outdoor temperature and wind speed in Halifax.

Table 5.1: Outdoor Temperature Statistics and Double Cosine Model Calibration Data for Halifax Nova Scotia Canada (Environment Canada, 2015; Chow and Levermore, 2007).

Month	N	T_{min} (°C)	$t_{T_{min}}$	T_{max} (°C)	$t_{T_{max}}$	T_{amp} (°C)	Wind (m s^{-1})
January	17	-8.2	14	-0.1	6	8.1	6.3
February	47	-7.5	14	0.4	6	7.9	6.2
March	75	-3.9	14	3.6	5	7.5	6.1
April	105	1.0	15	8.7	5	7.7	5.6
May	135	5.8	15	14.4	4	8.6	5.0
June	162	10.7	16	19.6	4	8.9	5.0
July	198	14.4	15	23.1	4	8.7	4.4
August	228	15.1	15	23.1	5	8.0	4.2
September	258	11.8	15	19.3	5	7.5	4.5
October	288	6.4	14	13.4	6	7.0	5.3
November	318	1.5	14	8.1	6	6.6	6.2
December	344	-4.3	14	2.8	7	7.1	6.4

From the data presented in Table 5.1, an average wind speed of 5.3 m s^{-1} is assumed. The BIMP interior and exterior surface are assumed to be equivalent, and to have thermophysical properties akin to glass. For a depth of 6 mm, the glass interior and exterior BIMP surface is assumed to have a mass of 14 kg (Duffie and Beckman, 2006). The BIMP culture medium is assumed to have a depth of 0.05 m. The outdoor temperature is variable throughout the day, as described in Eq. 3.50-3.52, meaning that the effective sky temperature T_{sky} will also be variable, as per Eq. 3.49. Table 5.2 presents the numerical values for the parameters used in the temperature model.

Table 5.2: Summary of BIMP Heat Transfer Model Parameters.

Parameter	Nomenclature	Value	Unit	Reference
Thickness of glass	d_1, d_2	0.006	m	(-)
Mass of glass	m_1, m_2	14	kg	Duffie and Beckman, (2006)
Heat capacity of glass	$C_{p,1}, C_{p,2}$	750	J kg^{-1} K^{-1}	Incropera et al., (2007)
Conductivity of glass	k_1, k_2	1.4	W m^{-1} K^{-1}	Incropera et al., (2007)
Absorptivity of glass	α_1, α_2	0.05	(-)	Goetz et al., (2011)
Emissivity of glass	$\varepsilon_1, \varepsilon_1$	0.92	(-)	Goetz et al., (2011)
Transmissivity of glass	τ_1, τ_2	0.95	(-)	Goetz et al., (2011)
Thickness of water	d_w	0.05	m	(-)
Mass of water	m_w	50	kg	(-)
Heat capacity of water	$C_{p,w}$	4180	J kg^{-1} K^{-1}	Goetz et al., (2011)
Absorptivity of water	α_w	0.90	(-)	Goetz et al., (2011)
Transmissivity of water	τ_w	0.10	(-)	Bechet et al., 2010)
Wind velocity	V	5.43	m s^{-1}	Table 5.1
Indoor temperature	T_i, T_{sur}	294	K	(-)
Outdoor conv. coefficient	$h_{c,1}$	26.35	W m^{-2} K^{-1}	Eq. 5.9
Indoor conv. coefficient	$h_{c,2}$	5.7	W m^{-2} K^{-1}	Carlos et al., (2011)
Conduction coefficient	$h_{k,1}$, $h_{k,2}$	233.33	W m^{-2} K^{-1}	Eq. 510

For the purposes of the analysis presented in the Results section, the dynamics of temperature-growth in the BIMP system were simulated for the four equinox months of March, June, September, and December. It is assumed that these four months are sufficient to characterize temperature in the BIMP system.

5.3.2 Biological model

The growth of microalgae in the BIMP system is assumed to follow batch dynamics, as described by Eq. 3.12. The specific biological parameters for *C. vulgaris* that were used in the simulation are summarized in Table 5.3. It is assumed that the physical characteristics of *C. vulgaris* described in Table 5.3 do not change during the length of the simulation.

Table 5.3: Summary of BIMP Temperature Model Parameters for Microalgae Species *C. vulgaris*.

Parameter	Nomenclature	Value	Unit	Reference
Activation energy	E_a	62.5	kJ mol^{-1}	Cen and Sage, (2005)
Gas constant	R	8.314	J K^{-1} mol^{-1}	(-)
Optimal temperature	T_{opt}	305.4	K	Mayo, (1997)

5.4 Results

The variation in daily temperature for each of the four months here considered is based on data for average outdoor conditions in Halifax over an approximately 30-year time span. The daily variations in outdoor temperature calculated from Eq. 3.50-3.52 for the equinox months are presented in Fig. 5.2. These data represent the initial system temperature, and the hourly outdoor temperatures used in the analysis of the BIMP temperature dynamics. The temperature change in the indoor and outdoor BIMP surface temperatures, as well as the BIMP culture temperature that occur during this diurnal temperature variation are also presented in Fig. 5.2.

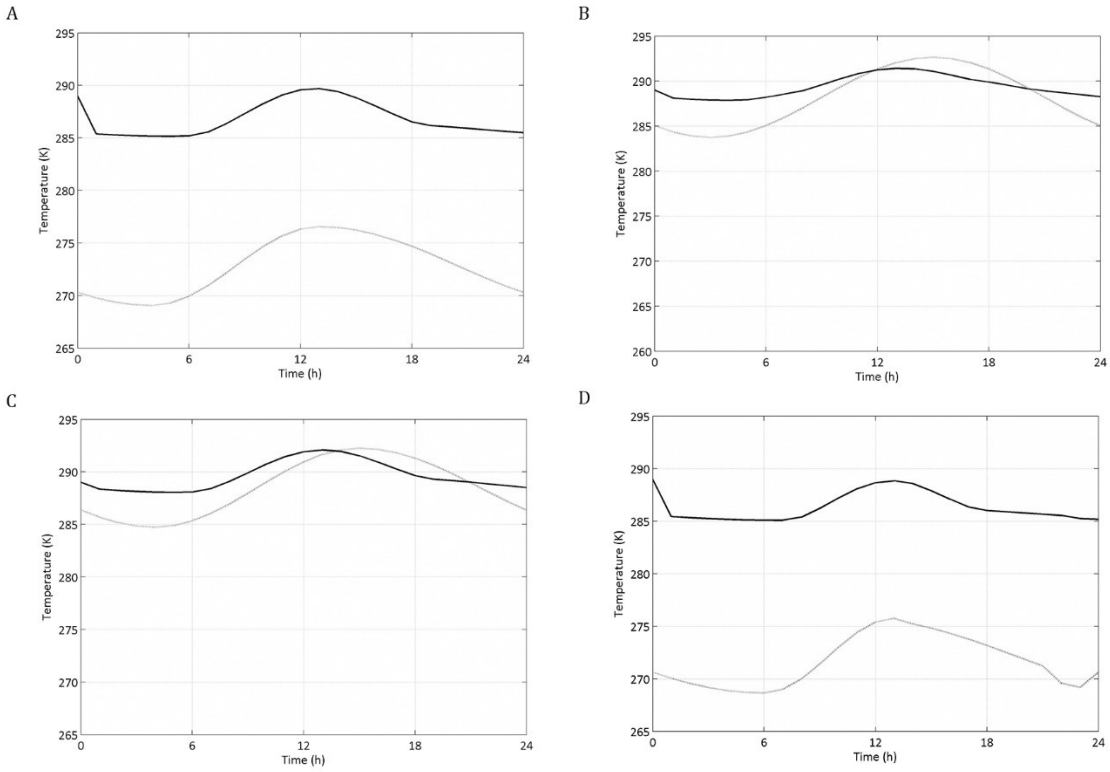

Fig. 5.2. MATLAB simulation of daily variation in outdoor temperature (dashed line) and the resultant BIMP culture temperature (solid line) for the four equinox months in Halifax Nova Scotia Canada. (A) March (B) June (C) September (D) December. Parameterization based on values given in Table 5.2

These temperature dynamics were used in a seven-day simulation was run in MATLAB using and Euler approximation with a time step of 0.042, and an initial microalgae concentration of 1 g L^{-1} for each of the four equinox months with the multiplicative growth dynamics described by Eq. 5.21. An initial system temperature for all months is assumed to be equal to the indoor temperature, or 294 K. These results are compared to the growth dynamics achieved using Monod kinetics in Chapter 4, and are presented in Fig. 5.3.

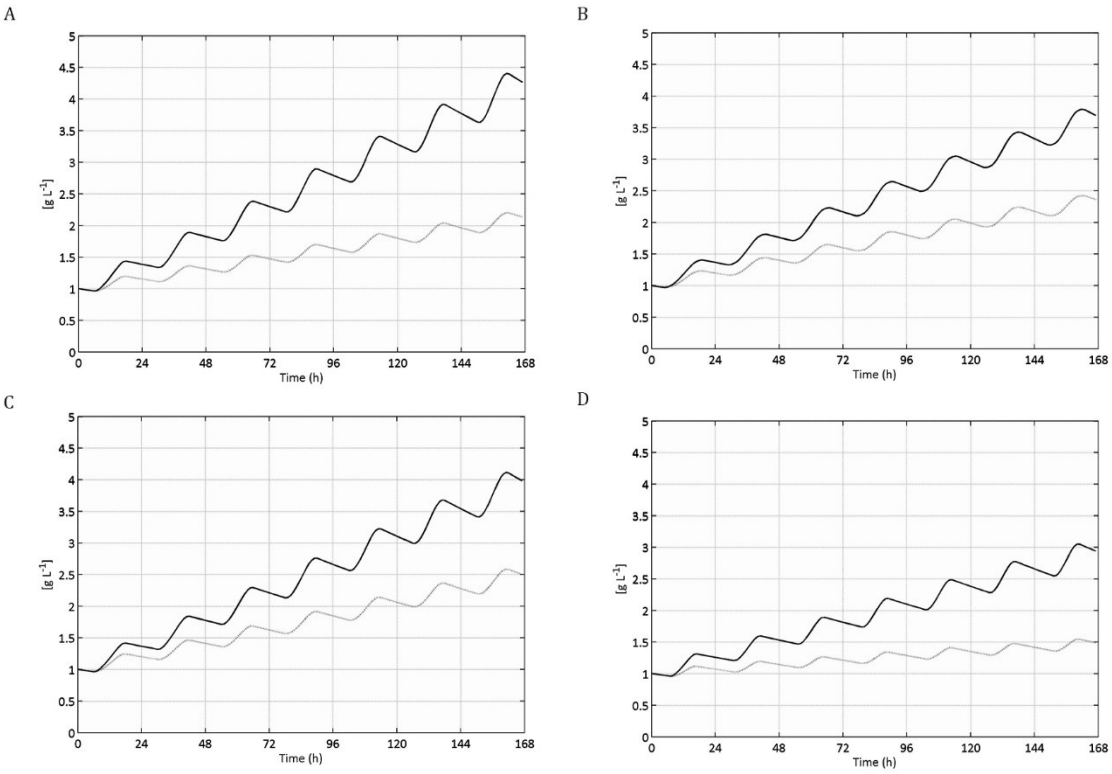

Fig. 5.3. MATLAB simulation of BIMP biomass growth dynamics over 7 days as characterized by Monod (solid line) kinetics for light, and multiplicative (dashed line) kinetic for light-temperature, in Halifax NS Canada. (A) March (B) June (C) September (D) December. Parameterization based on values given in Table 4.1 for solar model, and Tables 5.1 and 5.2 for temperature model, and Tables 4.2 and 5.3 for light and temperature biological models, respectively.

The final microalgae density in the BIMP system for each of the four months described in Fig. 5.3 is summarized in Table 5.4.

Table 5.4: Final BIMP Biomass Concentrations after Seven-Day Growth Simulation for the Four Equinox Months When Starting from a Concentration of 1 g L^{-1} Microalgae Biomass in the System.

Month	Monod (g L^{-1})	Multiplicative (g L^{-1})	Reduction
March	4.40	2.20	-50.0%
June	3.79	2.42	-36.1%
September	4.11	2.58	-37.2%
December	3.05	1.55	-49.2%

5.5 Sensitivity Analysis

The most significant new parameter with a high level of sensitivity presented in this chapter is the optimal growth temperature of the microalgae species, or T_{opt} as described in Table 5.3. Here, this value has been parameterized based on published data for the *C. vulgaris* species. However, if this value were to be lowered from its current value of 32.4 ^{0}C to 25 ^{o}C, the biomass output in September would be equal to 3.87 g L^{-1} after seven-days of growth, or at the industry standard of 3 g L^{-1} for growth in outdoor PBR systems during the same time span.

5.6 Discussion

Apparent from Fig. 5.3 is the damped growth dynamic of the temperature-light multiplicative growth kinetic as compared with the Monod analysis completed in the previous chapter. Counterintuitively, this drastic reduction in overall biomass yield after the seven-day simulation is not a result of too much heat in the system, but instead not enough. As described in Fig. 5.2, the diurnal increase in BIMP system temperature lags behind the increase in outdoor temperature, as would be expected. However, the BIMP system does not increase in temperature, even during the summer months, in any appreciable manner. This is a consequence of three system factors. First, the empirical relationships used to estimate the diurnal change in the hourly outdoor temperature value may underestimate the actual conditions. For instance, the model predicts for September (N = 258) a maximum daily temperature of 19.3 ^{o}C, whereas a simple survey of recent Environment Canada would suggest an average maximum daily temperature at least 3 ^{o}C warmer for the same September day of year. Secondly, variations in the indoor diurnal temperature profile are not considered at all, and instead a constant indoor temperature of 21 ^{o}C is assumed to be continuously maintained. However, to model the indoor temperature more accurately, a specific architectural scenario would have to be considered, which is outside the scope of this thesis.

The third factor affecting the temperature profile in Fig. 5.2 is a consequence of parameterizing the thermophysical properties of the system as akin to a window system, not a solar thermal device. However, such a parameterization is important to the adaptive design methodology used in this thesis, and will be discussed in more detail in Chapter 6. Of additional interest in the analysis presented in Chapter 6 is the improvement in overall biomass yield with a reduction in the optimal growth temperature described in Table 5.3.

Chapter 6 Conclusions

The work presented in this thesis toward the characterization of a building-integrated microalgae bioreactor (BIMP) system lends itself to several conclusions that can be used in an adaptive methodology. These conclusions are summarized in this chapter.

In Chapter 1, it was shown that urban regions require large extra-urban ecosystems both for the delivery of consumable materials, and for the discharge of waste generated through this consumption. This thesis investigated whether buildings can be designed as part of a larger urban metabolism theory, wherein the production of consumables is directly linked to the bioregeneration of wastes in the buildings themselves via a BIMP system. This chapter examines whether a BIMP system can be applied buildings to function in a similar way as the closed ecological life support systems (CELSS) developed by NASA. An important conclusion from Chapter 1 was reached in that, although similar to the CELSS systems in many respects, the BIMP system must consider both the indoor and outdoor environments through its design.

Chapter 2 described the design and function of the BIMP system, and how it will be based on flat-plate type photobioreactor (PBR) technology. Chapter 2 concludes that this type of PBR has the most appropriate set of design characteristics, for a BIMP system integrated in a building. The concept of a biological building system (BBS) is introduced, and is used to develop a criterion of analysis for the BIMP system. With respect to the abiotic waste/resource dynamics that are available in the BBS, it is concluded in this chapter that light, temperature, nutrients and CO_2 are the most important abiotic resource systems that must be characterized in the adaptive design of the BIMP system. Light is described as optimized in solar conditions that deliver a photosynthetically-active photon flux (PPFD) at or near the light saturation value of the microalgae, equivalent to a PPFD of approximately 200 μmol m^{-2} s^{-1} for most microalgae species. As typical solar PPFD intensities can reach at least ten times the

saturation, it is concluded in this chapter that characterizing the light-growth dynamic in the BIMP system is the most important adaptive design consideration. Temperature is described as affecting both light utilization and maximum growth rates in microalgae PBR systems. As a mediator between the indoor and outdoor environments, the characterization – and control - of the temperature-growth dynamic in the BIMP system is concluded to be the second most important characteristic in the adaptive design methodology. Both nutrients and CO_2 are described as waste products in the built environment, and their availability is concluded to be of sufficient quantity to not warrant consideration in the adaptive design methodology.

According to Chapter 3, the modeling of microalgae PBR systems is fundamentally akin to the modeling of biological continuously-stirred tank reactors (CSTR). The BIMP system is defined as operating as a batch system, with both Monod and Haldane kinetics governing the growth rate expression. According to Fig. 3.4, modeling light-growth dynamics using Monod kinetics in a PBR system results in a sawtooth-type behaviour, where the diurnal light/dark cycle describes system growth and decay, respectively. According to Fig. 3.5, using Haldane kinetics to describe inhibition results in a significant reduction in the growth rate in PBR system when substrate levels are above saturation concentrations. According to Fig. 3.6, applying multiplicative Monod kinetics will dampen the overall biomass yield in PBR systems. An important conclusion from these analyses is the need to include multiplicative kinetics when characterizing the BIMP system. A final important conclusion from this chapter is that the parameterization of models used to describe the BIMP growth dynamic involves a great deal of uncertainty, e.g the effect of glare from other buildings and snow that would provide a net photon gain on the BIMP surface, wind chill impacts, poisoning of the microalgae by unwanted chemicals in residential grey water or competition from unwanted bacteria, mould, and other microalgae for nutrients and light.

According to Chapter 4, the BIMP system is south-facing and vertically oriented. The incident solar resource is modeled using the Isotropic Diffuse Sky Model for Halifax Nova Scotia Canada. An important conclusion here is that the total solar intensity incident on a vertical surface must be attenuated by both biological and mechanistic considerations in the BIMP system. Toward the former, the PPFD useful for photosynthesis is defined as 45.8% of incident solar intensity. Toward the latter, the translucent exterior BIMP surface is defined as transmitting 89% of the incident PPFD. This PPFD is spatially averaged in the BIMP system using the Beer-Lambert expression, and both Monod and Haldane kinetics are considered in the MATLAB growth rate simulation. According to Fig. 4.2, the Isotropic Diffuse Sky Model is able to accurately predict the solar intensity on a vertical surface in Halifax. According to Fig. 4.3, the BIMP system does not show a significant reduction in biomass density after a seven-day growth period as a result of photoinhibition, and is able to produce biomass densities consistent with those reported in the literature for similar growth periods. Of the four equinox months for which the BIMP growth dynamics were simulated, March produced the highest biomass density; from an initial microalgae density of 1 g L^{-1} in the BIMP system, the model predicts a final biomass density of 4.12 g L^{-1} after the seven-day simulation, with a reduction of 6.7% when utilizing inhibitory kinetics. According to Fig. 4.4, the BIMP-light growth model is most sensitive to the parameterization of the maximum growth rate μ_{max}. An important conclusion from the sensitivity analysis is that the growth rate is inversely proportional to the culture depth d of the BIMP system. This means that for shorter light paths, microalgae in the BIMP system grow faster. If the growth rate is faster in short light path conditions, then density will increase to harvest levels in a shorter time span. To support these faster growth dynamics, the BIMP system will require nutrient and CO_2 resources at an accelerated rate, perhaps beyond the rate that they are produced within an urban environment. The design of the BIMP system will therefore need to adapt to the availability of these resources, with the culture depth and microalgae density optimized for the bioregeneration of these resources.

According to Chapter 5, modeling the temperature dynamics in the BIMP system presents a novel scenario not seen in the literature, as it is dependent on both the indoor and outdoor environmental conditions. The heat transfer mechanisms considered in the mathematical analysis presented in this chapter include solar gain, radiation from the BIMP, convection from the outer surfaces of the BIMP, and conduction from the BIMP culture to the indoor and outdoor environments. The diurnal variation in outdoor temperature in Halifax is described using the Double Cosine Model. The effect of temperature on the growth dynamic in the BIMP system is based on the activation of RuBisCo enzyme, with multiplicative kinetics. According to Fig. 5.2, the increase in BIMP temperature during the diurnal cycle is not significant. This is due to the temperature model being parameterized with properties consistent with those of a window system, rather than those of a solar thermal device. An important design conclusion is that these parameters need careful consideration to optimize the growth rate of the microalgae, but to also afford light penetration through the BIMP to the indoor environment. According to Fig. 5.3, the growth in the BIMP is significantly reduced as a result of using multiplicative kinetics to describe the light-temperature dynamics in the system. Of the four equinox months for which the BIMP growth dynamics were simulated, September produced the highest biomass density; from an initial microalgae density of 1 g L^{-1} in the BIMP system, the model predicts a final biomass density of 2.58 g L^{-1} after the seven-day simulation. Compared to the Monod kinetics described in Chapter 4, the use of multiplicative kinetics reduces the biomass yield in the BIMP system by 37.2% after the seven-day simulation. A sensitivity analysis on the parameters used in the RuBisCo activation kinetics demonstrates that the dramatic decrease in biomass density in the BIMP system is highly dependent on the optimal growth temperature for the specific microalgae species grown in the system. When the optimal temperature is reduced from the 32.4 ^{o}C defined for *C. vulgaris*, to 25 ^{o}C, the density in the BIMP system for June increases to 3.87 g L^{-1}. This leads to the conclusion that microalgae species selection is very important to the performance of the BIMP, with respect to both

optimizing the growth rate, and for the utilization of the system for the bioregeneration of urban wastes in buildings.

A summary of the adaptive design principles for the BIMP system determined through the research presented in this thesis are as follows. For a southward facing design, the BIMP system does not show a significant reduction in biomass yield due to photoinhibition if it were built in Halifax. This means light augmentation would not required, resulting in a significant reduction in prototyping costs. When the thermophysical properties of the BIMP are defined as akin to a window system, there is no over-heating in the system, and in fact, the performance of the BIMP system suffers from having a culture temperature far below the optimum value. However, these thermophysical properties can be optimized for heat retention, thereby improving the growth dynamics, while at the same time still allowing light penetration to the interior environment. Finally, the selection of a microalgae species that is both cold tolerant and able to bioregenerate urban waste streams is crucial for the overall performance of the BIMP system.

References

Aiba, S. (1982). Growth kinetics of photosynthetic microorganisms. In Fiechter, A. (Ed.). *Microbial reactions*. Berlin, DE. Springer, 85-156.

Asenjo, J., and Merchuk, J. (1995). *Bioreactor system design* (Bioprocess technology; v. 21). New York, US: M. Dekker.

Bae, W., and Rittmann, B. (1996). A structured model of dual-limitation kinetics. *Biotechnology and bioengineering*, 49(6), 683-689.

Bailey, J., and Ollis, D. (1986). *Biochemical engineering fundamentals* (2nd ed., McGraw-Hill chemical engineering series). New York US: McGraw-Hill.

Baquerisse, D., Nouals, S., Isambert, A., dos Santos, P. F., and Durand, G. (1999). Modelling of a continuous pilot photobioreactor for microalgae production. *Journal of biotechnology*, *70*(1), 335-342.

Bechet, Q., Shilton, A., and Guieysse, B. (2013). Modeling the effects of light and temperature on algae growth: State of the art and critical assessment for productivity prediction during outdoor cultivation. *Biotechnology advances*, 31(8), 1648-1663.

Bechet, Q., Shilton, A., Fringer, O. B., Munoz, R., and Guieysse, B. (2010). Mechanistic modeling of broth temperature in outdoor photobioreactors. *Environmental science & technology*, 44(6), 2197-2203.

Bequette, B. (1998). *Process dynamics: Modeling, analysis, and simulation*. Upper Saddle River, US: Prentice Hall PTR.

Bernard, O., and Rémond, B. (2012). Validation of a simple model accounting for light and temperature effect on microalgal growth. *Bioresource Technology,* 123, 520-527.

Bilbao, J., De Miguel, A., and Kambezidis, H. (2002). Air temperature model evaluation in the north Mediterranean belt area. *Journal of Applied Meteorology*, 41(8), 872-884.

Borowitzka, M. (2013). High-value products from microalgae—their development and commercialisation. *Journal of Applied Phycology,* 25(3), 743-756.

Canada Mortgage and Housing Corporation. (2004). *Strategies for reducing building energy use via innovative building envelope technologies*. Ottawa: CMHC.

Cai, T., Park, S., and Li, Y. (2013). Nutrient recovery from wastewater streams by microalgae: Status and prospects. *Renewable and Sustainable Energy Reviews,* 19, 360-369.

Carlos, J., Corvacho, H., Silva, P., and Castro-Gomes, J. (2011). Modelling and simulation of a ventilated double window. *Applied Thermal Engineering*, 31(1), 93-102.

Carlozzi, P., and Sacchi, A. (2001). Biomass production and studies on Rhodopseudomonas palustris grown in an outdoor, temperature controlled, underwater tubular photobioreactor. *Journal of Biotechnology, 88*(3), 239-249.

Carvalho, A., Silva, P., Baptista, S., and Malcata, F. (2011). Light requirements in microalgal photobioreactors: An overview of biophotonic aspects. *Applied Microbiology and Biotechnology,* 89(5), 1275-1288.

Carvalho, A., Meireles, L., and Malcata, F. (2006). Microalgal reactors: a review of enclosed system designs and performances. *Biotechnology progress*, 22(6), 1490-1506.

Cen, Y., and Sage, R. (2005). The regulation of Rubisco activity in response to variation in temperature and atmospheric CO2 partial pressure in sweet potato. *Plant physiology*, 139(2), 979-990.

Chisti, Y. (1989). *Airlift Bioreactors*. London, UK: Elsevier

Chisti, Y. (2007). Biodiesel from microalgae.*Biotechnology Advances,* 25(3), 294-306.

Chisti, Y. (1989). *Airlift Bioreactors*. London: Elsevier.

Christenson, L., and Sims, R. (2011). Production and harvesting of microalgae for wastewater treatment, biofuels, and bioproducts. *Biotechnology Advances,* 29(6), 686-702.

Chwieduk, D. (2009). Recommendation on modelling of solar energy incident on a building envelope. *Renewable Energy*, 34(3), 736-741.

Concas, A., Lutzu, G. A., Pisu, M., and Cao, G. (2012). Experimental analysis and novel modeling of semi-batch photobioreactors operated with Chlorella vulgaris and fed with 100%(v/v) CO 2. *Chemical Engineering Journal*, 213, 203-213.

Cooney, M., Young, G., and Pate, R. (2011). Bio-oil from photosynthetic microalgae: case study. *Bioresource Technology.* 102 (1): 166-77.

Chow, D., and Levermore, G. (2007). New algorithm for generating hourly temperature values using daily maximum, minimum and average values from climate models. *Building Services Engineering Research and Technology*,28(3), 237-248.

Chow, T., Li, C., and Lin, Z. (2011a). The function of solar absorbing window as water-heating device. *Building and Environment*, 46(4), 955-960.

Chow, T., Li, C., and Lin, Z. (2011b). Thermal characteristics of water-flow double-pane window. *International Journal of Thermal Sciences*, 50(2), 140-148.

Cuaresma, M., Janssen, M., Vílchez, C., and Wijffels, R. (2011). Horizontal or vertical photobioreactors? How to improve microalgae photosynthetic efficiency. *Bioresource Technology,* 102(8), 5129-5137.

Dalrymple O., Halfhide T., Udom I., Gilles B., Wolan J., Zhang Q., and Ergas S. (2013). Wastewater use in algae production for generation of renewable resources: A review and preliminary results. *Aquatic Biosystems, 9*(1), 2.

Dauta, A., Devaux, J., Piquemal, F., and Boumnich, L. (1990). Growth rate of four freshwater algae in relation to light and temperature. *Hydrobiologia,* 207(1), 221-226.

Decker, E., Elliott, S., Smith, F., Blake, D., & Rowland, F. (2000). Energy and material flow through the urban ecosystem. *Annual Review of Energy and the Environment,* 251 (1), 685-740.

Despins, C., Farahbakhsh, K., and Leidl, C. (2009). Assessment of rainwater quality from rainwater harvesting systems in Ontario, Canada. *Aqua*, 58(2), 117.

Douskova, D., Doucha, J., Livansky, K., Machat, J., Novak, P., Umysova, D., Zachleder, V., and Vitova, M. (2009). Simultaneous flue gas bioremediation and reduction of microalgal biomass production costs. *Applied Microbiology and Biotechnology,* 82(1), 179-185.

Duffie, J., and Beckman, W. (2006). *Solar engineering of thermal processes* (3rd Ed.). Hoboken, US: Wiley.

Dunn, I., Heinzle, E., Ingham, J., and Prenosil, J. (2003). *Biological reaction engineering*. New York US: Wiley-VCH.

Eckart, P. (1996). Bioregenerative Life Support Concepts. In *Spaceflight life support and biospherics*. Dordrecht, NU: Springer, 249-364.

England, A., Duffin, A., Schwartz, C., Uejio, J., Prendergast, D., and Saykally, R. (2011). On the hydration and hydrolysis of carbon dioxide. *Chemical Physics Letters*, 514(4), 187-195.

Environment Canada. (2015). 1981-2010 Climate Normals & Averages for Halifax Citadel [Data file]. Retrieved from http://climate.weather.gc.ca/climate_normals/index_e.html

Eppley, R. (1972). Temperature and phytoplankton growth in the sea. *Fishery Bulletin*, 70(4), 1068-1085.

Erickson, L., Curless, C., and Lee, H. (1987). Modeling and Simulation of Photosynthetic Microbial Growtha. *Annals of the New York Academy of Sciences*, 506(1), 308-323.

Evers, E. (1991). A model for light-limited continuous cultures: Growth, shading, and maintenance. *Biotechnology and bioengineering*, 38(3), 254-259.

Evseev, E., and Kudish, A. (2009). The assessment of different models to predict the global solar radiation on a surface tilted to the south. *Solar Energy*, 83(3), 377-388.

Fernandez, F., Sevilla, J. and Grima, E. (2012). Principles of photobioreactor design. In Posten, C., Walter, C. (Eds.). *Microalgal biotechnology potential and production*. Boston, US: Walter de Gruyter, 151-180

Fernandez, F., Camacho, F., Perez, J., Sevilla, J., and Grima, E. (1998). Modeling of biomass productivity in tubular photobioreactors for microalgal cultures: Effects of dilution rate, tube diameter, and solar irradiance. *Biotechnology and Bioengineering,* 58(6), 605-616.

Filali, R., Tebbani, S., Dumur, D., Isambert, A., Pareau, D., and Lopes, F. (2011). Growth modeling of the green microalga Chlorella vulgaris in an air-lift photobioreactor. TIC, 10, 2.

Folke, C., Jansson, A., Larsson, J., and Constanza, R. (1997). Ecosystem appropriation by cities. *Ambio,* 26(3), 167-172.

Frey, H., and Patil, S. (2002). Identification and review of sensitivity analysis methods. *Risk analysis*, 22(3), 553-578.

Frost, B., and Franzen, N. (1992). Grazing and iron limitation in the control of phytoplankton stock and nutrient concentration: A chemostat analogue of the Pacific equatorial upwelling zone. *Marine Ecology Progress Series,* 83, 291-303.

Ganzer, B., and Messerschmid, E. (2009). Integration of an algal photobioreactor into an environmental control and life support system of a space station. *Acta Astronautica,* 65(1), 248-261.

Gavis, J., and Ferguson, J. (1975). Kinetics of carbon dioxide uptake by phytoplankton at high pH. *Limnology and Oceanography,* Mar (2), 211-221.

Gitelson, I., Lisovsky, G., and MacElroy, R. (2003). *Manmade closed ecological systems* (Earth space institute book series). London, UK: Taylor & Francis.

Goetz, V., Le Borgne, F., Pruvost, J., Plantard, G., and Legrand, J. (2011). A generic temperature model for solar photobioreactors. *Chemical Engineering Journal*, 175, 443-449.

Goldman, J., and Carpenter, E. (1974). A kinetic approach to the effect of temperature on algal growth 1. *Limnology and Oceanography,* 19(5), 756-766.

González-López, C., Acién Fernández, F., Fernández-Sevilla, J., Sánchez Fernández, J., and Molina Grima, E. (2012). Development of a process for efficient use of CO_2 from flue gases in the production of photosynthetic microorganisms. *Biotechnology and Bioengineering,* 109(7), 1637-50.

Green Power Labs Inc. (2009). Solar suitability assessment of Dalhousie University, Halifax NS. Retrieved from https://www.dal.ca/content/dam/dalhousie/pdf/sustainability/Dalhousie_Solar_Suitability_Assessment.pdf

Grima, E., Fernandez, F., Camacho, F., and Chisti, Y. (1999). Photobioreactors: light regime, mass transfer, and scaleup. *Journal of biotechnology*, 70(1), 231-247.

Grobbelaar, J. (2010). Microalgal biomass production: challenges and realities. *Photosynthesis research*, 106(1-2), 135-144.

Grobbelaar, J. (2004). Algal nutrition: mineral nutrition. In Richmond, A. (Ed.). *Handbook of microalgal culture: biotechnology and applied phycology*. Oxford, UK: Blackwell Science, 97-124.

Gutierrez, J., Porta-Gandara, M., and Fernandez, J. (2008). Passive temperature solar control of an outdoor photobioreactor. *Renewable Energy*, 33(8), 1892-1903.

Heilig, G. (2012). World urbanization prospects: the 2011 revision. *United Nations, Department of Economic and Social Affairs (DESA), Population Division, Population Estimates and Projections Section, New York*.

Harun, R., Singh, M., Forde, G., and Danquah, M. (2010). Bioprocess engineering of microalgae to produce a variety of consumer products. *Renewable and Sustainable Energy Reviews,* 14(3), 1037-1047.

Hausladen, G., Saldanha, M., and Liedl, P. (2012). *Building to suit the climate: A handbook*. Basel, CH: Birkhauser.

Ho, S., Chen, C., Lee, D., and Chang, J. (2011). Perspectives on microalgal CO_2 -emission mitigation systems — A review. *Biotechnology Advances,* 29(2), 189-198.

Hsieh, C., and Wu, W. (2009). Cultivation of microalgae for oil production with a cultivation strategy of urea limitation. *Bioresource technology*, 100(17), 3921-3926.

Hu, Q., Guterman, H., and Richmond, A. (1996). A flat inclined modular photobioreactor for outdoor mass cultivation of photoautotrophs. *Biotechnology and Bioengineering*, 51(1), 51-60.

Huesemann, M., Van Wagenen, J., Miller, T., Chavis, A., Hobbs, S., and Crowe, B. (2013). A screening model to predict microalgae biomass growth in photobioreactors and raceway ponds. *Biotechnology and bioengineering*, 110(6), 1583-1594.

Hulatt, C., and Thomas, D. (2011). Energy efficiency of an outdoor microalgal photobioreactor sited at mid-temperate latitude. *Bioresource technology*, 102(12), 6687-6695

Huisman, J., Matthijs, H., Visser, P., Balke, H., Sigon, C., Passarge, J., Weissing, F., and Mur, L. (2002). Principles of the light-limited chemostat: Theory and ecological applications. *Antonie Van Leeuwenhoek,* 81(1), 117-133.

Incropera, F., DeWitt, D., Bergman, T., and Lavine, A. (2007). *Fundamentals of heat and mass transfer* (6th ed.). Hoboken, US: Wiley.

Kalogirou, S. (2009). *Solar energy engineering processes and systems*. Burlington, US: Elsevier/Academic Press.

Kennedy, C., Pincetl, S., and Bunje, P. (2011). The study of urban metabolism and its applications to urban planning and design. *Environmental Pollution,* 159(8), 1965-1973.

Kibert, C., Sendzimir, J., and Guy, B. (2000). Construction ecology and metabolism: Natural system analogues for a sustainable built environment. *Construction Management and Economics,* 18(8), 903-916.

Kumar, K., Dasgupta, C., Nayak, B., Lindblad, P., and Das, D. (2011). Development of suitable photobioreactors for CO 2 sequestration addressing global warming using green algae and cyanobacteria. *Bioresource technology*, 102(8), 4945-4953.

Kurano, N., Ikemoto, H., Miyashita, H, Hasegawa, T., Hata, H., and Miyachi, S. (1995). Fixation and utilization of carbon dioxide by microalgal photosynthesis. *Energy Conversion and Management,* 36(6), 689-692.

Labis, Paulino E., Visande, Rey G., Pallugna, Reuel C., & Caliao, Nolan D. (2011). The contribution of renewable distributed generation in mitigating carbon dioxide emissions.*Renewable and Sustainable Energy Reviews, 15*(9), 4891-4896.

Laamanen, C., Shang, H., Ross, G., and Scott, J. (2014). A model for utilizing industrial off-gas to support microalgae cultivation for biodiesel in cold climates. *Energy Conversion and Management,* 88, 476-483.

Lacerda, L., Queiroz, M., Furlan, L., Lauro, M., Modenesi, K., Jacob-Lopes, E., and Franco, T. (2011). Improving refinery wastewater for microalgal biomass production and CO2 biofixation: Predictive modeling and simulation. *Journal of Petroleum Science and Engineering,* 78(3), 679-686.

Li, M., Hu, D., Liu, H. Hu, E., Xie, B., and Tong, L.. (2013). Chlorella vulgaris culture as a regulator of CO2 in a bioregenerative life support system. *Advances in Space Research,* 52(4), 773-779.

Liu, B., and Jordan, R. (1960). The interrelationship and characteristic distribution of direct, diffuse and total solar radiation. *Solar energy*, 4(3), 1-19.

Lee, Y. (2001). Microalgal mass culture systems and methods: their limitation and potential. *Journal of applied phycology*, 13(4), 307-315.

Loutzenhiser, P., Manz, H., Felsmann, C., Strachan, P., Frank, T., and Maxwell, G. (2007). Empirical validation of models to compute solar irradiance on inclined surfaces for building energy simulation. *Solar Energy*, 81(2), 254-267.

Mandalam, R., and Palsson, B. (1998). Elemental balancing of biomass and medium composition enhances growth capacity in high-density Chlorella vulgaris cultures. *Biotechnology and Bioengineering,* 59(5), 605-11.

Masojidek, J., Koblizek, M., and Torzillo, G. (2004). Photosynthesis in microalgae. In Richmond, A. (Ed.). *Handbook of microalgal culture: biotechnology and applied phycology*. Oxford, UK: Blackwell Science, 20-39

Mata, T., Martins, A., and Caetano, N. (2010). Microalgae for biodiesel production and other applications: A review. *Renewable and Sustainable Energy Reviews,* 14(1), 217-232.

Mayo, A. (1997). Effects of temperature and pH on the kinetic growth of unialga Chlorella vulgaris cultures containing bacteria. *Water environment research*, 64-72.

Miron, A., Garcia, M., Camacho, Francisco, Grima, E., and Chisti, Y. (2002). Growth and biochemical characterization of microalgal biomass produced in bubble column and airlift photobioreactors: Studies in fed-batch culture. *Enzyme and Microbial Technology,*31(7), 1015-1023.
Monod, J. (1949). The Growth of Bacterial Cultures. *Annual Reviews in Microbiology,* 3(11), 371-394.

Nelson, M., Pechurkin, N., Allen, J., Somova, L.., and Gitelson, J. (2010). Closed ecological systems, space life support and biospherics. In Wang, L., Ivanov, V., Tay, J., Hung, Y. (Ed.). *Environmental Biotechnology*. New York, US: Humana Press, 517-565.

O'Brien, W. (1974). The Dynamics of Nutrient Limitation of Phytoplankton Algae: A Model Reconsidered. *Ecology, 55*(1), 135-141.

Ogbonna, J., and Tanaka, H. (2000). Light requirement and photosynthetic cell cultivation–development of processes for efficient light utilization in photobioreactors. *Journal of applied phycology*, 12(3-5), 207-218.

Ogbonna, J., Yada, H., and Tanaka, H. (1995). Kinetic study on light-limited batch cultivation of photosynthetic cells. *Journal of fermentation and Bioengineering*, 80(3), 259-264.

Osborne, B., and Geider, R. (1987). The minimum photon requirement for photosynthesis. *New phytologist*, 106(4), 631-644.

Panikov, N. (1995). *Microbial growth kinetics*. London; New York: Chapman & Hall.

Pegallapati, A., and Nirmalakhandan, N. (2012). Modeling algal growth in bubble columns under sparging with CO 2-enriched air. *Bioresource technology*, 124, 137-145.

Pickett, J. (1975). Growth of Chlorella in a Nitrate-limited Chemostat. *Plant Physiology,* 55(2), 223-5.

Pruvost, J., Cornet, J., Goetz, V., and Legrand, J. (2011). Modeling dynamic functioning of rectangular photobioreactors in solar conditions. *AIChE Journal*, 57(7), 1947-1960.

Pulz, O., and Gross, W. (2004). Valuable products from biotechnology of microalgae. *Applied Microbiology and Biotechnology,* 65(6), 635-648.

Quinn, J., De Winter, L., and Bradley, T. (2011). Microalgae bulk growth model with application to industrial scale systems. *Bioresource technology*, 102(8), 5083-5092.

Ras, M., Steyer, J. and Bernard, O. (2013). Temperature effect on microalgae: A crucial factor for outdoor production. *Reviews in Environmental Science and Bio/Technology,* 12(2), 153-164.

Ratledge, C., and Kristiansen, B. (Eds.). (2006). Basic biotechnology. Cambridge UK: University Press.

Razzak, S., Hossain, M., Lucky, R., Bassi, A., and De Lasa, H. (2013). Integrated CO2 capture, wastewater treatment and biofuel production by microalgae culturing—A review. *Renewable and Sustainable Energy Reviews,* 27, 622-653.
Richmond, A. (2004). *Handbook of microalgal culture: biotechnology and applied phycology*. Oxford, UK: Blackwell Science.

Richmond, A., and Cheng-Wu, Z. (2001). Optimization of a flat plate glass reactor for mass production of Nannochloropsis sp. outdoors. *Journal of Biotechnology,* 85(3), 259-269.

Riebesell, U., Wolf-Gladrow, D., and Smetacek, V. (1993). Carbon dioxide limitation of marine phytoplankton growth rates. *Nature,* 361(6409), 249.

Rorrer, G., and Mullikin, R. (1999). Modeling and simulation of a tubular recycle photobioreactor for macroalgal cell suspension cultures. *Chemical Engineering Science.* 54 (15-16): 3153-3162.

Ruiz, A., Álvarez-Díaz, G., Barragán, J., and Perales, J. (2013). Photobiotreatment model (PhBT): A kinetic model for microalgae biomass growth and nutrient removal in wastewater. *Environmental Technology,* 34(8), 979-991.

Sasi, D., Mitra, P., Vigueras, A., and Hill, G. (2011). Growth kinetics and lipid production using Chlorella vulgaris in a circulating loop photobioreactor. *Journal of Chemical Technology and Biotechnology*, 86(6), 875-880.

Sharma, R., Singh, G., and Sharma, V. (2011). Comparison of different media formulations on growth, morphology, and chlorophyll content of green alga, *Chlorella Vulgaris*. *International Journal of Pharma and Bio Sciences,* 2(2), 509-516.

Shurin, J., Abbott, R., Deal, M., Kwan, G., Litchman, E., McBride, R., Mandal, S., and Smith, V. (2013). Industrial-strength ecology: Trade-offs and opportunities in algal biofuel production. *Ecology Letters,* 16(11), 1393-1404.

Sierra, E., Acien, F., Fernandez, J., Garcia, J., Gonzalez, C., and Molina, E. (2008). Characterization of a flat plate photobioreactor for the production of microalgae. *Chemical Engineering Journal*, 138(1), 136-147.

Silva, H., and Pirt, S. (1984). Carbon dioxide inhibition of photosynthetic growth of Chlorella. *Journal of general microbiology*, 130(11), 2833-2838.

Soratana, K., and Landis, A. (2011). Evaluating industrial symbiosis and algae cultivation from a life cycle perspective. *Bioresource Technology,* 102(13), 6892-6901.

Sorokin, C., and Krauss, R. (1962). Effects of temperature & illuminance on chlorella growth uncoupled from cell division. *Plant Physiology*, 37(1), 37.

Stumm, W., and Morgan, James J. (1996). *Aquatic chemistry: Chemical equilibria and rates in natural waters* (3rd ed., Environmental science and technology). New York, US: Wiley.

Suh, I., and Lee, S. (2003). Photobioreactor engineering: Design and performance. *Biotechnology and Bioprocess Engineering,* 8(6), 313-321.

Talbot, P., Gortares, M., Lencki, R., and De la Noue, J. (1991). Absorption of CO2 in algal mass culture systems: A different characterization approach. *Biotechnology and Bioengineering,* 37(9), 834-842.

Tans, P., and Keeling, R. (2015). Trends in Atmospheric Carbon Dioxide. Retrieved May 2015 from http://www.esrl.noaa.gov/gmd/ccgg/trends/global.html

Torzillo, G., Pushparaj, B., Masojidek, J., and Vonshak, A. (2003). Biological constraints in algal biotechnology.*Biotechnology and Bioprocess Engineering,* 8(6), 338-348.

Tredici, M. (2004). Mass production of microalgae: photobioreactors. In Richmond, A. (Ed.). *Handbook of microalgal culture: biotechnology and applied phycology*. Oxford, UK: Blackwell Science, 178- 214

Tuantet, K., Temmink, H., Zeeman, G., Janssen, M., Wijffels, R., and Buisman, C. (2014a). Nutrient removal and microalgal biomass production on urine in a short light-path photobioreactor. *Water research*, 55, 162-174.

Tuantet, K., Janssen, M., Temmink, H., Zeeman, G., Wijffels, R., and Buisman, C. (2014b). Microalgae growth on concentrated human urine. *Journal of applied phycology*, 26(1), 287-297.

Udert, K., Larsen, T., Biebow, M., and Gujer, W. (2003a). Urea hydrolysis and precipitation dynamics in a urine-collecting system. *Water Research*, 37(11), 2571-2582.

Udert, K., Larsen, T., and Gujer, W. (2003b). Estimating the precipitation potential in urine-collecting systems. *Water Research*, 37(11), 2667-2677.

Ugwu, C.U., Aoyagi, H., and Uchiyama, H. (2008). Photobioreactors for mass cultivation of algae. *Bioresource Technology,* 99(10), 4021-4028.

Wang, B., Lan, C., and Horsman, M. (2012). Closed photobioreactors for production of microalgal biomasses. *Biotechnology Advances,* 30(4), 904-912.

Wang, L., Min, M., Li, Y., Chen, P., Chen, Y., Liu, Y., Wang, Y., and Ruan, R. (2010). Cultivation of Green Algae Chlorella sp. in Different Wastewaters from Municipal Wastewater Treatment Plant. *Applied Biochemistry and Biotechnology,* 162(4), 1174-1186.

Weyer, K., Bush, D., and Willson, B. (2010). Theoretical Maximum Algal Oil Production. *BioEnergy Research.* 3 (2): 204-213.

Wiley, P., Campbell, J., and Mckuin, B. (2011). Production of biodiesel and biogas from algae: A review of process train options. *Water Environment Research: A Research Publication of the Water Environment Federation,* 83(4), 326-38.

Yamane, T. (1995). Bioreactor operation modes. In Asenjo, J., and Merchuk, José C. (Ed.). *Bioreactor system design* (Bioprocess technology; v. 21). New York, US: M. Dekker, 479-509

Yen, H., Hu, I., Chen, C., and Chang, J. (2014). Design of photobioreactors for algal cultivation. In Pandy, A., Lee, D., Chisti, Y., and Soccol, C. (Ed.). *Biofuels from Algae*. Amsterdam, NL: Elsevier, 23-45.

Yun, Y., and Park, J. (2003). Kinetic modeling of the light-dependent photosynthetic activity of the green microalga Chlorella vulgaris. *Biotechnology and bioengineering*, 83(3), 303-311.

Zonneveld, C. (1998). Light-limited microalgal growth: A comparison of modelling approaches. *Ecological Modelling,* 113(1), 41-54.

Appendix A Equilibrium Equations for BIMP Nutrient System

The equilibrium equations for BIMP rainwater system are given as (adapted from Concas et al., 2012):

$$[H_2CO_3]^* = [CO_2]_L + [H_2CO_3] \quad \text{C.13}$$

$$[H_2CO_3]^* = H_C \cdot p_{CO_2} \quad \text{C.14}$$

$$[CO_2]_L = \frac{H_C \cdot p_{CO_2}}{1 + K_{C1}} \quad \text{C.15}$$

$$[H_2CO_3] = \frac{K_{C1} \cdot H_C \cdot p_{CO_2}}{1 + K_{C1}} \quad \text{C.16}$$

$$[HCO_3^-] = \frac{K_{C2} \cdot H_C \cdot p_{CO_2}}{[H^+]} \quad \text{C.17}$$

$$[CO_3^{-2}] = \frac{K_{C2} \cdot K_{C3} \cdot H_C \cdot p_{CO_2}}{[H^+]^2} \quad \text{C.18}$$

The equilibrium equations for BIMP nutrient system are given as (adapted from England et al 2011):

$$[CO_2]_L = \frac{[H^+]^2 \cdot [TIC]}{[H^+]^2 + K_{C1} \cdot [H^+]^2 + K_{C2} \cdot [H^+] + K_{C2} \cdot K_{C3}} \quad \text{C.19}$$

$$[H_2CO_3] = \frac{K_{C1} \cdot [H^+]^2 \cdot [TIC]}{[H^+]^2 + K_{C1} \cdot [H^+]^2 + K_{C2} \cdot [H^+] + K_{C2} \cdot K_{C3}} \quad \text{C.20}$$

$$[HCO_3^-] = \frac{K_{C2} \cdot [H^+] \cdot [TIC]}{[H^+]^2 + K_{C1} \cdot [H^+]^2 + K_{C2} \cdot [H^+] + K_{C2} \cdot K_{C3}} \quad \text{C.21}$$

$$[CO_3^{-2}] = \frac{K_{C2} \cdot K_{C3} \cdot [TIC]}{[H^+]^2 + K_{C1} \cdot [H^+]^2 + K_{C2} \cdot [H^+] + K_{C2} \cdot K_{C3}} \quad \text{C.22}$$

$$[H_3PO_4] = \frac{[H^+]^3 \cdot [P_T]}{[H^+]^3 + K_{P1} \cdot [H^+]^2 + K_{P1} \cdot K_{P2} \cdot [H^+] + K_{P1} \cdot K_{P2} \cdot K_{P3}} \quad \text{C.23}$$

$$[H_2PO_4^-] = \frac{K_{P1} \cdot [H^+]^2 \cdot [P_T]}{[H^+]^3 + K_{P1} \cdot [H^+]^2 + K_{P1} \cdot K_{P2} \cdot [H^+] + K_{P1} \cdot K_{P2} \cdot K_{P3}} \quad \text{C.24}$$

$$[HPO_4^{-2}] = \frac{K_{P1} \cdot K_{P2} \cdot [H^+] \cdot [P_T]}{[H^+]^3 + K_{P1} \cdot [H^+]^2 + K_{P1} \cdot K_{P2} \cdot [H^+] + K_{P1} \cdot K_{P2} \cdot K_{P3}} \quad \text{C.25}$$

$$[PO_4^{-3}] = \frac{K_{P1} \cdot K_{P2} \cdot K_{P3} \cdot [P_T]}{[H^+]^3 + K_{P1} \cdot [H^+]^2 + K_{P1} \cdot K_{P2} \cdot [H^+] + K_{P1} \cdot K_{P2} \cdot K_{P3}} \quad \text{C.26}$$

$$[NH_3] = \frac{K_{N1} \cdot [N_T]}{[H^+] + K_{N1}} \quad \text{C.27}$$

$$[NH_4^+] = \frac{[H^+] \cdot [N_T]}{[H^+] + K_{N1}} \quad \text{C.28}$$

The equilibrium equations for the BIMP nutrient system are presented in Table A.1.

Table A.1: Equilibrium Reactions for BIMP Nutrient System

Reaction	Equilibrium Constant	Reference
$H_2O \overset{K_W}{\leftrightarrow} [H^+] + [OH^-]$	$pK_W = 14.00$	Concas et al., (2012)
$[CO_2]_G + H_2O \overset{H_C}{\leftrightarrow} [H_2CO_3]^*$	$H_C = 3.4 \cdot (10)^{-2}$ mol L·atm^{-1}	Stumm and Morgan, (1970)
$[CO_2]_L + H_2O \overset{K_{C1}}{\leftrightarrow} [H_2CO_3]$	$pK_{C1} = 2.77$	England et al., (2011)
$[H_2CO_3]^* \overset{K_{C2}}{\leftrightarrow} [H^+] + [HCO_3^-]$	$pK_{C2} = 6.35$	England et al., (2011)
$[HCO_3^-] \overset{K_{C3}}{\leftrightarrow} [H^+] + [CO_3^{-2}]$	$pK_{C3} = 10.33$	England et al., (2011)
$[H_3PO_4] \overset{K_{P1}}{\leftrightarrow} [H^+] + [H_2PO_4^-]$	$pK_{P1} = 2.16$	Concas et al., (2012)
$[H_2PO_4^-] \overset{K_{P2}}{\leftrightarrow} [H^+] + [HPO_4^{-2}]$	$pK_{P2} = 7.21$	Udert et al., (2003a, b)
$[HPO_4^{-2}] \overset{K_{P3}}{\leftrightarrow} [H^+] + [PO_4^{-3}]$	$pK_{P3} = 12.35$	Udert et al., (2003a, b)
$[NH_4^+] \overset{K_{N1}}{\leftrightarrow} [H^+] + [NH_3]$	$pK_{N1} = 9.24$	Udert et al., (2003a, b)

Appendix B MATLAB Code

B.1 Monod

```
% ---------------------------------------------------------
% ---------------------------------------------------------
% Bioreactor Modeling Review
% Nutrient substrate with Monod kinetics
% Version 1.0
%
% MATLAB code written by Aaron Outhwaite (2015)
% ---------------------------------------------------------

clc
clear all
close all

%variables related to growth model
mu_max = 0.05;                          %(hour^-1) max. specific growth
mu_loss = 0.01;                         %(hour^-1) specific loss
Ks = 0.5;                               %(g L^-1) half-sat. constant
Ys = 1;                                 %(g X g^-1 S) yield coeffient

%BIMP simulation parameters
X_now = 1;                              %(g L^-1) initial algae []
S_now = 3;                              %(g L^-1) initial substrate []
X(1) = X_now;                           %set initial microalgae []
S(1) = S_now;                           %set initial substrate []

%BIMP simulation
days = 7;                               %(day) simulation length
hours = 24;
dt = 1;                                 %(hour) simulation timestep
total_tstep = hours*days*dt;            %(-) number of timestep
t = 1;                                  %start simulation at hour 1
time(1) = t;                            %set initial time

while t < total_tstep

   %calculate algae growth
   mu = mu_max*S(t)/(Ks + S(t));
   dX = (mu - mu_loss)*X(t);
   dS = -mu*X(t)/Ys;

   %Eulers method to determine algae and substrate at next time step
   X(t+1) = X(t) + dX*dt;
   S(t+1) = S(t) + dS*dt;

   %step forward in time
   X(t) = X(t+1);
```

```
    S(t) = S(t+1);
    t = t + 1;
    time(t) = t;

end

%analysis of results
figure
hold on
plot(0:length(time)-1,X,'b')
plot(0:length(time)-1,S,'k')
% ---------------------------------------------------------
```

B.2 Haldane

```
% ---------------------------------------------------------
% ---------------------------------------------------------
% Bioreactor Modeling Review
% Haldane limitation
% Version 1.0
%
% MATLAB code written by Aaron Outhwaite (2015)
% ---------------------------------------------------------

clc
clear all
close all

%variables related to growth model
mu_max = 0.05;                          %(hour^-1) max. specific growth
Ks = 0.5;                               %(g L^-1) half-sat. constant
Ki = 5;                                 %(g L^-1) inhibition constant

%BIMP simulation parameters
mu_M = 0;                               %(h^-1) initial growth rate
mu_M(1) = mu_M;
mu_I = 0;
mu_I(1) = mu_I;
S = 0;                                  %(g L^-1) initial substrate []
S(1) = S;

%BIMP simulation
i=1;
step = 0.01;
time = step;
simlength = 5;

while time < simlength

   S(i) = time;
   mu_M(i) = mu_max*S(i)/(Ks + S(i));                   %(h^-1) Monod growth rate
   mu_I(i) = mu_max*S(i)/(Ks + S(i)+ (S(i)^2/Ki));      %(h^-1) Haldane growth rate

   time = time + step;
   i = i + 1;
end

%analysis of results
figure
hold on
plot(S,mu_M,'b')
plot(S,mu_I,'r')
% ---------------------------------------------------------
```

B.3 Light Main

```
% ---------------------------------------------------------
% ---------------------------------------------------------
% BIMP Characterization
% Sunlight with Monod and Haldane kinetics
% Version 1.0
%
% MATLAB code written by Aaron Outhwaite (2015)
% ---------------------------------------------------------
clc
clear all
close all

%Define solar parameters
N = 75;                                 %(-) day of year
H = 12.64;                              %(MJ m^-2 d^-1) avg. solar radiation on horizontal surface
Kt = 0.48;                              %(-) clearness index factor
albedo = 0.40;                          %(-) ground reflectance

%Define solar profile
h_I = Solar(N, H, Kt, albedo);

%variables related to growth model
mu_max = 0.07;                          %(hour^-1) max. specific growth rate
mu_loss = 0.006;                        %(hour^-1) specific loss rate
Ks = 15.9;                              %(umol m^-1 s^-1) half-sat. constant
Ki = 200;                               %(umol m^-1 s^-1) inhibition constant
X = zeros(1,24);
X_now = 1;                              %(g L^-1) initial algae []
X(1) = X_now;

%variables related to Beer-Lambert expression
Km = 0.334;                             %(m^2 g^-1) mass attenuation coefficient
d = 0.05;                               %(m) BIMP culture depth

%BIMP simulation
days = 7;
day = zeros(1,24);
dy = 1;
day(1) = dy;
hours = 23;
hour = zeros(1,24);
hr = 1;
hour(1) = hr;
X_sim = zeros(1,0);
simlength = zeros(1,days*(hours+1));
dt = 1;

for dy = 1:days

   %determine algae growth at each sunlight hour
```

```
    for hr = 1:hours
        %Beer-lambert correlation for spatially averaged light
        h_Iavg(hr) = h_I(hr)*(1-exp(-Km*(X(hr)*1000)*d))/(Km*(X(hr)*1000)*d);

        %calculate algae growth
        %Monod
        %fLight = mu_max*h_Iavg(hr)/(Ks + h_Iavg(hr));
        %Haldane
        fLight = mu_max*h_Iavg(hr)/(Ks + h_Iavg(hr) + (h_Iavg(hr)^2)/Ki);

        %growth rate expression
        dX = (fLight-mu_loss)*X(hr);

        %Eulers method to determine algae at next time step
        X(hr+1) = X(hr) + dX*dt;
        hour(hr+1) = hour(hr) + dt;

    end

    %populate array with daily values for t = days of simulation
    X_sim = [X_sim X];
    dX = X(hr) - X(hr+1);
    X(1)= X(hr+1) - dX;
    %run simulation for t = days
    simlength = 1:days*(hours+1);
    day(dy+1) = day(dy) + 1;

end

%analysis of results
figure
hold on
plot(0:length(simlength)-1,X_sim,'b')
% ---------------------------------------------------------
```

B.4 Solar Function

```
% ---------------------------------------------------------
% ---------------------------------------------------------
% BIMP Characterization
% Light solar model
% Version 1.0
%
% MATLAB code written by Aaron Outhwaite (2015)
% ---------------------------------------------------------
function h_Solar = Solar_T(N, H, Kt, albedo)

lat = 44.4;                                 %(degree) latitude
tilt = 90;                                  %(degree) BIMP tilt
n = 1.0;                                    %(hr) timestep for light/dark

%Preliminary calculations
decl = 23.45*sind((360/365)*(284+N));
h_sunset = acosd(-tand(lat)*tand(decl));

d_light = round((2/15)*h_sunset);
d_light_half = 0.5*d_light;
h_light = 0.5:n:d_light_half;

h_angle = 0.25*60*h_light;
h_count = numel(h_angle);

if h_sunset <= 81.4
   Hd = H*(1.391-(3.560*Kt)+(4.189*Kt^2)-(2.137*Kt^3));
else
   Hd = H*(1.311-(3.022*Kt)+(3.427*Kt^2)-(1.821*Kt^3));
end
Hb = H-Hd;

a_rt = 0.409+0.5016*sind(h_sunset-60);
b_rt = 0.6609-0.4767*sind(h_sunset-60);

 for i = 1:h_count
    %Ratio of mth.avg.hr to mon.avg.day horizontal solar radiation
    rt_w(i) = (pi/24)*(a_rt+(b_rt*cosd(h_angle(i))))*((cosd(h_angle(i))-cosd(h_sunset))/(sind(h_sunset)-
((pi*h_sunset)*cosd(h_sunset)/180)));
    rd_w(i) = (pi/24)*((cosd(h_angle(i))-cosd(h_sunset))/(sind(h_sunset)-
((pi*h_sunset)*cosd(h_sunset)/180)));

    %Total mth.avg.hr horizontal radiation
    I_h(i) = rt_w(i)*H;
    Id_h(i) = rd_w(i)*Hd;
    Ib_h(i) = I_h(i) - Id_h(i);

    %Ratio of mth.avg.hr horizontal to vertical surface solar radiation
    cos_0(i) = cosd(lat-tilt)*cosd(decl)*cosd(h_angle(i))+sind(lat-tilt)*sind(decl);
    cos_0z(i) = cosd(lat)*cosd(decl)*cosd(h_angle(i))+sind(lat)*sind(decl);
```

```
    Rb(i) = cos_0(i)/cos_0z(i);

    %total mth.avg.hr vertical radiation
    Ib_t(i) = Ib_h(i)*Rb(i);
    Id_t(i) = Id_h(i)*((1+cosd(tilt))/2);
    Ir_t(i) = I_h(i)*((1-cosd(tilt))/2)*albedo;

    %sum postive values
    a = [Ib_t(i) Id_t(i) Ir_t(i)];
    pos = a>0;
    %convert from MJ m^-2 h^-1 to umol m^-2 s^-1 on vertical culture
    %surface
    I_t(i) = sum(a(pos))*509.525;
 end

%populate solar array for use in 24 hr growth model
h_Solar = zeros(1,24);
d_dark = 24-2*h_count;
d_dark_half = 0.5*d_dark;
h_morning = h_count;
for j = d_dark_half+1:d_dark_half+h_count
   h_Solar(j) = I_t(h_morning);
   h_morning = h_morning - 1;
end

for k = 1:h_count
   h_Solar(12+k) = I_t(k);
end
% ------------------------------------------------------------
```

B.5 Light-Temperature Main

```
% ---------------------------------------------------------
% ---------------------------------------------------------
% BIMP Characterization
% Temperature with RuBisCo activation kinetics
% Version 1.0
%
% MATLAB code written by Aaron Outhwaite (2015)
% ---------------------------------------------------------
clc
clear all
close all

%define solar parameters
N = 258;                                %(-) day of year
H = 14.33;                              %(MJ m^-2 d^-1) avg. solar radiation on horizontal surface
Kt = 0.50;                              %(-) clearness index factor
albedo = 0.20;                          %(-) ground reflectance

%define solar profile
h_I = Solar(N, H, Kt, albedo);

%define temperature parameters
h_T = Temperature();

%variables related to light and temperature growth model
mu_max = 0.07;                          %(hour^-1) max. specific growth rate
mu_loss = 0.006;                        %(hour^-1) specific loss rate
Ks = 15.9;                              %(umol m^-1 s^-1) half-sat. constant
Ea = 62.5*1000;                         %(J mol^-1) RuBisCo activation energy
R = 8.314;                              %(J K^-1 mol^-1) universal gas constant
Topt = 305.4;                           %(K) Optimal temp for C. vulgaris

X = zeros(1,24);
X_now = 1;                              %(g L^-1) initial algae []
X(1) = X_now;

%variables related to Beer-Lambert expression
Km = 0.334;                             %(m^2 g^-1) mass attenuation coefficient
d = 0.05;                               %(m) BIMP culture depth

%BIMP simulation
days = 7;
day = zeros(1,7);
dy = 1;
day(1) = dy;
hours = 23;
hour = zeros(1,24);
hr = 1;
hour(1) = hr;
X_sim = zeros(1,0);
```

```
simlength = zeros(1,days*(hours+1));
dt = 1;

for dy = 1:days

   %determine algae growth at each sunlight hour
   for hr = 1:hours

      %Beer-lambert correlation for spatially averaged light
      h_Iavg(hr) = h_I(hr)*(1-exp(-Km*(X(hr)*1000)*d))/(Km*(X(hr)*1000)*d);
      %calculate algae growth

      %Monod
      fLight = h_Iavg(hr)/(Ks + h_Iavg(hr));

      %calculate temperature limitation
      aTemp = exp((Ea/(R*Topt))-(Ea/(R*h_T(hr))));
      fTemp = ((2*aTemp)/(1+aTemp^2));

      %growth rate expression
      dX = (mu_max*fTemp*fLight-mu_loss)*X(hr);
      %Eulers method to determine algae at next time step
      X(hr+1) = X(hr) + dX*dt;
      %step forward in time
      hour(hr+1) = hour(hr) + dt;

   end
   %populate array with daily values for t = days of simulation
   X_sim = [X_sim X];
   dX = X(hr) - X(hr+1);
   X(1)= X(hr+1) - dX;
   %run simulation for t = days
   simlength = 1:days*(hours+1);
   day(dy+1) = day(dy) + 1;

end

%analysis of results
figure
hold on
plot(0:length(simlength)-1,X_sim,'b')
% ---------------------------------------------------------
```

B.6 Temperature function

```
% ---------------------------------------------------------
% ---------------------------------------------------------
% BIMP Temperature Characterization
% Version 1.0
%
% MATLAB code written by Outhwaite (2015)
% ---------------------------------------------------------

function Tw_dt = Temperature()

%define solar parameters
N = 258;                                    %(-) day of year
H = 14.33;                                  %(MJ m^-2 d^-1) avg. solar radiation on horizontal surface
Kt = 0.50;                                  %(-) clearness index factor
albedo = 0.20;                              %(-) ground reflectance

%define solar profile
h_I = Solar_T(N, H, Kt, albedo);

%To = xlsread('Temperature.xlsx','HFX-Temp-Mar','D15:D39');
%To = xlsread('Temperature.xlsx','HFX-Temp-Jun','D15:D39');
To = xlsread('Temperature.xlsx','HFX-Temp-Sep','D15:D39');
%To = xlsread('Temperature.xlsx','HFX-Temp-Dec','D15:D39');

To = To';

Ti = 294;
Tsur = 294;

sb = 5.67037e-8;

A1 = 1;
A2 = A1;
Aw = A1;

d1 = 0.006;
d2 = d1;
dw = 0.05;

m1 = 14;
m2 = m1;
mw = 50;

Cp1 = 750;
Cp2 = Cp1;
Cpw = 4180;

k1 = 1.4;
k2 = k1;
```

```
a1 = 0.05;
a2 = a1;
aw = 0.9;

e1 = 0.92;
e2 = e1;

tau1 = 0.95;
tau2 = tau1;
tauw = 0.1;

V = 5.43;
hc1 = 26.35;
hc2 = 5.7;
hk1 = 233.33;
hk2 = hk1;

T1 = zeros(1,3600);
T1_now = 294;
T1(1) = T1_now;

T2 = zeros(1,3600);
T2_now = 294;
T2(1) = T2_now;

Tw = zeros(1,3600);
Tw_now = 294;
Tw(1) = T1_now;

seconds = 3599;
second = zeros(1,3600);
sec = 1;
second(1) = sec;
dt = 1;

hours = 24;
hour = zeros(1,24);
hr = 1;
hour(1) = hr;
dh = 1;

T1_sim = [T1_now];
T2_sim = [T2_now];
Tw_sim = [Tw_now];

for hr = 1:hours

   for sec = 1:seconds

      %outer BIMP surface
      Qs1 = a1*A1*h_I(hr);
      Qr1 = e1*sb*A1*((T1(sec)^4)-(0.0552*To(hr)^1.5)^4);
```

```
        Qc1 = hc1*A1*(T1(sec)-To(hr));
        Qk1 = hk1*A1*(T1(sec)-Tw(sec));

        %inner BIMP surface
        Qs2 = tau1*tauw*a2*A2*h_I(hr);
        Qr2 = e2*sb*A2*(T2(sec)^4-Tsur^4);
        Qc2 = hc2*A2*(T2(sec)-Ti);
        Qk2 = hk2*A2*(T2(sec)-Tw(sec));

        %culture
        Qsw = tau1*aw*Aw*h_I(hr);

        %temperature expression
        dT1 = (Qs1-Qr1-Qc1-Qk1)/(m1*Cp1);
        dT2 = (Qs2-Qr2-Qc2-Qk2)/(m2*Cp2);
        dTw = (Qsw+Qk1+Qk2)/(mw*Cpw);

        %Eulers method to determine temp at next time step
        T1(sec+1) = T1(sec) + dT1*dt;
        T2(sec+1) = T2(sec) + dT2*dt;
        Tw(sec+1) = Tw(sec) + dTw*dt;

        %step forward in time
        second(sec+1) = second(sec) + dt;

    end
    %populate arrays with daily values for t = days of simulation
    T1_sim = [T1_sim median(T1)];
    T2_sim = [T2_sim median(T2)];
    Tw_sim = [Tw_sim median(Tw)];

    dT1(1)= T1(sec);
    dT2(1)= T2(sec);
    dTw(1)= Tw(sec);
    %run simulation for t = hours
    hour(dh+1) = hour(dh) + 1;
end
Tw_dt = Tw_sim
% ------------------------------------------------------
```